Fabrication of Copper Plated Carbon Fiber Dispersed Iron Matrix Composites and Thermal Conductivity Calculation by Two-Dimensional Microstructure Images

（銅めっき炭素繊維を添加した鉄基複合材料の作製と二次元微細構造画像を用いた熱伝導率の計算）

Dissertation for the Degree of Doctor of Engineering

Department of Mechanical Science and Engineering

Graduate School of Engineering

Hiroshima University, Japan

Advisor: Prof. Gen Sasaki

Wu　Di

ウ　デイ

2023. May

CONTENTS

List of Figures

List of Tables

Table 5-2 Relative density of monolithic SKD6l block and composite prepared by spark plasma sintering.

Chapter 1

Background and objective

1.1 Introduction

With the warming of the climate and the melting of glaciers, the emission reduction of carbon dioxide (CO_2) has become a major global issue. Among them, the CO_2 emitted by transportation is second only to electricity, and about 90% of the CO_2 emissions in transportation come from automobiles[1]. Now, automobiles have become the most used travel means of transportation. Lightweight vehicles not only improve the fuel efficiency and reduce CO_2 emissions, but also improve the safety and comfort of vehicles[2,3]. Every 10 % reduction in a car's weight can improve fuel efficiency by nearly 2.5%[4,5]. Light weighting of the car is achieved by using thinner parts with higher strength. To achieve a perfect match between the strength and density of the part, the preferred materials are magnesium alloy, aluminum alloy and steel, whose strength, density, and specific strength are listed in Table 1-1.

Table 1-1 Tensile strength, density, and specific strength of various sheet metals.

Sheet	Tensile strength / MPa	Density / $g \cdot cm^{-3}$	Specific strength/N·m/kg
Magnesium alloy	250~343	1.8	1389~1906
Aluminum alloy	110~270	2.7	407~1000
Ordinary steel	340~600	7.8	436~769
high strength steel	490~1500	7.8	928~1923
ultra-high strength steel	1620~1700	7.8	2077~2179

Specific strength is the ratio of tensile strength to density. Magnesium alloy has high specific strength, but its tensile strength is not enough to ensure the safety of automobiles, and it is expensive. Although aluminum alloys are inexpensive and readily available and attractive for automotive light weighting, their specific strengths are much lower than steel. Magnesium alloy sheet and aluminum alloy sheet are mainly produced by warm and hot stamping process[6-9]. The specific strength of ultra-high strength steel is 3 to 5 times that of ordinary steel. Therefore, high-strength steel and ultra-high-strength steel become the best choice for auto parts.

In the process of producing high-strength steel plates by the traditional cold stamping, the forming difficulty is large, the resilience is large, the required stamping load is large, and the formability is low. As shown in Figure 1-1, short die life and severe wear[10-12]. Therefore, the hot stamping process is essential for the production of high-strength and ultra-high-strength steel auto parts, which has contributed to the prosperity of the automotive industry[13-15].

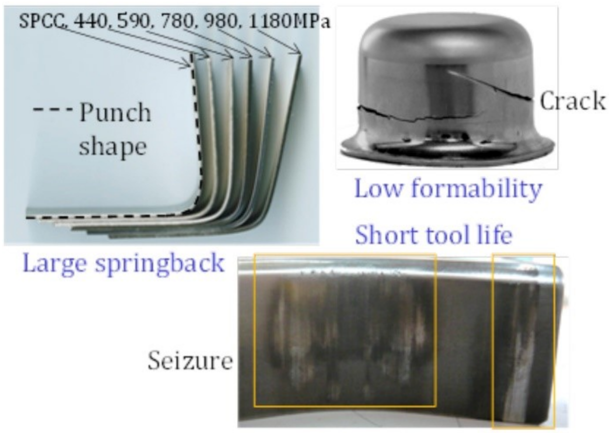

Figure 1-1 Problems in cold stamping of high strength steel sheets.

Currently, the number of auto parts produced by the hot stamping process is 2-7 per minute, which cannot meet the growing demand for auto parts. As shown in Figure 1-2, the automotive industry uses hot stamped parts for chassis components such as A-pillars, B-pillars, bumpers, roof rails, rocker rails, and tunnels. As shown in Figure 1-3, Hot stamping parts used in automobiles are increasing year by year.

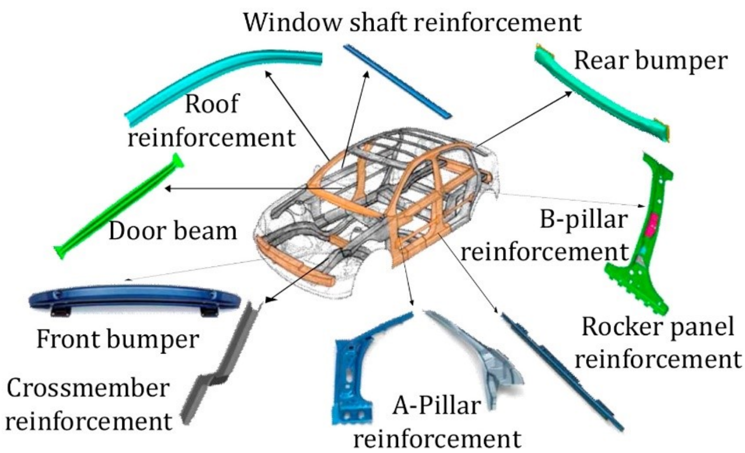

Figure 1-2 Automobile parts produced by hot stamping.

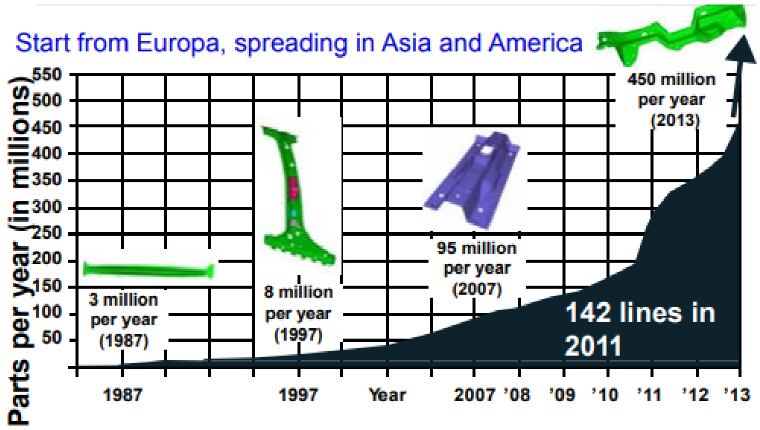

Figure 1-3 Number of parts produced by hot stamping.

With the rapid development of the processing and manufacturing industry, the production efficiency of automobile parts needs to be further improved. The heating and heat dissipation of the die accounts for 30% of the total time and improving the thermal conductivity (TC) of the die can improve production efficiency. Increasing the TC of the die also helps to reduce the thermal stress accumulation of the die and improves the service life of the die. To meet the development of the automobile industry, the production efficiency of auto parts also needs to be further improved. Hot stamping dies used to produce automotive parts must have the following mechanical and thermal properties[16].

1. High hardness and low aging index: high yield strength ratio (σs /σb) ensures the dimensional accuracy of stamping parts.

2. Greater toughness: not easy to crack.

3. Good machinability: easy to design and process the shape of the die.

4. Good chemical stability and high temperature stability: It is not easy to undergo phase change and corrosion under high temperature and low temperature cyclic working conditions. The life of the die is long.

5. Cost control and competition requirements: easy to process, cheap and easy to obtain, suitable for industrialized large-scale production.

6. High TC: Quickly homogenize and dissipate heat in the die to improve production efficiency.

The currently high TC hot stamping die is based on pure iron, and trace elements such as C, Si, Mn, W, Mo, Cr, V, S, and P are added to adjust the mechanical and thermal properties of the die. Heat conduction in materials is determined by phonons and electrons. These trace elements cause distortion of the iron lattice, and the phonons of the lattice vibration hinder the movement of electrons and hinder the conduction of heat[17]. Therefore, in this study, pure iron (Fe) was selected as the matrix in order to obtain a die with high TC.

Pure metal can no longer meet the needs of the increasingly complex working environment of the current industry. We can enhance the composite TC by adding these high TC fillers[18,19], which can obtain high TC and good mechanical properties of the metal matrix[20,21]. Diamond (C)[22,23], silicon carbide (SiC)[24,25], carbon nanotubes (CNT)[26-28], graphite (GF)[29-31] and carbon fiber (C_f)[32-37] have attracted great attention as high TC fillers to improve the TC of composites. Both diamond and SiC require surface plating to improve surface wettability[38-41]. Diamonds are expensive. The TC of SiC is small, which has negligible effect on the enhancement of composite TC. Although these particles can improve the thermal properties of the composite, the volume fraction of the reinforcing material required to increase the TC is as high as 60%, Which in turn makes the diamond and SiC reinforced composite difficult to machine. To seek the balance between machinability and thermal performance, graphite, CNT and C_f with significant anisotropic thermal conductivity have become the most used thermally conductive fillers[42]. Graphite has low strength and adding it as a filler to a hot work die will result in a reduction in die strength. The industrial cost of CNT is high, and it is often used in the field of electrical conductivity, which is not suitable for large-scale industrial production of hot stamping dies. C_f possesses excellent mechanical properties, high-cost performance, and other characteristics. C_f reinforced Fe-based composites have good TC and workability and are extremely suitable for hot stamping die materials and are suitable for mass production of dies.

As a two-dimensional TC material, C_f is highly anisotropic in the TC[32,43-45], and has excellent TC in the axial direction[37,46-49]. The TC of C_f reinforced composites is also anisotropic. TC of Fe (54 $Wm^{-1}K^{-1}$) is between axial TC (580 $Wm^{-1}K^{-1}$) and radial

TC (5 $Wm^{-1}K^{-1}$) of C_f. Therefore, the orientation of C_f has a significant effect on the TC of the composites[35,36,50-55]. Moreover, to prevent C_f from contacting and reacting with the iron matrix and causing C_f to be destroyed, C_f needs electroless copper plating to obtain copper-plated C_f (C_f-Cu).

To be able to predict the TC of C_f reinforced composites, scholars have proposed many theoretical calculation models[45,56-61]. However, due to the anisotropy of the TC of C_f, these models are not suitable for the calculation of the effective TC (ETC) of C_f-Cu/Fe. Usually, to evaluate the interfacial thermal resistance(ITR) inside C_f reinforced metal matrix composites such as C_f-Cu/Fe, researchers have established some models such as the phonon diffusion mismatch model (DMM)[62] and acoustic mismatch model (AMM)[63] under ideal conditions. However, these theoretical models are far from the ITR of actual composites. The actual state of the contact interface is affected by many factors, which make its microstructure extremely complex. Such as the shape, wettability, specific heat capacity, thermal expansion coefficient and other influencing factors of the contacting phase, as well as the pressure, temperature, equipment pressure transfer and heat transfer capacity in the composite manufacturing process. So far, it has been almost impossible to determine the numerical relationship between these influencing factors and the microstructure of the contact interface. Therefore, these models calculate ITR that are much smaller than the ITR of actual composites.

The main purpose of this thesis is to investigate the method of improvement of TC of C_f-Cu reinforced iron composites TC, the influencing factors and degree of influence of TC, to fabricate C_f-Cu/Fe hot stamping die with high TC, speed up heat conduction to improve production efficiency and Extend die life. In this study, a novel 2D image-based simulation method[64-66] was employed to calculate the simulated TC of C_f-Cu/Fe composites, and the influence degree of various heat conduction hindering factors on the composite material was calculated. Research methods: The model of C_f-Cu/Fe composite TC was calculated based on two-dimensional images simulation. By comparing the TC of the composites obtained by different models with the actual TC, the factors hindering the thermal conduction of the C_f-Cu/Fe composites were analyzed.

Research contents: 1, Analyze the spatial position of C_f in the actual composite, determine its orientation and calculate the simulated TC of the composite by combining the finite element analysis method; 2, Through the layer-in-parallel (ROM) and the effective medium approximation (EMA) models calculated composite TC and TC by finite element simulation compared with measured TC to evaluate the degree of influence of the voids, the orientation and aspect ratio of C_f-Cu, the thermal contact resistance and the experimental error on TC of C_f-Cu/Fe composites.

1.2 Experimental study on die composites

1.2.1 Metal matrix composites

The properties of single metal materials or alloys can deteriorate significantly in relatively harsh environments, thereby limiting their availability in critical components[67]. Metal matrix composites are new materials made of metals and one or more reinforcing fillers to make up for the defects of a certain characteristic of metals. These reinforcing fillers can significantly improve hardness, tensile strength, elastic modulus, and other mechanical properties in metal matrices. Few other properties such as TC, coefficient of thermal expansion (CTE), coefficient of friction, wear resistance, corrosion resistance, and fatigue resistance are available depending on the application requirements of metal matrix composites. Prashanth et al.[68] found that adding high thermal conductivity BeCu to the tool steel material die, in the production process of a cosmetic product cap, uniform temperature distribution and reduce warpage. Compared to tool steel, the cycle time is reduced by nearly 3 seconds, which greatly increases production efficiency.

In Metal matrix composites, the matrix, reinforcement, and matrix/reinforcement interface will determine the properties of the composite[69-71]. In traditional cognition, the matrix is only used to fix the reinforcing material, and the reinforcing filler is used to strengthen one or several characteristics of the overall composite material. However, with in-depth research, researchers found that the interaction between the matrix and the reinforcement also seriously affects the mechanical and thermal properties of the composite. For example, a chemical reaction occurs between the matrix and the reinforcement, which destroys the structure of the reinforcement or generates a new phase that weakens a certain property of the composite. The poor wettability between the matrix and the reinforcement leads to voids in the contact between the two during the preparation process, which hinders the continuity of atomic and phonon vibrations, and hinders the process of force and heat transfer.

1.2.2 Advantages of high thermal conductivity dies

Due to the increasing competition in the automotive industry, shortening the production cycle time and process reliability of components is essential to improve the competitiveness of automotive manufacturers[72-75]. More and more scholars improve the thermal cycle process mainly through two methods to offset the production cost that cannot be passed on to customers[76]. One is to improve the heat transfer process by designing the thermal cycle structure of the die, which has been studied by many scholars[13,73-75,77-79]. However, such cooling channels have complex design, high machining and maintenance costs, and limited cooling capacity (TC is lower than that of the substrate). The other is to fundamentally change the TC of the die by adding high TC materials, reasonable compositional structure, and compositional combination. This method of increasing the TC of die is rarely studied. High TC can not only accelerate the thermal diffusion of the die, improve the stability and production efficiency of the equipment, but also accelerate the cooling of the parts to obtain high-strength martensite.

1.2.3 C_f reinforced metal matrix composites

Generally, materials containing more than 92 wt% carbon and forming the shape of fibers are defined as C_f [80]. C_f has excellent mechanical properties, high tensile strength (2-7 GPa), high Young's modulus (200-900 GPa), low density (1.75- 2.20 g/cm3), low thermal expansion, excellent electrical and thermal conductivity (800 $Wm^{-1}K^{-1}$), which can significantly enhance the mechanical and physical properties of the matrix[81]. C_f have high chemical resistance to almost all chemicals except hot air and flame, exhibiting extremely high chemical stability[82]. There have been many studies on C_f-reinforced metal matrix composites in recent years. When C_f as reinforcing fillers reinforce metal matrices such as Fe, Cu, Al and their alloys, chemical reactions will occur in direct contact, which will destroy the continuity of C_f and lead to poor final properties of the composites. The interface between C_f and the substrate plays an important role in the transfer of force and heat. If the bond between the two is weak; this may be due to wettability issues or lack of interaction; the final composite will have poor mechanical properties. We may need to adjust the fabrication process to improve the final properties of the composite. Baumli et al.[83] found that C_f was transferred into liquid aluminum by using a special flux containing K_2TiF_6 dissolved in NaCl-KCl. This flux ensures the removal of oxides from the interface and the formation of a wettable TiC layer at the interface with perfect wettability with liquid Al for spontaneous composite formation. In squeeze casting, in order to solve the non-wetting behavior of molten aluminum to carbon fibers, Hasan et al.[84] adopted a laminated squeeze casting method to force the two to quickly and intimately contact, penetrate, wet, and cool quickly to reduce the contact time and chemical reaction of the interface between C_f and molten aluminum.

If the wettability and mutual contact between C_f and metal cannot be handled by the preparation process, we can change the wettability of C_f by copper/nickel plating. Nickel and copper plating on the carbon fiber surface enhances its wettability with molten aluminum[85].In order to avoid contact between C_f and Al, Bhav Singh et al.[86] performed electroless copper plating on the surface of C_f to form a protective layer to protect C_f. Korb et al.[87] improved the thermal expansion coefficient of carbon fiber by plating copper, so that the axial thermal expansion coefficient of the famous Schapery model is consistent with the prediction of the model derived by Kural and Min, and produced an isotropic in-plane thermomechanical material cross-plying composite.

1.2.4 Fabrication method of metal matrix composites

In previous studies, C_f reinforced various metal matrix composites have been shown to exhibit excellent mechanical and thermal properties, such as Aluminum (Al)[83-85,88,89], Magnesium (Mg)[90], Nickel (Ni)[91], Copper (Cu)[49,92-94] and Titanium (Ti)[95-98] and its alloy etc. Summarizing the above literature, we can find that the manufacturing methods of C_f reinforced metal matrix composites are Solid state processing, Liquid state processing and Deposition processing. The research on C_f reinforced iron matrix composites is rarely involved. Considering that iron has a melting point of 1808K, the Liquid state processing method is extremely equipmentintensive and expensive to produce, it is suitable for the fabrication of C_f-reinforced low-melting-point metal matrix composites. Deposition treatment methods are mostly used for the modification of C_f. Before solid-state treatment and liquid treatment methods, metal coatings are deposited on the surface of C_f to change the wettability and thermal expansion coefficient between C_f and metal or to protect C_f from damage. Solid state processing methods including Powder metallurgy and Diffusion bonding.

1.2.4.1 Powder metallurgy

Powder metallurgy is a process technology that uses metal powder or a mixture of metal powder and other metal powder (non-metallic materials) as raw materials, after forming and sintering, to fabricate metal or composite and various types of products. It is an important production process for the fabrication of metals and metal matrix composites. Powder metallurgy processes include spark plasma sintering (SPS) and vacuum hot pressing. Powder metallurgy provides an effective sintering method for low temperature rapid sintering of C_f reinforced iron matrix composites. Figure 1-4 shows the Schematic representation of a SPS process and vacuum hot pressing.

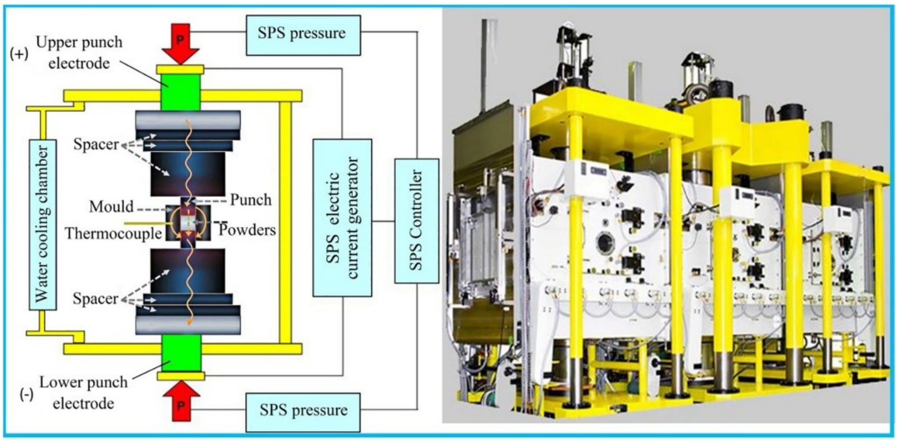

Figure 1-4 The schematic representation of a SPS process and vacuum hot pressing[99].

In 1933, patents were published to describe methods of using electrical discharge or electrical current to facilitate powder sintering or metal sintering joining[99,100]. Through the tireless efforts of Lenel of RPI, scientists from Lockheed Missile and Space Corporation of California, and Inoue of Japan, the so-called "spark sintering" was identified[100,101].Spark plasma sintering can prepare metals, ceramics, nanomaterials, amorphous materials, composite materials, gradient materials and materials with complex shapes[99,102-106]. Spark plasma sintering technology has significantly advanced the advancement of materials science research.

Compared with traditional powder metallurgy methods such as pressure less sintering (PLS), hot pressing sintering (HP) and hot isostatic pressing (HIP), SPS can ensure that the high temperature is only distributed in the die, rather than filling the entire cavity, Rapid heating can achieve rapid sintering. Spark plasma sintering has many distinct advantages[99,107-109]. Factors such as the initial powder, the type and size of the die, and the capacity of the equipment can affect the heating rate of the SPS. In general, most SPS devices can reach up to 1000 K/min[110]. Rapid heating can make it too late for the newly formed grain boundaries to adjust themselves to a stable state[111]. The dislocations and slips of the crystal planes hinder each other so that this high-energy state is preserved[112]. Therefore, rapid high temperature can effectively suppress the grain growth in the early sintering of SPS[113]. Liu et al.[113] found that the ultrafast heating and high-pressure technique can doubly suppress the coarsening of MgO particles during SPS sintering. As shown in Figure 1-5, under the SPS sintering conditions of 170MPa and a heating rate of 1880K/min, and holding pressure for 60s, MgO ceramics with a relative density of 99.1% and an average grain size of 50 nm were obtained by ultrafast heating and high-pressure technology[113].

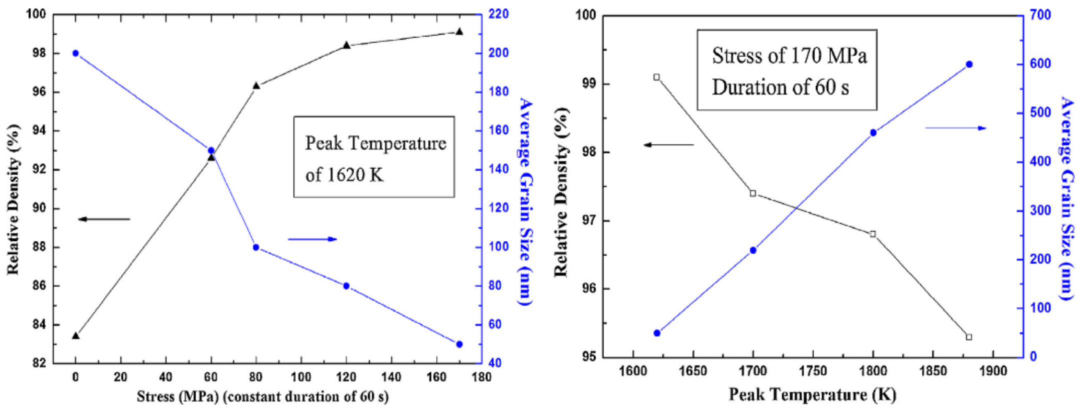

Figure 1-5 The relationship between the average grain size of MgO and pressure[113].

During the sintering process of SPS, the sputtering and discharge impact of high-temperature plasma will generate local high temperature, and various particles can be rapidly densified through various diffusion mechanisms to achieve rapid densification[114,115]. Compared with most traditional sintering methods, the densification temperature of SPS is about 200-300K lower, which provides a simple and effective method for the densification of heat-resistant bulk materials. The rapid densification of SPS greatly shortens the production cycle, improves production efficiency and reduces production costs. In the study of Raichenko et al.[116], it was found that SPS only required 1.5-1.75 min to form a uniform and dense alloy of Ni and Mo powders. Using the traditional sintering method to achieve the same effect requires sintering at a temperature of 1727K for 2h.

Therefore, SPS is becoming an effective way to carry out material design and material genome engineering research because of its simplicity, rapidity, high efficiency and low cost.

1.2.4.2 Extrusion process

In the introduction in Section 1.1, we already know that C_f is a two-dimensional high TC material, and the TC of C_f-enhanced metal matrix composites also has anisotropy. The orientation of C_f significantly affects the TC of the composite, which will be detailed in section 1.3. In order to achieve the purpose of establishing a TC channel in the composite and improving the TC of the composite, we need to change the orientation of C_f through external force.

There are generally two types of external forces acting on C_f. One is to align the C_f in the direction of the material's design and make composites by diffusion bonding. Diffusion bonding means that directly under the action of external factors (pressure, temperature, vacuum, etc.), the contact surfaces of C_f and the metal are brought close to each other, plastic deformation occurs locally, and the atoms diffuse each other and bond into a whole[117,118]. Diffusion bonding can directly join metals and non-metals together to form a strong connection. The absence of the diffusion agent in diffusion bonding does not cause macroscopic deformation, melting, or relative motion of the parts[119-121]. This technique is particularly suitable for the manufacture of anisotropic cast iron parts, forgings, and connections between powder metallurgy parts with large differences in part thickness[120]. Diffusion bonding is an integral heating process with small deformation of composites and high dimensional accuracy. Therefore, diffusion bonding is suitable for the manufacture of large-area parts, laminates, hollow components, porous materials or complex internal passages (such as turbine blades and jet elements), closed internal joints (such as honeycomb siding), and other bonding methods are less feasible for the manufacture of parts[122]. Furthermore, the technology is environmentally friendly and easy to automate, making it suitable for large-scale industrial production. Koráb et al.[123] wound C_f-Cu on a steel plate, put the steel plate into a die, and diffusion-bonded it under vacuum conditions of 100 MPa and 873 K for 15 minutes to fabricate a composite with a thickness of about 0.25 mm.

Another method is that the external force acts on C_f indirectly, and the orientation of C_f is adjusted by the deformation of the composite material. The most common method is extrusion, including cold extrusion and hot extrusion. Extrusion has been used as one of the most common secondary processes due to its good axial preferential orientation of discontinuous fibers. Cold extrusion uses compressive and shear stresses to push or pull composite materials in or out of a die to produce the required complex cross-sections and brittle work materials. Cold extrusion can also form finished parts with a surface finish. In this paper, discontinuous C_f (chopped to 5 mm) is used as reinforcement, and C_f cannot be oriented by cold extrusion process. This is because to achieve the same compression effect (compression ratio), the pressure of cold extrusion is much greater than that of hot extrusion, which places high demands on equipment, and the compressive stress and shear stress will cause the composite to be easily crushed. The research shows that the variation of the strain rate of the workpiece with the process temperature is an important factor for the success of the hot extrusion process of metal matrix composites. The melting point (T_m) of pure iron is 1811K, the minimum recrystallization temperature is 724.4K ($0.4T_m$), and the softening temperature is higher than the recrystallization temperature. If the temperature of the metal exceeds its recrystallization temperature when extruding, the process is called "hot extrusion", otherwise called "cold extrusion". The extrusion of pure iron is hot extrusion, and the hot extrusion temperature is about 50% to 75% of the T_m of the metal matrix[124], that is, 905.5-1358.25K. Hot extrusion works in a high-temperature and high-pressure environment, and the use of a suitable lubricant between the extrusion billet and the die can improve the life of the die and other components. Oil and graphite work at lower temperatures, while glass frit is used at higher temperatures. When the traditional lubrication is insufficient, the hydrostatic extrusion process can be applied, and the hydrostatic extrusion can be considered as an extension of the lubricated hot extrusion process[124]. Pure iron is usually hot extruded without lubrication.

In the process of hot extrusion, we need to control the strain rate within a certain range to avoid peeling at the interface between Cf and the substrate, and to prevent Cf from breaking and weakening its efficiency of strengthening[125]. The classical composite hot extrusion metal forming process can refine particles (large particle or agglomerates are broken), reduce porosity and improve the bonding interface of non-metallic reinforcements and metals, improve the mechanical properties of metal matrix composites[126]. In order to make the orientation of C_f perpendicular to the pressing direction on the cross-section of the Al matrix to be consistent, Yi et al.[127] fabricated a nickel-plated C_f-reinforced Al composite by a hot extrusion process (Figures 1-6).

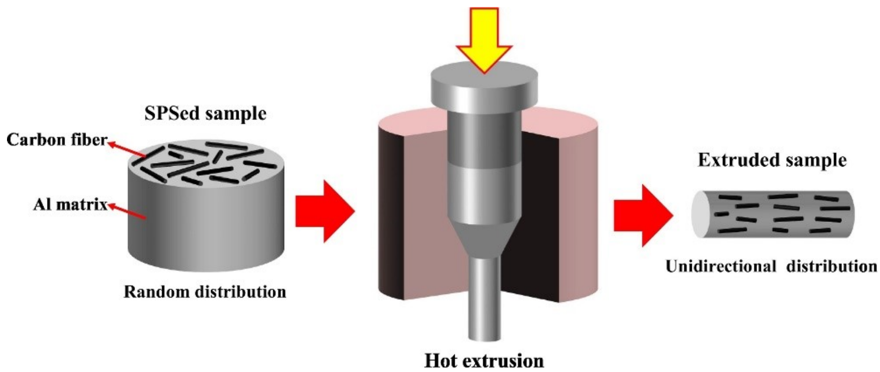

Figure 1-6 Schematic illustration of preparation method of unidirectionally oriented C_f/Al composites[127].

Daoud et al.[128] and Ramesh et al.[129] It was found that hot extrusion can significantly reduce the porosity of the composites, refine the grains, and bind the metal matrix more tightly to the reinforcement compared to the as-cast material. Under the same conditions in various experiments, the extruded composites are more wear-resistant than the cast composites[129].

1.3 Influencing factors of TC of C_f reinforced composites

There are two main considerations for improving the TC of composites[130]. One is to improve the thermal conductivity of raw materials, including switching to a higher TC matrix and thermal fillers and modifying thermally conductive fillers. Another is to reduce the thermal contact resistance between the reinforcing material and the substrate. Typically, the reinforcing thermal fillers for composites are oxides (Al_2O_3, MgO), nitride (Si_3N_4, BN, AlN), and carbon materials (C_f, CNTs, and GFs).

Compared with the granular shape, the linear reinforced thermal filler can form a thermal conduction channel, and the effect of improving the TC of the composite is more obvious[131-133]. Commonly used linear reinforcement materials include GF, CNT, and C_f, which have high anisotropy, and the TC of the reinforced composites also has anisotropy. Many scholars' studies have shown that the TC of C_f-reinforced composites is affected by various factors. Li et al.[50] believed that the TC of composites depends on the TC of the matrix material, the ITR and the percentage content of C_f. The aspect ratio of C_f in the direction of heat flow is also a key factor for obtaining high TC of composite. Xu et al.[134] believed that one is that a large amount of phonon scattering in the discontinuous network will occur at the filler/matrix interface because the sound of different atoms does not match[135]. The other is that the ITR at the contact between the matrix and C_f plays a major role in reducing the TC of the composite.

Changing the content and orientation of C_f, building a thermally conductive network structure, or changing the interface between C_f and the substrate can enhance the TC of the composite. Wei et al.[34] found that not only the content of C_f would seriously affect the TC of the composite, but the TC of the composite decreased with the increase of temperature [136]. This phenomenon can be attributed to the Umklapp resistance, which increases with temperature[136,137].

Xu et al.[134] prepared a C_f-GF three-dimensional (3D) network structure to establish the path of thermal conduction and improve the TC of polyamide-imide composites. When the filler content was 4.25 wt%, the vertical TC of the composites

(TC) reaches 0.53 W m, which is 165% higher than that of pure polyamide-imide.

1.4 Theoretical calculation for ETC and ITR of composites

1.4.1 Theoretical calculation models for TC of composites

C_f reinforced iron composites belong to heterogeneous medium structure materials. A number of models have been proposed to predict the macroscopic properties of such composites[138]. TC is one of the most important properties of heterogeneous media composites. In his famous work on electromagnetism, Maxwell was the first to give the expression of the inhomogeneous medium ETC, K_{eff}[139].

$$\frac{K_{eff}}{K_m} = 1 + \frac{3\varphi}{\left(\frac{K_1 + 2K_m}{K_1 - K_m}\right) - \varphi}$$

…… (1-1)

Where K_{eff} is the ETC of the composite, K_m is the TC of the continuous matrix, K_1 is the TC of the reinforcement, and φ is the volume fraction of the reinforcement. This equation solves the calculation of the ETC in a homogeneous medium with spherical particles dispersed, ignoring thermal interactions between particles. Many researchers have modified Maxwell's model to include various effects. Eucken expanded the reinforcement material from one to many. Burger and Hamilton and Crosser[140] extended spherical reinforcements to different particle shapes.

C_f is a long axis reinforcing material. Rayleigh[141] assumes that C_f is uniformly distributed in a continuous matrix and that all C_f axes are parallel to each other (Figure 1-7). TC is closely related to the measurement direction. Assuming that the C_f axis is parallel to the z axis, the Rayleigh formula is:

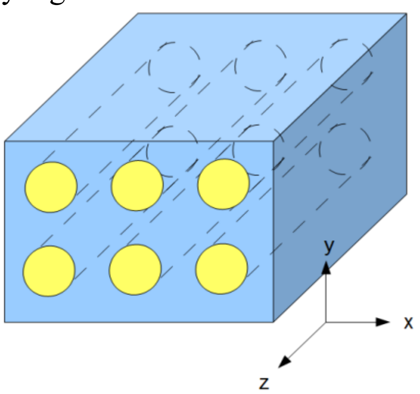

Figure 1-7 The schematic of the composite medium considered by Rayleigh[141].

$$\frac{K_{eff,ZZ}}{K_m} = 1 + \left(\frac{K_1 - K_m}{K_m}\right)\varphi$$

…… (1-2)

$$\frac{K_{eff,XX}}{K_m} = \frac{K_{eff,YY}}{K_m} = 1 + \frac{2\varphi}{C_1 - \varphi + C_2(0.30584\varphi^4 + 0.1013363\varphi^8) + \cdots}$$

$$C_1 = \frac{K_1 + K_m}{K_1 - K_m} \quad C_2 = \frac{K_1 - K_m}{K_1 + K_m}$$

…… (1-3)

The Rayleigh model ignores the shape parameter of C_f when calculating the composite ETC. However, we all know that the shape parameter of C_f affects the size of the thermal conduction channel, which in turn directly affects the TC of the composite. Hasselman and Johnson[142] considered the shape parameters of the filler and the non-zero ITR at the interface when they studied the effect of the interfacial gap between the filler and the matrix on the thermal diffusivity and TC of Ni-glass composites. Their simple modification of the Maxwell and Rayleigh model to derive a new Hasselman-Johnson formulation for calculate ETC of cylindrical filler (C_f) reinforced homogeneous media with non-zero ITR.

$$K_{eff} = K_m \frac{\left[2\left(\frac{K_1}{K_m} - \frac{K_1}{ah_c} - 1\right)\varphi + \frac{K_1}{K_m} + \frac{2K_1}{ah_c} + 2\right]}{\left[\left(1 - \frac{K_1}{K_m} + \frac{K_1}{ah_c}\right)\varphi + \frac{K_1}{K_m} + \frac{2K_1}{ah_c} + 2\right]}$$

…… (1-4)

Where, a is the radius of C_f, hc is the interfacial TC, which is the reciprocal of the ITR(R). With the advancement of basic mathematics to advanced mathematics, especially the introduction of differential equations, the calculation accuracy of composite TC has been greatly improved. Scholars divide the material to be tested into infinitely small units, and gradually calculate the ETC of the overall composite through the study of the ETC of the unit. This method of finding global approximate solutions using differential equations is called the effective medium approximation (EMA) method or the differential effective medium (DEM) Method. The most typical model established by EMA is the Bruggeman model, which provides a new method for the TC calculation of composite materials with a large φ value[143].

$$(1-\varphi)^3=\frac{K_m}{K_{eff}}\left(\frac{K_c-K_1}{K_m-K_1}\right)$$

…… (1-5)

Every and Tzou[144] obtained an expression for the ETC of granular composites by modifying Bruggeman's results[145].

$$(1-\varphi)^3=\left(\frac{K_m}{K_{eff}}\right)^{(1+2\alpha)/(1-\alpha)}\left[\left(\frac{K_{eff}-K_1(1-\alpha)}{K_m-K_1(1-\alpha)}\right)\right]^{3/(1-\alpha)}$$

…… (1-6)

Where, α is depending on ITR between filler and matrix. It is defined as $\alpha = a_k/a$, where a is the particle radius, and a_k is the Kapitza radius ($a_k = R\cdot k_m$). The value of a_k will be listed in the next section. Only when the TC of the reinforcing filler is much larger than that of the matrix, the reinforcing filler can greatly improve the TC of the composite material. Equation (1-6) can be simplified as:

$$\frac{K_1}{K_m}=\frac{1}{(1-\varphi)^{3(1-\alpha)/(1+2\alpha)}}$$

…… (1-7)

Through long-term experimental exploration, scholars have not only developed a series of computational models for ETC of composite, but also summarized and established some empirical models for the convenience of calculation. Even without considering ITR, the Lewis-Nielsen model is the most commonly used in the literature due to its convenience and inclusion of most particle shapes and patterns and gives better results. It is suitable for medium filling volume fractions (a can be as high as 40%). When the value of φ is larger, the Lewis-Nielsen model becomes inaccurate[146].

$$K_{eff}=\frac{1+AB\varphi}{1-B\delta\varphi},\quad B=\left(\frac{K_1/K_m-1}{K_1/K_m+A}\right),\quad \delta=1+\left(\frac{1-\varphi_m}{{\varphi_m}^2}\right)\varphi$$

…… (1-8)

Where, A is the shape factor of the filler particles (refer to Table 1-2)[147] and φ_m is the maximum filler volume fraction (refer to Table 1-3)[148].

Table 1-2 Values of A for several dispersed types.

Shape of particles	Aspect ratio of particles(P=L/D)	A
Spheres	1	1.5
Randomly	2	1.58
Oriented rods	4	2.08
	6	2.8
	10	4.93
	15	8.38

Where, the aspect ratio(P) of the particle is a shape parameter of the columnar filler, and its value is the ratio of the length (L) and the diameter (D) of the particle.

Table 1-3 Maximum packing fractions for different arrangements

Shape of particles	Type of packing	φ_m
Spheres	Face-centered cubic	0.7405
	Hexagonal close	0.7405
	Body-centered cubic	0.6
	Simple cubic	0.524
	Random close	0.637
	Random loose	0.601
Rods or fibers	Uniaxial hexagonal close	0.907
	Uniaxial simple cubic	0.785
	Uniaxial random	0.82
	Three-dimensional Random	0.52

The above models are all used when the value of φ is small. As the value of φ increases, the density of fillers in the composite increases, and the probability of the fillers in contact with each other increases. When φ will eventually reach a certain value, φ_m, the particles of the filler come into contact. For C_f-reinforced composites, C_f has a high TC, and the heat transfer between two C_fs is easier than that between C_f and the matrix. The connection of C_f each other forms a new thermal conduction channel, which helps to improve the TC of the composite, which also brings difficulties to the establishment of a model to calculate the ETC of the composite. As shown in Figure 1-8, The curve of ETC with φ has changed from a gentle growth to a sharp growth, which is the intuitive manifestation of this effect[146]. The corresponding φ value when the gentle change curve begins to change sharply is called the percolation threshold, φ_m.

The EMA model has been unable to accurately predict the ETC of multiphase media close to the seepage threshold (volume fraction of filler not less than 40%). Numerical simulation to simulate seepage has become one of the most effective methods to solve this problem. As shown in Figure 1-8, the Nielsen model becomes inaccurate above 40vol.%, while the ETC of the composite by EMA (EMT)model[149] is lower than that of the experimental value. By modeling percolation and ITR, Devpura et al.[146] used matrix algebra calculations to predict the TC of composites, which fit the trend of the experimental curves well and allowed one to predict the upper limit of the ETC of composite with higher filler volume fractions. The numerically simulated seepage model is more accurate in predicting the ETC of high-filler composites, and the numerical simulation is simple and low-cost, making it the most attractive tool for predicting composite TC in the composite design process.

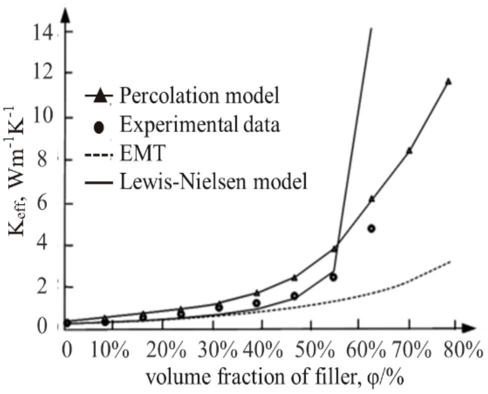

Figure 1-8 ETC of Al_2O_3 reinforced polyethylene matrix predicted by different models, compared with experimental results.

The calculation model used in the seepage model is far from the actual situation of the filler and matrix inside the material, which is the main reason for the difference between the two. The finite element method (FEM) can reflect the actual situation inside the material. The computation of ETC is then extended mathematically from a two-dimensional plane to a three-dimensional space.

FEM is frequently used to the Simulation of heat transfer and the calculation of ETC in composite[150-153]. It is often used as an additional method to verify results obtained by other methods. The complex geometric structure and long-term meshing inside the composite, as well as the extremely severe computing power, limit the large-scale application of the FEM. However, with the development of computer science, these shortcomings can be compensated by the development of computing software. By using MATLAB 7.0® and COMSOL Multiphysics™ to automatically generate 3D finite element model of rod or cube-shaped filler reinforced continuous matrix composite, Floury et al.[154] investigated the effects of shape, orientation, TC, and volume fraction of filler on the composites ETC. The cubic and rod fillers with different TC were compared under the conditions of heat flow direction orientation and random distribution, the ETC calculated by various calculation models and EMT, and the change of ETC with the volume fraction of the continuous matrix was explored.

In this paper, the calculation software developed in our experiment is used to carry out the simulation ETC of composites by FEM. This method has the advantages of a seepage model and can reflect the real condition of the composite. Characteristic of simplicity, save money and ease of operation, which makes FEM a useful and attractive tool for estimating ETC of composite in the composite design process.

1.4.2 Theoretical calculation models for ITR of composites

Typically, heat conduction in composite materials is achieved by vibrating atoms and phonons. The traditional heat conduction mechanism believes that when heat enters a substance, the heat causes the atoms in the substance to vibrate and collide with the atoms in the substance, and in this way, the heat is transferred to the entire substance and the surrounding space. The heat dissipation of this vibration heat transfer method is closely related to the atomic spacing and atomic species, and the macroscopic performance is that both the material composition and the unit cell structure affect the heat transfer. The macroscopic manifestation of thermal energy dissipation is that when heat is conducted in the composite material, the temperature will be transferred at the interface between the components to decrease. ITR can be applied to describe this heat conduction hindering effect. We define ITR as the heat flow efficiency per unit area per 1 K decrease in the temperature of the material. ITR is the combined effect of the two thermal resistances. The first is heat loss due to weak physical and chemical bonding between the continuous phases during heat transfer, which is called thermal contact resistance (TCR). The second is the heat loss due to the difference in the physical properties of the two different phases during the heat generation process, which is called thermal boundary resistance (TBR), also known as Kapitza thermal resistance. Kapitza was the first to observe the drop in temperature in the boundary of liquid helium and metal[155]. The ITR is defined as the ratio of the temperature change (△T) that occurs at the interface to the heat rate ($Q=I^2R$) passing per unit area (A), according to equation (1.4.2-1):

$$R_{int} = \frac{\triangle T}{Q/A}$$

…… (1-9)

where R_{int} is the ITR. Even if the atoms near the interface are perfectly aligned, the interface will still generate thermal resistance. Differences in vibrational and electronic properties of different materials lead to the scattering of heat carriers (phonons or electrons) near the two-phase interface, and the probability of heat carrier transport after scattering will depend on the available energy states on both sides of the interface. At temperatures below 40K, interfacial heat transfer at solid-solid boundaries can be achieved by acoustic and diffusion mismatch models (AMM and DMM)[156]. ITR is inversely proportional to the cube of temperature.

$$R_{bd} = BT^{-3}$$

…… (1-10)

The value of B is related to the density of the heat carrier on both sides of the interface and the scattering when passing through the interface. Parameter B was collected by Swartz et al.[157] for some solid-solid interfaces is listed in Tables 1-4. The scattering-mediated acoustic mismatch model (SMAMM) developed by Prasher and Phelan can calculate the ITR at higher temperatures[158]. However, this model introduces additional parameters of material properties, which bring uncertainty to the calculation of ITR[159].

Table 1-4 The parameter B in the low-temperature thermal boundary resistances by AMM and DMM.

	Sapphire		Quartz		Silicon	
	AMM	DMM	AMM	DMM	AMM	DMM
	(K^4cm^2 / W)		(K^4cm^2 / W)		(K^4cm^2 / W)	
Aluminum	21.0	21.4	6.50	10.8	11.8	15.9
Copper	18.5	20.1	8.66	9.43	14.3	14.6
Nickel	19.7	21.1	9.32	10.5	15.5	15.6
Platinum	20.8	18.7	13.0	8.10	21.3	13.2
Rhodium	20.8	23.6	13.0	13.0	19.2	18.1
Silver	18.2	18.7	8.66	8.06	13.8	13.2

Any factor that can affect the density and scattering of heat carriers on both sides of the contact surface may affect the ITR[138]. These factors include lattice distortion caused by thermal stress, voids caused by weak bonding or inconsistent thermal expansion of the two phases[160], thin layers caused by interdiffusion of the two phases or surface plating, etc. Zhao et al.[161] looked for ways to reduce ITR by studying thermal interface materials (TIMs). The ITR decreases with increasing pressure, the ITR of carbon-based materials decreases with increasing temperature, and the ITR of thermal pads is not affected by temperature. The increase in surface roughness leads to an increase in the ITR of the thermal pad and carbon-based materials. Shaikh et al.[162] also found that TIMs with CNTs can promote thermal conduction between aluminum and graphite more than direct contact of aluminum and graphite or graphite coatings.

With further research on composites, scholars have found that ETC decreases with the decreases of reinforcement average particle radius, the contact area on the surface per unit volume increases, and ITR cannot be ignored. Therefore, in the process of model building to predict the ETC of composites, ignoring the ITR will have a very important impact on the evaluation results. The numerical models proposed by Devpura et al.[146] to predict the ETC of composite materials include the seepage model and the ITR model. They investigated the effect of ITR and particle size on ETC. To characterize the value of ITR, the Biot number is introduced, and the Biot number of spherical particles is expressed as:

$$B_i = \frac{R_{int}K_m}{2a}$$

…… (1-11)

where a is the particle radius. Larger Biot numbers and particle radii result in higher ITR, which increases the percentage of enhancement required to reach the permeation threshold. When Biot > 1, the reinforcement will cause the ETC of the composite to drop below that of the pure matrix. Knowing the value of ITR, we can calculate the particle radius (critical radius) for Bi = 1. The addition of smaller radius reinforcements to the matrix results in a decrease in ETC rather than increase. These theories are of great significance to the design of composite materials.

1.4.3 Theoretical calculation for ETC and ITR of C_f-Cu/Fe composites

In order to evaluate the ETC and ITR of C_f-Cu/Fe composites, the historical process of ETC and ITR research of composites was explored, and various models were established, ranging from spherical particles to fiber reinforcement, considering the percolation threshold, the internal thermal resistance, orientation of reinforcement, and the actual situation inside the composite.

In this paper, considering the structure of C_f-Cu/Fe composites, in order to study the influence of various hindering heat conduction factors on ETC, the mixing rule, Nan model and FEM in the EMT method are most suitable.

The mixing rule can be expressed:

$$K_{ROM} = K_C^X = K_{Cf-Cu}^X \times V_{Cf-Cu} + K_m \times (1 - V_{Cf-Cu})$$

…… (1-12)

$$\frac{1}{K_C^{Y/Z}} = \frac{V_{Cf-Cu}}{K_{Cf-Cu}^{Y/Z}} + \frac{1 - V_{Cf-Cu}}{K_m}$$

…… (1-13)

Where, K_C^X , $K_C^{Y/Z}$ and K_{ROM} is the TC of composite, K_{Cf-Cu}^X and $K_{Cf-Cu}^{Y/Z}$ are the axial and radial TC of C_f-Cu, respectively, and K_m is the TC of matrix. $V_{Cf\text{-}Cu}$ is the volume fraction of C_f-Cu in the composite. When the axial direction of C_f-Cu is parallel and perpendicular to the heat flow direction, the ETC of the composite can be evaluated by equations (1-12) and (1-13), respectively. However, the rule of mixture only considers the volume fraction of C_f-Cu, assuming that all C_f-Cu is uniformly distributed in the composite and oriented parallel to the direction of heat flow, regardless of ITR, the calculated TC of the composite is much larger than the measured TC. Considering the effect of the internal thermal resistance and on the TC of the composite, the effective TC of C_f-Cu (K_{Cf-Cu}^{eff}) can be modified by the equation:

$$K_{Cf-Cu}^{eff} = \frac{K_{Cf-Cu}}{1 + \frac{2K_{Cf-Cu}}{hd}}$$

…… (1-14)

Where, K_{Cf-Cu}^{eff} is the corrected ETC of the axial and radial TC of C_f-Cu considering ITR. D is the diameter of C_f-Cu. h is the interfacial thermal conductivity, which is the reciprocal of ITR (abbreviated R), h=1/ R. When the value of h is known, $K_{Cf-Cu}^{Y/Z}$ and K_{Cf-Cu}^X in equation 1.4.3-1 and 1.4.3-2 can be replaced by K_{Cf-Cu}^{eff}, respectively. It is also possible to reversely derive h under the condition of known measured TC, and then obtain the ITR (equation 1.4.3-4) under the condition of the rule of mixture.

$$\mathrm{h} = \frac{2}{d\left[\frac{V_{Cf-Cu}}{K_C - K_m(1 - V_{Cf-Cu})} - \frac{1}{K_{Cf-Cu}}\right]}$$

…… (1-15)

Nan's model is based on the effective medium approximation (EMA) theory to predict the ETC of C_f-Cu. The model assumes that all C_f-Cu is uniformly distributed along the heat flow direction, taking into account the volume fraction and aspect ratio of C_f-Cu, orientation and ITR. Figure 1-9 shows that the X axis is parallel to the axis of C_f-Cu.

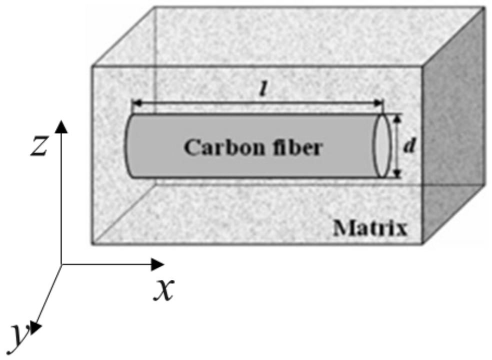

Figure 1-9 The schematic of the C_f-Cu in composite in the EMA model.

In Nan's theory, the ellipsoid is taken as an example and the calculation equation of TC is given as follows:

$$K_{EMA} = K_C^{Y/Z} = K_m\left(\frac{2 + V_{Cf-Cu}[\beta_{11}(1-L_{11})(1+\langle\cos^2\theta\rangle) + \beta_{33}(1-L_{33})(1-\langle\cos^2\theta\rangle)]}{2 - V_{Cf-Cu}[\beta_{11}L_{11}(1+\langle\cos^2\theta\rangle) + \beta_{33}L_{33}(1-\langle\cos^2\theta\rangle)]}\right)$$

…… (1-16)

$$K_C^X = K_m\left(\frac{1 + V_{Cf-Cu}[\beta_{11}(1-L_{11})(1-\langle\cos^2\theta\rangle) + \beta_{33}(1-L_{33})\langle\cos^2\theta\rangle]}{1 - V_{Cf-Cu}[\beta_{11}L_{11}(1-\langle\cos^2\theta\rangle) + \beta_{33}L_{33}\langle\cos^2\theta\rangle]}\right)$$

…… (1-17)

$$\langle\cos^2\theta\rangle = \frac{\int \rho(\theta)\cos^2\theta\sin\theta\, d\theta}{\int \rho(\theta)\sin\theta\, d\theta}$$

…… (1-18)

where, θ is the angle between the axial direction of C_f-Cu and the direction of heat flow. $K_C^{Y/Z}$, K_C^X, are the TC of the composite material in the direction of heat flow and perpendicular to the direction of heat flow, respectively. L_{ii} is the geometric factor of C_f-Cu, determined by its aspect ratio(P=L/d). L and d are the length and radius of the cross section of C_f-Cu, respectively. The geometric factor can be obtained by equation.

$$L_{11} = L_{22} = \begin{cases} \frac{P^2}{P^2 - 1} - \frac{P}{(1 - P^2)^{3/2}} \cosh^{-1} P, & P > 1 \\ \frac{P^2}{P^2 - 1} - \frac{P}{(1 - P^2)^{3/2}} \cosh^{-1} P, & P < 1 \end{cases}$$

$$L_{33} = 1 - 2L_{11}$$

$$\cdots\cdots \text{(1-19)}$$

Considering the impact of ITR on TC, β_{ii} (i =1,2,3) can be expressed as:

$$\beta_{22} = \beta_{11} = \frac{K^C_{Y/Z} - K_m}{K_m + L_{11}\left(K^C_{Y/Z} - K_m\right)} \qquad \beta_{33} = \frac{K^C_X - K_m}{K_m + L_{33}\left(K^C_X - K_m\right)}$$

$$K^C_{Y/Z} = \frac{d \cdot K^{Y/Z}_{Cf-Cu} \cdot K_m}{dK_m + 2R_{EMA}K^{Y/Z}_{Cf-Cu}} \qquad K^C_X = \frac{L \cdot K^X_{Cf-Cu} \cdot K_m}{LK_m + 2R_{EMA}K^X_{Cf-Cu}}$$

$$\cdots\cdots \text{(1-20)}$$

where, R_{EMA} is the ITR in the EMA model. It is also possible to reversely derive R_{EMA} under the condition of known measured TC.

1.5 Objective of this thesis

C_f has the characteristics of high TC in direction of axial, which can improve the TC of composites by establishing thermal conduction channels in the composites. The C_f surface can be prevented from directly contacting and reacting with iron by electroless copper plating. C_f has high anisotropy, the axial TC is larger than the matrix TC, which can improve the TC of the composite, and the radial TC is much smaller than the matrix TC, which will reduce the TC of the composite. Therefore, it is crucial to control the orientation of C_f-Cu in the composites. In this thesis, the method of hot rolling was used to align the axial direction of C_f-Cu in the measurement direction of TC. Although most of the C_f-Cu can be aligned by hot rolling, a small amount of C_f-Cu not parallel to the heat flow direction has a great influence on the TC of the composite, which brings difficulties to the prediction of TC of C_f-Cu/Fe composites. Many theoretical models and simulation calculations have been explored to predict C_f-reinforced metal matrix composites. However, the complex structure and composition of the composite are far from theoretical models. Previous studies have shown that voids in composites, orientation and aspect ratio of C_f, ITR affect heat transfer in composites.

Due to the irregular distribution of C_f in 3D composites, various theoretical models of C_f distribution assumptions in composites are proposed to evaluate the ETC of C_f-reinforced composites. Some theoretical models only consider the calculation of TC perpendicular and parallel to the heat flow direction, but the orientation of C_f has a great influence on TC, and the influence of C_f in other directions on TC cannot be ignored. Some theoretical models assume that C_f is distributed according to a certain rule or depends on a certain existing component distribution, which is not consistent with the actual distribution of C_f in the composite. However, the influencing degree of influencing factors on TC has not been investigated.

C_f is randomly oriented in the 3D space of the composite, which brings difficulties to predict the composite TC through model-building calculations. Some scholars hope to obtain the ETC of C_f reinforced composites through the simulation of 3D models. This simulation method is achieved by obtaining a series of images from ultra-high-resolution X-ray computed tomography, which results in the simulation of 3D models costing a lot of time and money. Since the C_f orientations in 2D images are quite different from those in their corresponding composites, few studies have used 2D image simulations to evaluate the ETC of C_f-reinforced composites. Most scholars have only qualitatively analyzed the voids, C_f content, orientation and aspect ratio, ITR will affect the heat transfer ability of the composites. With the increase of C_f content, the contact area between C_f and the substrate increases, and the voids and contact thermal resistance both increases. We all know that TC increases with the increase of C_f content, and with the increase of void and contact thermal resistance. However, in real-world situations, the TC of the composites changes in various ways with increasing C_f. When the increasing effect of orientation of C_f on TC is greater than the weakening effect of voids, orientation of C_f and ITR on TC, the TC of the composite increases with the increase of C_f, and the growth rate gradually decreases. The increased effect and decreased effect of C_f content on TC of composite will be equal at a certain content of C_f, which is closely related to the complex actual situation of composite.

The purpose of this study includes three aspects. One is to determine the relationship between the orientation of C_f in 2D cross-section and 3D space and calculate the TC of composite by 2D image simulation. The second is to explore the influencing factors and degree of influence of TC in C_f-Cu/Fe composites, according to the comparison of the TC, which was obtained by the simulation method, calculation model and measurement. The third is to improve the TC of SKD61(40CrMoV5) alloy by adding C_f-Cu and evaluate the thermal conductivity of the composite based on 2D image analysis.

1.6 Outline of this thesis

Chapter 1 Background and objective

In this Chapter, discusses the development of dies with high TC and investigates methods to improve TC of hot stamping dies, the necessity of dies with high TC to produce steel parts with high strength, the choice of matrix and reinforcement for composites, the preparation method of C_f-Cu/Fe composites, Some influencing factors on TC of C_f-reinforced composites, some research procedure of calculation models of theoretical TC and simulation methods to calculate the TC of C_f-reinforced composites, and the purpose of this thesis.

Chapter 2 Fabrication, mechanical properties, and thermal conductivity of C_f - Cu/Fe composite

In this Chapter, C_f obtains discontinuous C_f-Cu by electroless copper plating. 10~40vol.% C_f-Cu/Fe composites were fabricated by SPS. The relative density of the C_f-Cu/Fe composites was measured by the Archimedes method, and the TC of the void-containing matrix was corrected. The C_f-Cu, elemental distribution of C_f and Cu, and C_f-Cu/Fe composites were investigated by optical microscopy (OM) and electron probe microanalysis (EPMA). The most suitable sintering temperature for C_f-Cu/Fe was determined and ensured that C_f-Cu in C_f-Cu/Fe would not be destroyed by XRD The measured TC was obtained by the steady-state measurement.

Chapter 3 Effective thermal conductivity of C_f-Cu/Fe composites by 2D Image Analysis

In this Chapter, 5~25vol.% C_f-Cu/Fe composites were fabricated by SPS. The composites were hot rolled to control the orientation of C_f-Cu in the composite. The relative density of the C_f-Cu/Fe composites was measured Archimedes method, and the TC of the void-containing matrix was corrected. The measured TC is obtained by the steady state measurement method. The mathematical equation between the orientation of C_f-Cu in the 3D model, the orientation of C_f-Cu on the 2D cross-section, and the aspect ratio an ellipse was obtained by C_f-Cu intersects with cross-section was determined by establishing a model of the orientation of C_f-Cu in 3D space. The simulated TC of the composite was calculated by 2D image simulation. The effect of the orientation of C_f-Cu on the TC of composites with different C_f-Cu contents was investigated.

Chapter 4 Influencing factors and degrees of thermal conductivity of C_f-Cu/Fe composites

In this Chapter, the ETC of the C_f-Cu/Fe composites was calculated by the ROM model and the EMA model, respectively. Based on the second step, the TC calculated by the ROM model (K_{ROM}), TC calculated by EMA model (K_{EMA}), TC calculated by 2D image simulation ($K_{simulated}$) and TC measured by steady state method ($K_{measured}$) were compared to investigate the degree of influence of Voids, orientation and aspect ratio of C_f-Cu, ITR, and experimental error on the TC of C_f-Cu/Fe composites with different C_f-Cu contents.

Chapter 5 Thermal conductivity of C_f-Cu dispersed SKD61(40CrMoV5) composite

In this Chapter, 0/3/5vol.% C_f-Cu/Fe composites were fabricated by SPS. The relative density of the C_f-Cu/Fe composites was measured by the Archimedes method. The microstructure was investigated by optical microscopy (OM) and electron probe microanalysis (EPMA). The measured TC is obtained by the steady-state measurement method. According to the investigation of the calculation of TC of Cf-Cu/Fe composite by 2D cross-sectional simulation and the influencing factors and degree on TC, 3/5vol.%Cf-Cu was added to SKD61 (40CrMoV5) alloy to improve the TC of the die and improving the production efficiency.

Chapter 6 Conclusions, discussion and future work

The background and purpose of this research, the selection of experimental materials will be discussed, and the conclusions were summarized in this chapter. Also, the details of this study and the future work will be discussed in this chapter.

1.7 References

[1]Mori K, Bariani P F, Behrens B A, Brosius A, Bruschi S, Maeno T, Merklein M,Yanagimoto J. Hot stamping of ultra-high strength steel parts.CIRP Annals. 2017;66(2):755-777.

[2]Merklein M,Lechler J. Investigation of the thermo-mechanical properties of hot stamping steels.Journal of Materials Processing Technology. 2006;177(1-3):452-455.

[3]Mori K, Maki S,Tanaka Y. Warm and Hot Stamping of Ultra High Tensile Strength Steel Sheets Using Resistance Heating.CIRP Annals. 2005;54(1):209-212.

[4]Kiani M, Gandikota I, Rais-Rohani M,Motoyama K. Design of lightweight magnesium car body structure under crash and vibration constraints.Journal of Magnesium and Alloys. 2014;2(2):99-108.

[5]Tong C, Rong Q, Yardley V A, Li X, Luo J, Zhu G,Shi Z. New Developments and Future Trends in Low-Temperature Hot Stamping Technologies: A Review.Metals. 2020;10(12):1652.

[6]Doege E, Kurz G,Doege E. Development of a formulation to describe the work softening behaviour of magnesium sheets for heated deep drawing processes.CIRP Annals. 2001;50(1):177-180.

[7]Groche P, Huber R, Dörr J,Schmoeckel D. Hydromechanical Deep-Drawing of Aluminium-Alloys at Elevated Temperatures.CIRP Annals. 2002;51(1):215-218.

[8]Siegert K, Jäger S,Vulcan M. Pneumatic Bulging of Magnesium AZ 31 Sheet Metals at Elevated Temperatures.CIRP Annals. 2003;52(1):241-244.

[9]Kleiner M, Geiger M,Klaus A. Manufacturing of Lightweight Components by Metal Forming.CIRP Annals. 2003;52(2):521-542.

[10]Abe Y, Ohmi T, Mori K,Masuda T. Improvement of formability in deep drawing of ultra-high strength steel sheets by coating of die.Journal of Materials Processing Technology. 2014;214(9):1838-1843.

[11]Mori K-i, Abe Y,Suzui Y. Improvement of stretch flangeability of ultra high strength steel sheet by smoothing of sheared edge.Journal of Materials Processing Technology.

2010;210(4):653-659.

[12]Mori K, Akita K,Abe Y. Springback behaviour in bending of ultra-high-strength steel sheets using CNC servo press.International Journal of Machine Tools and Manufacture. 2007;47(2):321-325.

[13]Lim W-S, Choi H-S, Ahn S-y,Kim B-M. Cooling channel design of hot stamping tools for uniform high-strength components in hot stamping process.The International Journal of Advanced Manufacturing Technology. 2013;70(5-8):1189-1203.

[14]Bok H-H, Lee M-G, Kim H-D,Moon M-B. Thermo-mechanical finite element analysis incorporating the temperature dependent stress-strain response of low alloy steel for practical application to the hot stamped part.Metals and Materials International. 2010;16(2):185-195.

[15]Choi H-s, Nam K-j, Lim W-s, Ko D-C,Kim B-M. The optimization of hot press bending for improving dimensional accuracy and mechanical strength of bent product.Metals and Materials International. 2010;16(6):1001-1007.

[16]Chantzis D, Liu X, Politis D J, El Fakir O, Chua T Y, Shi Z,Wang L. Review on additive manufacturing of tooling for hot stamping.The International Journal of Advanced Manufacturing Technology. 2020;109(1-2):87-107.

[17]Burger N, Laachachi A, Ferriol M, Lutz M, Toniazzo V,Ruch D. Review of thermal conductivity in composites: Mechanisms, parameters and theory.Progress in Polymer Science. 2016;61(1-28.

[18]Ramesh C S, Adarsha H, Pramod S,Khan Z. Tribological characteristics of innovative Al6061–carbon fiber rod metal matrix composites.Materials & Design. 2013;50(597-605.

[19]Kelly A. Composite materials after seventy years.Journal of Materials Science. 2006;41(3):905-912.

[20]Qu X-h, Zhang L, Wu M,Ren S-b. Review of metal matrix composites with high thermal conductivity for thermal management applications.Progress in Natural Science: Materials International. 2011;21(3):189-197.

[21]Srinivasan M, Maettig P, Glitza K W, Sanny B, Schumacher A, Duhovic

M,Schuster J. Out of Plane Thermal Conductivity of Carbon Fiber Reinforced Composite Filled with Diamond Powder.Open Journal of Composite Materials. 2016;06(02):41-57.

[22]Abyzov A M, Kidalov S V,Shakhov F M. Filler-matrix thermal boundary resistance of diamond-copper composite with high thermal conductivity.Physics of the Solid State. 2012;54(1):210-215.

[23]Yoshida K,Morigami H. Thermal properties of diamond/copper composite material.Microelectronics Reliability. 2004;44(2):303-308.

[24]Song J,Zhang Y. Vertically aligned silicon carbide nanowires/reduced graphene oxide networks for enhancing the thermal conductivity of silicone rubber composites.Composites Part A: Applied Science and Manufacturing. 2020;133(105873.

[25]Shen D, Zhan Z, Liu Z, Cao Y, Zhou L, Liu Y, Dai W, Nishimura K, Li C, Lin C T, Jiang N,Yu J. Enhanced thermal conductivity of epoxy composites filled with silicon carbide nanowires.Sci Rep. 2017;7(1):2606.

[26]Trinh P V, Luan N V, Phuong D D, Minh P N, Weibel A, Mesguich D,Laurent C. Microstructure, microhardness and thermal expansion of CNT/Al composites prepared by flake powder metallurgy.Composites Part A: Applied Science and Manufacturing. 2018;105(126-137.

[27]Miranda A, Barekar N,Mckay B J. MWCNTs and their use in Al-MMCs for ultra-high thermal conductivity applications: A review.Journal of Alloys and Compounds. 2019;774(820-840.

[28]Park J-M, Kwon D-J, Wang Z-J, Roh J-U, Lee W-I, Park J-K,Lawrence Devries K. Effects of carbon nanotubes and carbon fiber reinforcements on thermal conductivity and ablation properties of carbon/phenolic composites.Composites Part B: Engineering. 2014;67(22-29.

[29]Huang Y, Ouyang Q, Guo Q, Guo X, Zhang G,Zhang D. Graphite film/aluminum laminate composites with ultrahigh thermal conductivity for thermal management applications.Materials & Design. 2016;90(508-515.

[30]Wang X, Su Y, Wang X, Liu K, Zhang L, Ouyang Q,Zhang D. Fabrication,

mechanical and thermal properties of tungsten-copper coated graphite flakes reinforced copper matrix composites.Materials & Design. 2022;216(110526.

[31]Prieto R, Molina J M, Narciso J,Louis E. Fabrication and properties of graphite flakes/metal composites for thermal management applications.Scripta Materialia. 2008;59(1):11-14.

[32]Tian T,Cole K D. Anisotropic thermal conductivity measurement of carbon-fiber/epoxy composite materials.International Journal of Heat and Mass Transfer. 2012;55(23-24):6530-6537.

[33]Lee S B, Matsunaga K, Ikuhara Y,Lee S-K. Effect of alloying elements on the interfacial bonding strength and electric conductivity of carbon nano-fiber reinforced Cu matrix composites.Materials Science and Engineering: A. 2007;449-451(778-781.

[34]Wei J, Liao M, Ma A, Chen Y, Duan Z, Hou X, Li M, Jiang N,Yu J. Enhanced thermal conductivity of polydimethylsiloxane composites with carbon fiber.Composites Communications. 2020;17(141-146.

[35]Tokunaga T, Takahashi K, Ohno M, Sasaki K, Imanishi T,Matsuura K. Fabrication of Carbon Fiber Oriented Al-Based Composites by Hot Extrusion and Evaluation of Their Thermal Conductivity.Journal of the Japan Institute of Metals. 2016;80(10):640-645.

[36]Hou X, Chen Y, Dai W, Wang Z, Li H, Lin C-T, Nishimura K, Jiang N,Yu J. Highly thermal conductive polymer composites via constructing micro-phragmites communis structured carbon fibers.Chemical Engineering Journal. 2019;375(121921.

[37]Lee E, Cho C H, Hwang S H, Kim M G, Han J W, Lee H,Lee J H. Improving the Vertical Thermal Conductivity of Carbon Fiber-Reinforced Epoxy Composites by Forming Layer-by-Layer Contact of Inorganic Crystals.Materials (Basel). 2019;12(19):

[38]Qu X H, Zhang L, Wu M,Ren S B. Review of metal matrix composites with high thermal conductivity for thermal management applications.Progress in Natural Science-Materials International. 2011;21(3):189-197.

[39]Schubert T, Ciupiński Ł, Zieliński W, Michalski A, Weißgärber T,Kieback B. Interfacial characterization of Cu/diamond composites prepared by powder metallurgy

for heat sink applications.Scripta Materialia. 2008;58(4):263-266.

[40]Weber L,Tavangar R. On the influence of active element content on the thermal conductivity and thermal expansion of Cu–X (X=Cr, B) diamond composites.Scripta Materialia. 2007;57(11):988-991.

[41]Chu K, Liu Z, Jia C, Chen H, Liang X, Gao W, Tian W,Guo H. Thermal conductivity of SPS consolidated Cu/diamond composites with Cr-coated diamond particles.Journal of Alloys and Compounds. 2010;490(1-2):453-458.

[42]Wang H, Li L, Chen Y, Li M, Fu H, Hou X, Wu X, Lin C-T, Jiang N,Yu J. Efficient Thermal Transport Highway Construction Within Epoxy Matrix via Hybrid Carbon Fibers and Alumina Particles.ACS Omega. 2020;5(2):1170-1177.

[43]Zheng X, Kim S,Park C W. Enhancement of thermal conductivity of carbon fiber-reinforced polymer composite with copper and boron nitride particles.Composites Part A: Applied Science and Manufacturing. 2019;121(449-456.

[44]Han S,Chung D D L. Increasing the through-thickness thermal conductivity of carbon fiber polymer–matrix composite by curing pressure increase and filler incorporation.Composites Science and Technology. 2011;71(16):1944-1952.

[45] Rolfes R, Hammerschmidt U. Transverse thermal conductivity of CFRP laminates: A numerical and experimental validation of approximation formulae[J]. Composites Science and Technology, 1995, 54(1): 45-54.

[46]Lee M, Choi Y, Sugio K, Matsugi K,Sasaki G. Effect of aluminum carbide on thermal conductivity of the unidirectional CF/Al composites fabricated by low pressure infiltration process.Composites Science and Technology. 2014;97(1-5.

[47]Miranda A T, Bolzoni L, Barekar N, Huang Y, Shin J, Ko S-H,Mckay B J. Processing, structure and thermal conductivity correlation in carbon fibre reinforced aluminium metal matrix composites.Materials & Design. 2018;156(329-339.

[48]Khayyam H, Naebe M, Bab-Hadiashar A, Jamshidi F, Li Q, Atkiss S, Buckmaster D,Fox B. Stochastic optimization models for energy management in carbonization process of carbon fiber production.Applied Energy. 2015;158(643-655.

[49]Xia L, Jia B, Zeng J,Xu J. Wear and mechanical properties of carbon fiber

reinforced copper alloy composites.Materials Characterization. 2009;60(5):363-369.

[50]Li M, Ali Z, Wei X, Li L, Song G, Hou X, Do H, Greer J C, Pan Z, Lin C-T, Jiang N,Yu J. Stress induced carbon fiber orientation for enhanced thermal conductivity of epoxy composites.Composites Part B: Engineering. 2021;208(108599.

[51]Ibrahim Y, Elkholy A, Schofield J S, Melenka G W,Kempers R. Effective thermal conductivity of 3D-printed continuous fiber polymer composites.Advanced Manufacturing: Polymer & Composites Science. 2020;6(1):17-28.

[52] Mutnuri B. Thermal conductivity characterization of composite materials. West Virginia University, 2006.

[53]Cho J, Lee S-K, Eem S-H, Jang J G,Yang B. Enhanced mechanical and thermal properties of carbon fiber-reinforced thermoplastic polyketone composites.Composites Part A: Applied Science and Manufacturing. 2019;126(105599.

[54] Kontani H, Tokunaga T, Ohno M, et al. Fabrication of unidirectionally orientated carbon fiber reinforced cu-based composites by hot extrusion and evaluation of their thermal properties. Journal of the Japan Institute of Metals and Materials, 2018; 82(5): 125-129.

[55]Nan C W, Shi Z,Lin Y. A simple model for thermal conductivity of carbon nanotube-based composites.Chemical Physics Letters. 2003;375(5-6):666-669.

[56] Pilling M W, Yates B, Black M A, et al. The thermal conductivity of carbon fibre-reinforced composites. Journal of materials science, 1979; 14(6): 1326-1338.

[57]Ning Z, Liu R, Elhajjar R F,Wang F. Micro-modeling of thermal properties in carbon fibers reinforced polymer composites with fiber breaks or delamination.Composites Part B: Engineering. 2017;114(247-255.

[58]Wang M, Kang Q,Pan N. Thermal conductivity enhancement of carbon fiber composites.Applied Thermal Engineering. 2009;29(2-3):418-421.

[59]Dasgupta A, Agarwal R K, Bhandarkar S M. Three-dimensional modeling of woven-fabric composites for effective thermo-mechanical and thermal properties[J]. Composites science and technology, 1996, 56(3): 209-223.

[60]Villière M, Lecointe D, Sobotka V, Boyard N,Delaunay D. Experimental

determination and modeling of thermal conductivity tensor of carbon/epoxy composite.Composites Part A: Applied Science and Manufacturing. 2013;46(60-68.

[61] Kuniya K, Arakawa H, Kanai T, et al. Thermal conductivity, electrical conductivity and specific heat of copper-carbon fiber composites.Transactions of the Japan institute of metals, 1987;28(10): 819-826.

[62]Swartz E T,Pohl R O. Thermal boundary resistance.Reviews of Modern Physics. 1989;61(3):605-668.

[63] Little W A. "The transport of heat between dissimilar solids at low temperatures" From High-Temperature Superconductivity to Microminiature Refrigeration. Springer, Boston, MA, 1996;15-30.

[64]Sugio K, Choi Y-B,Sasaki G. Effect of the Interfacial Thermal Resistance on the Effective Thermal Conductivity of Aluminum Matrix Composites.Materials Transactions. 2016;57(5):582-589.

[65]Yang L, Miyoshi Y, Sugio K, Choi Y, Matsugi K,Sasaki G. Effect of graphite orientation distribution on thermal conductivity of Cu matrix composite.Materials Chemistry and Physics. 2021;257(123702.

[66]Zhao Y, Sugio K, Choi Y, Gen S, Xu Z,Yu J. Effect of Anisotropic Thermal Conductivity of Graphite Flakes and Interfacial Thermal Resistance on the Effective Thermal Conductivity of Graphite Flakes/Aluminum Composites.Materials Transactions. 2021;62(1):98-104.

[67] Surappa M K. Aluminium matrix composites: Challenges and opportunities. Sadhana. 2003; 28(1): 319-334.

[68]Prashanth Reddy K,Panitapu B. High thermal conductivity mould insert materials for cooling time reduction in thermoplastic injection moulds.Materials Today: Proceedings. 2017;4(2):519-526.

[69]Ghasali E, Alizadeh M, Ebadzadeh T, Pakseresht A h,Rahbari A. Investigation on microstructural and mechanical properties of B4C–aluminum matrix composites prepared by microwave sintering.Journal of Materials Research and Technology. 2015;4(4):411-415.

[70]Ghasali E, Pakseresht A, Rahbari A, Eslami-Shahed H, Alizadeh M,Ebadzadeh T. Mechanical properties and microstructure characterization of spark plasma and conventional sintering of Al–SiC–TiC composites.Journal of Alloys and Compounds. 2016;666(366-371.

[71]Ghasali E, Pakseresht A, Safari-Kooshali F, Agheli M,Ebadzadeh T. Investigation on microstructure and mechanical behavior of Al–ZrB2 composite prepared by microwave and spark plasma sintering.Materials Science and Engineering: A. 2015;627(27-30.

[72]Ji K, Fakir O E, Gao H,Wang L. Determination of Heat Transfer Coefficient for Hot Stamping Process.Materials Today: Proceedings. 2015;2(S434-S439.

[73]Lei C, Cui J, Xing Z, Fu H,Zhao H. Investigation of Cooling Effect of Hot-stamping Dies by Numerical Simulation.Physics Procedia. 2012;25(118-124.

[74]Hoffmann H, So H,Steinbeiss H. Design of Hot Stamping Tools with Cooling System.CIRP Annals. 2007;56(1):269-272.

[75]Caron E J F R, Daun K J,Wells M A. Experimental heat transfer coefficient measurements during hot forming die quenching of boron steel at high temperatures.International Journal of Heat and Mass Transfer. 2014;71(396-404.

[76]Li S, Zhou L, Wu X, Zhang Y,Li J. The Influence of Thermal Conductivity of Die Material on the Efficiency of Hot-Stamping Process.Journal of Materials Engineering and Performance. 2016;25(11):4848-4867.

[77]Steinbeiss H, So H, Michelitsch T,Hoffmann H. Method for optimizing the cooling design of hot stamping tools.Production Engineering. 2007;1(2):149-155.

[78]Ying X,Zhong-De S. Design parameter investigation of cooling systems for UHSS hot stamping dies.The International Journal of Advanced Manufacturing Technology. 2013;70(1-4):257-262.

[79]Chang Y, Tang X, Zhao K, Hu P,Wu Y. Investigation of the factors influencing the interfacial heat transfer coefficient in hot stamping.Journal of Materials Processing Technology. 2016;228(25-33.

[80]Bianco A, Kostarelos K,Prato M. Applications of carbon nanotubes in drug

delivery.Current Opinion in Chemical Biology. 2005;9(6):674-679.

[81]Shirvanimoghaddam K, Hamim S U, Karbalaei Akbari M, Fakhrhoseini S M, Khayyam H, Pakseresht A H, Ghasali E, Zabet M, Munir K S, Jia S, Davim J P,Naebe M. Carbon fiber reinforced metal matrix composites: Fabrication processes and properties.Composites Part A: Applied Science and Manufacturing. 2017;92(70-96.

[82]Frank E, Steudle L M, Ingildeev D, Sporl J M,Buchmeiser M R. Carbon fibers: precursor systems, processing, structure, and properties.Angew Chem Int Ed Engl. 2014;53(21):5262-5298.

[83]Baumli P, Sychev J, Budai I, Szabo J T,Kaptay G. Fabrication of carbon fiber reinforced aluminum matrix composites via a titanium-ion containing flux.Composites Part A: Applied Science and Manufacturing. 2013;44(47-50.

[84]Alhashmy H A,Nganbe M. Laminate squeeze casting of carbon fiber reinforced aluminum matrix composites.Materials & Design. 2015;67(154-158.

[85]Rajan T P D, Pillai R M, Pai B C. Reinforcement coatings and interfaces in aluminium metal matrix composites.Journal of materials science. 1998;33(14):3491-3503.

[86]Bhav Singh B,Balasubramanian M. Processing and properties of copper-coated carbon fibre reinforced aluminium alloy composites.Journal of Materials Processing Technology. 2009;209(4):2104-2110.

[87]Korb G, Koráb J, Groboth G. Thermal expansion behaviour of unidirectional carbon-fibre-reinforced copper-matrix composites.Composites Part A: Applied Science and Manufacturing. 1998;29(12):1563-1567.

[88]Daoud A. Microstructure and tensile properties of 2014 Al alloy reinforced with continuous carbon fibers manufactured by gas pressure infiltration.Materials Science and Engineering: A. 2005;391(1-2):114-120.

[89]Łągiewka M, Konopka Z. Properties of AlSi9Mg alloy matrix composite reinforced with short carbon fibre after remelting.Archives of Foundry Engineering. 2015;15.

[90]Hou L G, Wu R Z, Wang X D, Zhang J H, Zhang M L, Dong A P,Sun B D. Microstructure, mechanical properties and thermal conductivity of the short carbon

fiber reinforced magnesium matrix composites.Journal of Alloys and Compounds. 2017;695(2820-2826).

[91] Jackson P W, Marjoram J R. Compatibility studies of carbon fibres with nickel and cobalt.Journal of Materials Science. 1970; 5(1): 9-23.

[92]Korb G, Koráb J, Groboth G. Thermal expansion behaviour of unidirectional carbon-fibre-reinforced copper-matrix composites.Composites Part A: Applied Science and Manufacturing. 1998;29(12):1563-1567.

[93]Liu L, Tang Y, Zhao H, Zhu J,Hu W. Fabrication and properties of short carbon fibers reinforced copper matrix composites.Journal of Materials Science. 2007;43(3):974-979.

[94] Wan Y Z, Wang Y L, Luo H L, et al. Effects of fiber volume fraction, hot pressing parameters and alloying elements on tensile strength of carbon fiber reinforced copper matrix composite prepared by continuous three-step electrodeposition.Materials Science and Engineering: A. 2000;288(1):26-33.

[95]Hu C, Liu J, Xu L, Yu L,Zhu B. Effect of Sintering Temperature on Properties of Carbon Fiber-Reinforced Titanium Matrix Composites.ACS Omega. 2022;7(34):30087-30092.

[96]Jiao Y, Huang L,Geng L. Progress on discontinuously reinforced titanium matrix composites.Journal of Alloys and Compounds. 2018;767(1196-1215.

[97] Leyens C, Hausmann J, Kumpfert J. Continuous fiber reinforced titanium matrix composites: fabrication, properties, and applications.Advanced Engineering Materials, 2003;5(6):399-410.

[98]Even C, Arvieu C,Quenisset J M. Powder route processing of carbon fibres reinforced titanium matrix composites.Composites Science and Technology. 2008;68(6):1273-1281.

[99]Hu Z-Y, Zhang Z-H, Cheng X-W, Wang F-C, Zhang Y-F,Li S-L. A review of multi-physical fields induced phenomena and effects in spark plasma sintering: Fundamentals and applications.Materials & Design. 2020;191(108662.

[100]Munir Z A, Anselmi-Tamburini U,Ohyanagi M. The effect of electric field and

pressure on the synthesis and consolidation of materials: A review of the spark plasma sintering method.Journal of Materials Science. 2006;41(3):763-777.

[101]Guillon O, Gonzalez-Julian J, Dargatz B, Kessel T, Schierning G, Räthel J,Herrmann M. Field-Assisted Sintering Technology/Spark Plasma Sintering: Mechanisms, Materials, and Technology Developments.Advanced Engineering Materials. 2014;16(7):830-849.

[102]Decker S,Krüger L. Mechanical properties of a CrMnNi steel/Mg-PSZ-FGM processed by asymmetric Spark Plasma Sintering.Materials & Design. 2017;115(8-16.

[103]Mu X N, Cai H N, Zhang H M, Fan Q B, Zhang Z H, Wu Y, Ge Y X,Wang D D. Interface evolution and superior tensile properties of multi-layer graphene reinforced pure Ti matrix composite.Materials & Design. 2018;140(431-441.

[104]Yang J, Trapp J, Guo Q,Kieback B. Joining of 316L stainless steel by using spark plasma sintering method.Materials & Design (1980-2015). 2013;52(179-189.

[105]Liu W,Naka M. In situ joining of dissimilar nanocrystalline materials by spark plasma sintering.Scripta Materialia. 2003;48(9):1225-1230.

[106]Omori M. Sintering, consolidation, reaction and crystal growth by the spark plasma system (SPS).Materials Science and Engineering: A. 2000;287(2):183-188.

[107]Zheng B, Ashford D, Zhou Y, Mathaudhu S N, Delplanque J-P,Lavernia E J. Influence of mechanically milled powder and high pressure on spark plasma sintering of Mg–Cu–Gd metallic glasses.Acta Materialia. 2013;61(12):4414-4428.

[108]Lee S H, Oh H C, An B H,Kim H D. Ultra-low temperature synthesis of Al4SiC4 powder using spark plasma sintering.Scripta Materialia. 2013;69(2):135-138.

[109]Zoli L, Vinci A, Silvestroni L, Sciti D, Reece M,Grasso S. Rapid spark plasma sintering to produce dense UHTCs reinforced with undamaged carbon fibres.Materials & Design. 2017;130(1-7.

[110]Olevsky E A, Kandukuri S, Froyen L. Consolidation enhancement in spark-plasma sintering: Impact of high heating rates.Journal of Applied Physics. 2007;102(11):114913.

[111]Zhang J, Meng F, Todd R I,Fu Z. The nature of grain boundaries in alumina

fabricated by fast sintering.Scripta Materialia. 2010;62(9):658-661.

[112]Ji W, Parker B, Falco S, Zhang J Y, Fu Z Y,Todd R I. Ultra-fast firing: Effect of heating rate on sintering of 3YSZ, with and without an electric field.Journal of the European Ceramic Society. 2017;37(6):2547-2551.

[113]Liu J, Fu Z, Wang W, Zhang J, Wang H, Wang Y, Lee S,Niihara K. Ultra-high heating rate densification of nanocrystalline magnesia at high pressure and investigation on densification mechanisms.Journal of the European Ceramic Society. 2014;34(12):3095-3102.

[114]Deng S, Li R, Yuan T,Cao P. Effect of electric current on crystal orientation and its contribution to densification during spark plasma sintering.Materials Letters. 2018;229(126-129.

[115]Ortali C, Julien I, Vandenhende M, Drouet C,Champion E. Consolidation of bone-like apatite bioceramics by spark plasma sintering of amorphous carbonated calcium phosphate at very low temperature.Journal of the European Ceramic Society. 2018;38(4):2098-2109.

[116]Raichenko A I, Burenkov G L, Khrienko A F, et al. Electric discharge sintering of binary powder mixtures.Soviet Powder Metallurgy and Metal Ceramics. 1976;15(8):602-606.

[117]Burger K, Mader W,Rühle M. Structure, chemistry and diffusion bonding of metal/ceramic interfaces.Ultramicroscopy. 1987;22(1-4):1-13.

[118]Scheu C, Gao M, Oh S H, Dehm G, Klein S, Tomsia A P,Rühle M. Bonding at copper–alumina interfaces established by different surface treatments: a critical review.Journal of Materials Science. 2006;41(16):5161-5168.

[119]Derby B,Wallach E R. Theoretical model for diffusion bonding.Metal Science. 2013;16(1):49-56.

[120]Derby B,Wallach E R. Diffusion bonding: development of theoretical model.Metal Science. 2013;18(9):427-431.

[121] Derby B, Wallach E R. Joining methods in space: a theoretical model for diffusion bonding.Acta Astronautica. 1980;7(4-5): 685-698.

[122]Maehara Y, Komizo Y,Langdon T G. Principles of superplastic diffusion bonding.Materials Science and Technology. 2013;4(8):669-674.

[123]Korab J, Štefánik P, Kavecký Š, et al. Thermal conductivity of unidirectional copper matrix carbon fibre composites.Composites Part A: Applied Science and Manufacturing. 2002;33(4):577-581.

[124]Ramesh C S, Hirianiah A, Harishanad K, et al. A review on hot extrusion of Metal Matrix Composites (MMC's).International Journal of Engineering and Science. 2012;1(10): 30-35.

[125]Ye H Z, Liu X Y. Review of recent studies in magnesium matrix composites. Journal of materials science. 2004;39(20): 6153-6171.

[126]An J, Liu Y B, Lu Y, Zhang Q Y,Dong C. Dry sliding wear behavior of hot extruded Al–Si–Pb alloys in the temperature range 25–200 °C.Wear. 2004;256(3-4):374-385.

[127]Yi L-F, Yamamoto T, Onda T,Chen Z-C. Orientation control of carbon fibers and enhanced thermal/mechanical properties of hot-extruded carbon fibers/aluminum composites.Diamond and Related Materials. 2021;116(108432.

[128]Daoud A, Reif W, Rohatgi P. MICROSTRUCTURE AND TENSILE PROPERTIES OF EXTRUDED 7475 AL-AL2O3 PARTICLE COMPOSITES. Composite materials lab., Central Metallurigical Reasearch and Development institute, Helwan, Cario, Egypt. 2003.

[129]Ramesh C S,Safiulla M. Wear behavior of hot extruded Al6061 based composites.Wear. 2007;263(1-6):629-635.

[130]Li M, Li L, Hou X, Qin Y, Song G, Wei X, Kong X, Zhang Z, Do H, Greer J C, Han F, Cai T, Dai W, Lin C-T, Jiang N,Yu J. Synergistic effect of carbon fiber and graphite on reducing thermal resistance of thermal interface materials.Composites Science and Technology. 2021;212(108883.

[131]Tang L, He M, Na X, Guan X, Zhang R, Zhang J,Gu J. Functionalized glass fibers cloth/spherical BN fillers/epoxy laminated composites with excellent thermal conductivities and electrical insulation properties.Composites Communications.

2019;16(5-10.

[132]Ruan K, Guo Y, Tang Y, Zhang Y, Zhang J, He M, Kong J,Gu J. Improved thermal conductivities in polystyrene nanocomposites by incorporating thermal reduced graphene oxide via electrospinning-hot press technique.Composites Communications. 2018;10(68-72.

[133]Zhang C, Li T, Song H, Han Y, Dong Y, Wang Y,Wang Q. Improving the thermal conductivity and mechanical property of epoxy composites by introducing polyhedral oligomeric silsesquioxane-grafted graphene oxide.Polymer Composites. 2018;39(S3):E1890-E1899.

[134]Xu T, Zhou S, Cui S, Song N, Shi L,Ding P. Three-dimensional carbon fiber-graphene network for improved thermal conductive properties of polyamide-imide composites.Composites Part B: Engineering. 2019;178(107495.

[135]Zhang Y, Heo Y-J, Son Y-R, In I, An K-H, Kim B-J,Park S-J. Recent advanced thermal interfacial materials: A review of conducting mechanisms and parameters of carbon materials.Carbon. 2019;142(445-460.

[136]Zhang K, Zhang Y,Wang S. Effectively decoupling electrical and thermal conductivity of polymer composites.Carbon. 2013;65(105-111.

[137]Zhang R L, Gao B, Du W T, Zhang J, Cui H Z, Liu L, Ma Q H, Wang C G,Li F H. Enhanced mechanical properties of multiscale carbon fiber/epoxy composites by fiber surface treatment with graphene oxide/polyhedral oligomeric silsesquioxane.Composites Part A: Applied Science and Manufacturing. 2016;84(455-463.

[138]Pietrak K, Wiśniewski T S. A review of models for effective thermal conductivity of composite materials.Journal of Power Technologies. 2015; 95(1).

[139]JIN X, GONG Y, HAN X, et al. A review of current state and prospect of the manufacturing and application of advanced hot stamping automobile steels. Acta Metall Sin. 2020;56(4):411-428.

[140]Hamilton R L, Crosser O K. Thermal conductivity of heterogeneous two-component systems.Industrial & Engineering chemistry fundamentals. 1962;1(3): 187-

191.

[141]Bird R, Stewart W,Lightfoot E. Other mechanisms for mass transport.Transport Phenomena, John Wiley & Sons, Inc. 2007;

[142]Powell Jr B R, Youngblood G, Hasselman D,Bentsen L D. Effect of Thermal Expansion Mismatch on the Thermal Diffusivity of Glass-Ni Composites.Journal of the American Ceramic Society. 1980;63(9-10):581-586.

[143]Bruggeman V D. Berechnung verschiedener physikalischer Konstanten von heterogenen Substanzen. I. Dielektrizitätskonstanten und Leitfähigkeiten der Mischkörper aus isotropen Substanzen.Annalen der physik. 1935;416(7):636-664.

[144]Every A G, Tzou Y, Hasselman D P H, et al. The effect of particle size on the thermal conductivity of ZnS/diamond composites. Acta metallurgica et materialia. 1992;40(1):123-129.

[145]Benveniste Y. Effective thermal conductivity of composites with a thermal contact resistance between the constituents: Nondilute case.Journal of applied physics. 1987; 61(8): 2840-2843.

[146]Devpura A, Phelan P E, Prasher R S. Percolation theory applied to the analysis of thermal interface materials in flip-chip technology ITHERM 2000. The Seventh Intersociety Conference on Thermal and Thermomechanical Phenomena in Electronic Systems (Cat. No. 00CH37069). IEEE. 2000;1:21-28

[147]Bejan A, Kraus A D, eds. Heat transfer handbook. John Wiley & Sons. 2003; 1.

[148]Conway J H, Sloane N J A. Sphere packings, lattices and groups.Springer Science & Business Media, 2013.

[149]Davis L C, Artz B E. Thermal conductivity of metal-matrix composites.Journal of applied physics. 1995;77(10): 4954-4960.

[150]Han M, Zhou G, Huang J,Chen S. Optimization selection of the thermal conductivity of the top ceramic layer in the Double-Ceramic-Layer Thermal Barrier Coatings based on the finite element analysis of thermal insulation.Surface and Coatings Technology. 2014;240(320-326.

[151]Han M, Zhou G, Huang J,Chen S. A parametric study of the double-ceramic-layer

thermal barrier coatings part I: Optimization design of the ceramic layer thickness ratio based on the finite element analysis of thermal insulation (take LZ7C3/8YSZ/NiCoAlY DCL-TBC for an example).Surface and Coatings Technology. 2013;236(500-509.

[152]Wang L, Wang Y, Sun X G, He J Q, Pan Z Y,Wang C H. A novel structure design towards extremely low thermal conductivity for thermal barrier coatings – Experimental and mathematical study.Materials & Design. 2012;35(505-517.

[153]Wang Z, Kulkarni A, Deshpande S, Nakamura T,Herman H. Effects of pores and interfaces on effective properties of plasma sprayed zirconia coatings.Acta Materialia. 2003;51(18):5319-5334.

[154]Floury J, Carson J,Pham Q T. Modelling Thermal Conductivity in Heterogeneous Media with the Finite Element Method.Food and Bioprocess Technology. 2007;1(2):161-170.

[155]Kapitza P. E10. THE STUDY OF HEAT TRANSFER IN HELIUM II.Helium 4: The Commonwealth and International Library: Selected Readings in Physics. 2013;114.

[156]Swartz E T, Pohl R O. Thermal resistance at interfaces.Applied Physics Letters. 1987;51(26): 2200-2202.

[157]Swartz E T, Pohl R O. Thermal resistance at interfaces.Applied Physics Letters. 1987;51(26): 2200-2202.

[158]Prasher R S,Phelan P E. A Scattering-Mediated Acoustic Mismatch Model for the Prediction of Thermal Boundary Resistance.Journal of Heat Transfer. 2001;123(1):105-112.

[159]Devpura P E P, Ravi S. Prasher, Amit. Size effects on the thermal conductivity of polymers laden with highly conductive filler particles.Microscale Thermophysical Engineering. 2001;5(3):177-189.

[160]Furmański P, Wiśniewski T S, Banaszek J. Thermal contact resistance and other thermal phenomena at solid-solid interfance.Institute of Heat Engineering-Warsaw University of Technology. 2008.

[161]Zhao J-W, Zhao R, Huo Y-K,Cheng W-L. Effects of surface roughness, temperature and pressure on interface thermal resistance of thermal interface

materials.International Journal of Heat and Mass Transfer. 2019;140(705-716.

[162]Shaikh S, Lafdi K,Silverman E. The effect of a CNT interface on the thermal resistance of contacting surfaces.Carbon. 2007;45(4):695-703.

Chapter 2

Fabrication, mechanical properties, and thermal conductivity of C_f-Cu/Fe composite

2.1 Introduction

With the prosperity and development of the automobile industry, the demand for auto parts, especially high-strength and low-thickness parts, is increasing, which requires further improvement of production efficiency. High-strength and low-thickness auto parts can not only effectively reduce the weight of the body and reduce fuel consumption, but also ensure and improve the safety and comfort of the car[1,2]. A die with high TC can accelerate heat conduction and obtain martensite during hot stamping, improve production efficiency, and extend the service life of the die[3,4]. Taking advantage of the high TC characteristic of C_f in the axial direction, a thermal conduction channel is established in the composite, and the C_f-Cu/Fe composite with high TC is fabricated[5,6].

In chapter 1, it has been known that the die composite must have high hardness to ensure dimensional accuracy of parts, high temperature stability to ensure the life of the die and tensile strength to ensure the strength of the die does not crack[7]. The mechanical properties of these composites are related to their microstructure[8].

For C_f-Cu/Fe composites, due to the high anisotropy of C_f-Cu, both its orientation and content have a significant impact on the hardness and tensile strength of the composites. The 80% vol. C_f/polyetherimide (PEI) composite was investigated by Sharma et al.[9], and the effect of the angles (the angles between C_f and the loading direction were 0°, 30°, 45°, 60° and 90°) of C_f were evaluated on the mechanical properties of composites. It was observed that Young's modulus, Poisson's ratio, toughness and strain decreased with increasing angle of C_f. When C_f is parallel to the loading direction (angle of C_f is 0°), the wear rate of the composite (K_0=0.7 1×10^{-9} m^3/Nm) is almost three times higher than that of the composite with 90° of C_f. C_f, especially orientation of C_f parallel to the loading direction, can significantly enhance all the mechanical properties of PEI.

When exploring C_f-Ni-enhanced nickel coating materials, Shi et al.[10] found that due to the uniform distribution of C_f-Ni and metal carbides and the well bonding interface between C_f and the matrix, The microhardness and ultimate tensile strength of 6vol%C_f-Ni/Ni-coating composites reach 678 $HV_{0.2}$ and 608 MPa, respectively, which are 1.7 and 3.7 times that of the corresponding composite without C_f-Ni, respectively. Xiong et al.[11] found that an increase in the content of short Cf helps to improve the vicker hardness, ultimate tensile strength and fracture toughness of the composites.

There are many micropores, foreign bodies, crystals, etc. on the surface of C_f, which are important factors affecting the bonding properties between the matrix and the reinforcement in the composites[12], which will have a great effect on the properties of the composite. The surface of untreated C_f is smooth and chemically inert, and it has poor wettability with the matrix in the composite, reducing the interfacial bonding ability of the composite. The chemical reaction between C_f and Fe hinders the stability of C_f heat transfer. Through C_f electroless copper plating, C_f-Cu can be obtained, which not only protects C_f from its destruction but also enhances the mechanical properties (such as interlaminar shear strength and interfacial shear strength) of C_f materials. Copper plating is often used on the surface of C_f to hinder chemical reactions. Gao et al.[13] found that due to the interdiffusion of Cu and Al atoms, the synergistic effect of dispersion, precipitation and solid solution strengthening, the Vickers hardness, tensile strength and tensile strength of 9wt% Cu-C_f/Al composites were higher than those of pure Al. The tensile and flexural strengths were increased by 232.5%, 322% and 296.4%, respectively. In addition, the corrosion resistance of C_f-Cu/Al composites is better than that of uncoated C_f/Al composites.

In this chapter, hardness characterizes the resistance of composite to diamond indenters. When there are voids in the composite, the composite is compressed more densely when measuring the hardness, and the macroscopic appearance is that the hardness decreases. For C_f-Cu/Fe composites, due to the copper does not react with iron, voids easily exist at the interface between C_f-Cu and Fe. The decrease of the bonding strength of the contact surface can easily lead to the debonding of C_f-Cu, resulting in the decrease of the tensile strength of the composite[14-17]. Fei et al.[14] believe that as the resin content increases, the porosity decreases and the hardness and tensile strength of C_f reinforced paper-based friction (CFRPF) composites increase.

Taking into account the orientation of reinforcement, interfacial reaction, economy and residual stress, and other factors, powder metallurgy, hot pressing diffusion bonding, hot rolling hot pressing, squeeze casting and vacuum pressure infiltration are applied to fabricate C_f-reinforced metal composite products with excellent strength and TC. The most commonly used powder metallurgy method is SPS, and the advantages of this method for preparing C_f-reinforced iron composites have been presented in Chapter 1, Section 1.2.4.1.

The TC of the void is about 0.03 $W \cdot m^{-1}K^{-1}$. In the composite, the TC of pure iron is 54 $W \cdot m^{-1}K^{-1}$, and the axial and radial TC of C_f-Cu are 580 $W \cdot m^{-1}K^{-1}$, respectively. 1 and 5.3 $W \cdot m^{-1}K^{-1}$. The voids of the C_f-Cu/Fe composites seriously hinder the TC. Wang et al.[18] summarized the calculation model of the TC of the void-containing composites. The equations of the voids and TC of the material can be Expressed as:

$$\frac{K_{Effective}}{K_m} = (1-\omega)^n = \left(1 - \frac{V_p}{1-V_f}\right)^n \quad \cdots\cdots (2\text{-}1)$$

where, ω is the relative matrix porosity, $K_{Effective}$ and K_m are the ETC of the corrected material and the TC of the matrix, respectively. For different theoretical models, N has different values. n = 1.5, 1.65-1.85 and 1.55 for the Bruggeman model, Scaling relation and Progelhoff model, respectively. Solórzano[19] believed that n is a geometric factor of pores, which is related to the shape, connectivity and topology. Choosing a suitable processing method can simplify the operation and save money.

The porosity has a great influence on the mechanical properties of C_f-Cu/Fe composites. In this study, the Archimedes method was used to measure the density of the composites. In order to protect C_f from being damaged by the iron matrix, electroless copper plating was used in this study to obtain a uniform and dense copper layer. To ensure that the C_f-Cu in the composites is not destroyed by chemical reactions, XRD was used to investigate the phase composition of the C_f-Cu/Fe composites and determine the appropriate sintering temperature. The TC of Cu (K_{Cu}=398 $W \cdot m^{-1}K^{-1}$) is much higher than that of iron (K_{Fe}=54 W·m^{-1}K^{-1}). The distribution of Cu in the composite also has a great effect on the TC. The calculation of the radial TC of C_f-Cu by coating equation. EPMA was applied to observe the thickness of copper layers and the distribution of copper elements in the composites. In order to sinter the composites at low temperature and quickly obtain uniform and dense composites, the C_f-Cu/Fe composites were prepared by sintering method of SPS in this study. Steady-state method were used to obtain the measured TC of the C_f-Cu/Fe composites.

2.2 Experimental procedure

2.2.1 Raw materials

In this study, Fe powder (FEE14PB, 100% in purity, Kojundo Chemical Laboratory Co., Ltd., Japan, 7.874 kg m^{-3}) were used, and the average diameter was 5~10 μm. The pitched-based C_f (K13C6U, Mitsubishi Chemical Co., Ltd., Japan, 2.18 Mg m^{-3}, 8.6 μm of average diameter) was shortcut into about 5 mm. The properties parameter of C_f and graphite are shown in Table 2-1.

Table 2-2 Pitch based C_f (K13C6U, Mitsubishi Chemical Co.).

Purity	Diameter	Tensile Strength	Young's Modulus	Thermal conductivity Axial	Thermal conductivity radial
99%	8.6 mm	3.6 GPa	900 GPa	580Wm^{-1}K^{-1}	5 Wm^{-1}K^{-1}

Electroless copper plating is needed to prevent C_f from reacting with iron contacts and breaking its continuity. The TC of Fe is 54 Wm^{-1}K^{-1}, the axial TC of C_f is 580 Wm^{-1}K^{-1}, and the radial TC is 5 Wm^{-1}K^{-1}. The C_f were short cut into 5mm, which were roughened (10ml of acetone for 10min), acidified (68wt.% HNO_3 for 10min), sensitized (4g $SnCl_2$ and 0.5mL of 38.wt% HCl), activated (0.04g $PdCl_2$ and 5mL of 38 wt.% HCl) and other treatment procedures, in the electroless copper plating solution (OPC-750 electroless copper plating MA, MB and MC), under the conditions of 20 ~ 30 ℃, constant temperature, pH=12, A Cu layer (0.27μm) on the surface of C_f was obtained. The above procedures are all carried out in 100ml aqueous solution and under the action of ultrasonic vibration.

2.2.2 Mix the iron powder and C_f-Cu by V-tape mixer

In order to make the C_f-Cu in the composite evenly distributed in the matrix, the iron powder was suspended with alcohol, and then 0/10/20/30/40vol.% C_f-Cu was added to the suspension to make it uniformly mixed by a V-tape mixer (50r/min) for 2 hours. During the mixing process, Al_2O_3 balls (vol. Φ5: Φ8=3:2) were used to mix the C_f-Cu and iron powder more uniformly, and the corundum and composite materials were mixed in a volume ratio of 1:5. During the wet mixing process, the suspension can effectively reduce the mechanical friction between the iron powder and C_f-Cu, and the volume of the solution accounts for two-thirds of the volume of the mixing bottle, which is very important for the preparation of composites. The mixture was removed and dried at a temperature of 303K. The mixing process of iron powder and C_f-Cu was shown in Figure 2-1.

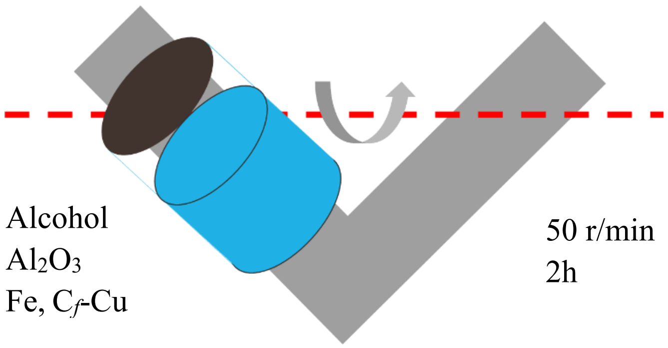

Figure 2-1 The schematic of V-type mixer.

2.2.3 Spark plasma sintering of C_f-Cu/Fe composite

The mixed iron powder and C_f-Cu were loaded into graphite dies and subjected to spark plasma sintering (pulsed spark sintering 0.9 ks, current was 300A, temperature was 1100-1200K, axial pressure was 50MPa, a vacuum of 1.3×10^{-2}Pa, and is kept for 10 minutes) in a graphite die to obtain a cylindrical composite of $65\times10\times10$ mm^3. These experimental parameters were set with reference to the parameters commonly used in the actual manufacturing process of sintering metals by SPS. The SPS device are shown in Figure 2-2. The sintering process and parameters of SPS are shown in Figure 2-3.

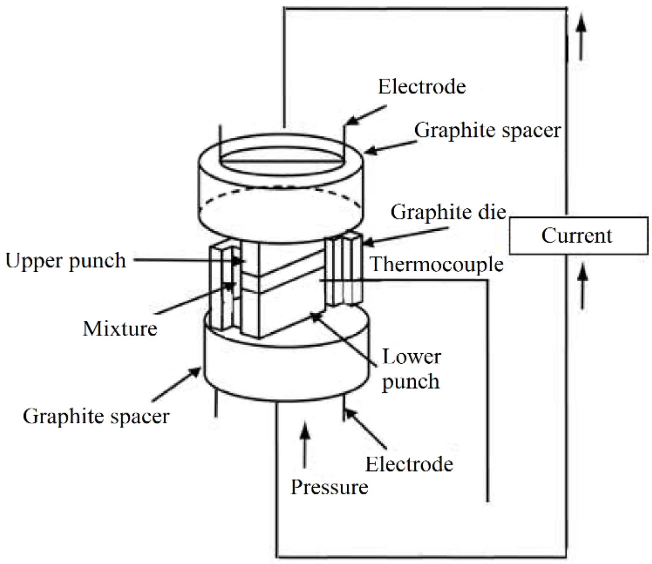

Figure 2-2 The schematic illustration of SPS.

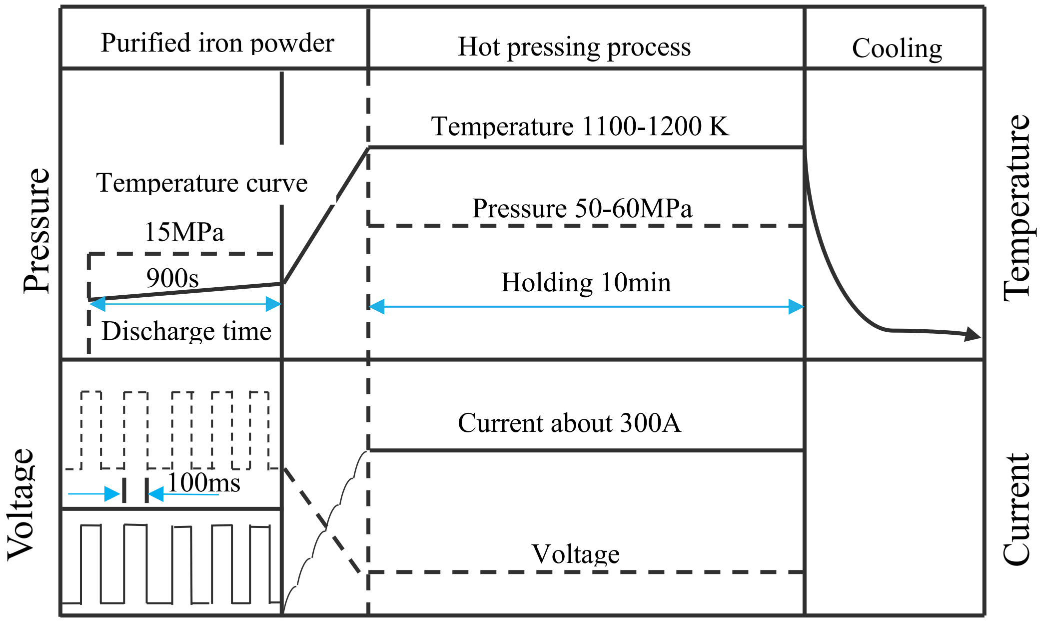

Figure 2-3 Flow chart of spark plasma sintering.

2.3 Mechanical and thermal properties evaluation

2.3.1 Relative density

The relative density of the composite material can be obtained by the following equation:

$$\omega = \frac{\rho_{measured}}{\rho_{theoretical}} \times 100\%$$

…… (2-2)

Where, ω is the relative density of the composite. $\rho_{measured}$ and $\rho_{theoretical}$ are the density measured by the Archimedes method and the theoretical density obtained by the mixing rule, respectively. The sum of ω and porosity is 1. The measured theoretical density can be obtained by the following equation:

$$\rho_{theoretical} = \boldsymbol{\rho_A} V_A + \boldsymbol{\rho_B} V_B + \boldsymbol{\rho_C} V_C + \cdots + \boldsymbol{\rho_X} V_X \qquad -\infty < x < \infty$$

…… (2-3)

Where, ρ_x is density of x, V_x is volume fraction of x. The density of pure aqueous solution is 1 g·cm^{-3}. The measured theoretical density can be obtained by the following equation:

$$\rho_{measured} = \frac{M_3 - M_1}{M_2 - M_1}$$

…… (2.3.1-3)

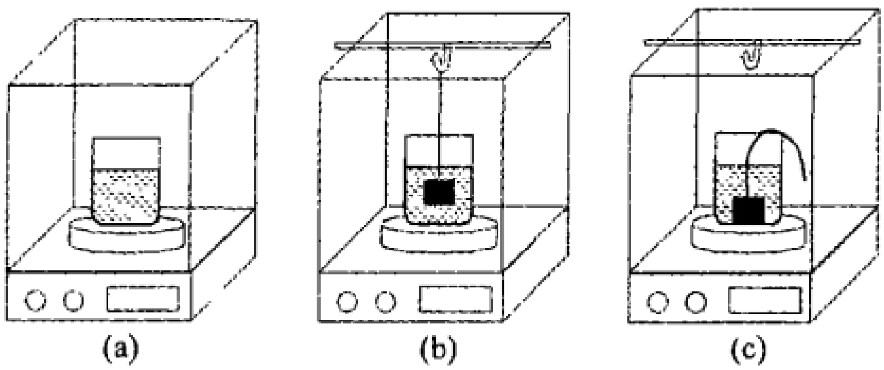

M_1 M_2 M_3

Figure 2-4 Schematic diagram of measurement of the density by the Archimedes method.

2.3.2 Hardness and tensile strength

The hardness of the composite was measured with a Vickers hardness tester under the conditions of loading 10kg/20kg and maintaining the pressure for 10s.

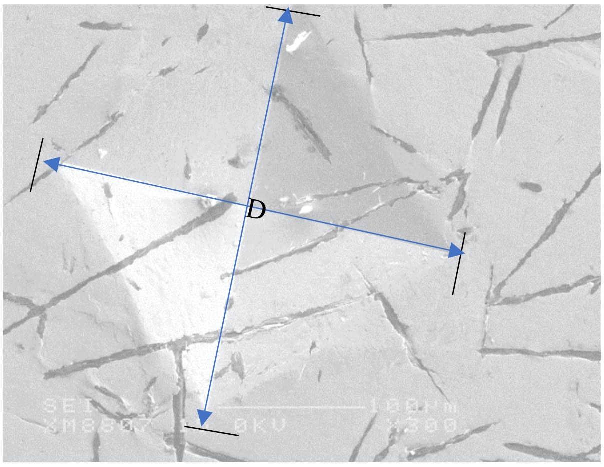

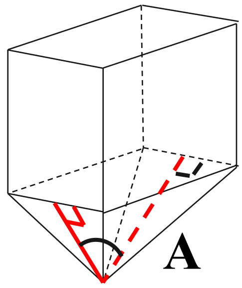

$$HV = \frac{F}{S} = \frac{2F\sin(A/2)}{D^2} = \frac{1.854F}{D^2} \quad \cdots\cdots (2\text{-}4)$$

Figure 2-5 Schematic diagram of hardness tester forming a diamond on composite.

The tensile strength of the composite was measured under the conditions of a tensile force of 5t and a tensile speed of 0.5mm/min, and the tensile specimens were machined by electric spark wire cutting as shown in Figure 2-6.

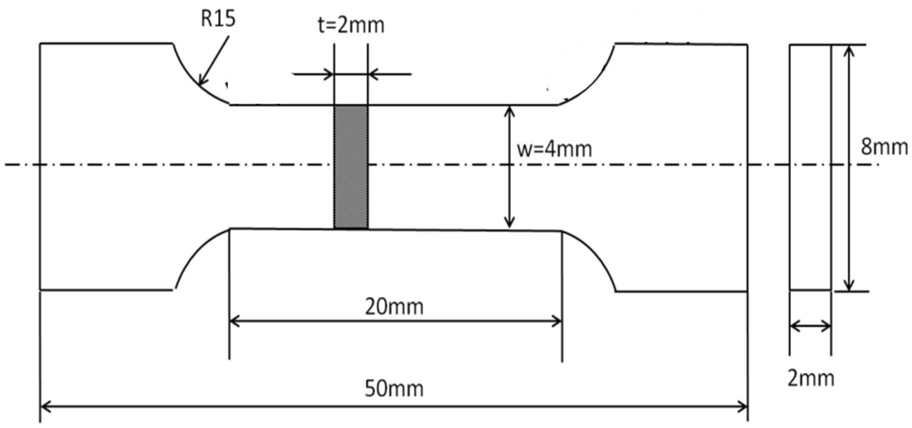

Figure 2-6 Schematic diagram of tensile test specimen.

2.3.3 Phase components of composites

When the C_f-Cu is damaged during the mixing, sintering and rolling process, for example, the C_f-Cu is interrupted, the Cu on the surface of the C_f is exfoliated, and the Cf reacts with the iron. The composition of the phase components of the composites can be investigated by means of X-ray powder diffraction (XRD) (D/MAX-2500/PC). The measurement conditions are listed in Table 2-2.

Table 2-2 The measurement conditions of composites by XRD.

Target	Wavelength (10^{-10}m)	Power (KW)	Voltage (KV)	Current (mA)	Sampling step (degree)	Scan speed (degree/min)
Cu	1.54 ($K_{\alpha1}$)	≤ 18	20	200	0.02	4

2.3.4 Microstructure of composite

The C_f-Cu and the cross-section microstructure of the sintered composites were observed by EPMA. An optical microscope (OM)was used for observing the aspect ratio and orientation of C_f-Cu in the sintered composites.

2.3.5 Effective thermal conductivity by steady state method

Steady-state TC measurement has become the most commonly used method for TC measurement of Cf-reinforced metal composites due to its simple operation and low cost[20]. The schematic diagram of the measuring device is shown in Figure 2-7.

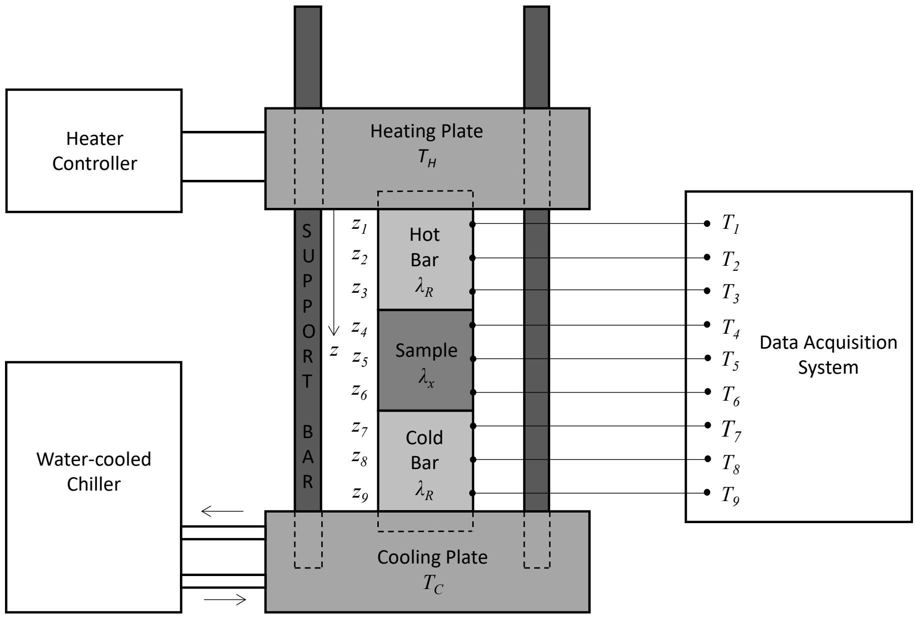

Figure 2-7 Schematic of steady state thermal conductivity measuring device[20].

The sample is placed between the hot column and the cold column, with the hot column above the sample and the cold column below the sample. The surfaces of the samples in contact with the hot and cold pillars were polished and coated with a high

TC thermal paste (Arctic Silver R5, Arctic Silver Inc., U.S.) to reduce the thermal resistance at the interface. Both the hot and cold columns are made of copper cylinders with a diameter of 10 mm and a length of 30 mm. As shown in Figure 2-7, nine thermocouples are mounted on the hot column, the sample, and the cold column in sequence. Heat the hot column, circulate water to cool the cold column, and after the temperature of the hot column and the cold column is stabilized, obtain the thermal gradient temperature from thermocouples 1 to 9 at 1-second intervals for about 300 seconds. Then, the temperature gradients a_h, a_s and a_c of the hot rod, sample, and cold rod were calculated by the least squares method as follows:

$$a_h = \sum_{i=1}^{3}(z_i - \bar{z}_h)(T_i - \bar{T}_h) \Big/ \sum_{i=1}^{3}(z_i - \bar{z}_h)^2, \quad \bar{z}_h = \frac{1}{3}\sum_{i=1}^{3} z_i, \quad \bar{T}_h = \frac{1}{3}\sum_{i=1}^{3} T_i$$

$$a_s = \sum_{i=4}^{6}(z_i - \bar{z}_s)(T_i - \bar{T}_s) \Big/ \sum_{i=4}^{6}(z_i - \bar{z}_s)^2, \quad \bar{z}_s = \frac{1}{3}\sum_{i=4}^{6} z_i, \quad \bar{T}_s = \frac{1}{3}\sum_{i=4}^{6} T_i$$

$$a_c = \sum_{i=7}^{9}(z_i - \bar{z}_c)(T_i - \bar{T}_c) \Big/ \sum_{i=7}^{9}(z_i - \bar{z}_c)^2, \quad \bar{z}_c = \frac{1}{3}\sum_{i=7}^{9} z_i, \quad \bar{T}_c = \frac{1}{3}\sum_{i=7}^{9} T_i$$

…… (2-5)

Where, in a thermally stable state, T_i is the temperature of the i-th thermocouple, and zi is the distance from the i-th thermocouple to the hot end. Finally, the ETC of the sample, $K_{Measured}$, can be calculated by the following formula:

$$K_{Measured} = \frac{K_{Cu} C \, (a_h + a_c)}{2\Delta a_s}$$

…… (2-6)

In this research, The TC of copper cylinders is 385 W m^{-1} K^{-1}, C is a constant value (i.e C=236/257).

2.4 Results and discussion

2.4.1 Relative density of composites

It can be seen from Figure 2-8 that the relative density of C_f-Cu/Fe composites decreases with the increase of C_f-Cu content, and the relative density of all composites is higher than 93%. As the sintering temperature increases, the sensitivity of the relative density to the change of C_f-Cu content decreases. When the sintering temperature is 1200K, the deviation of the relative density of the composites is 1%.

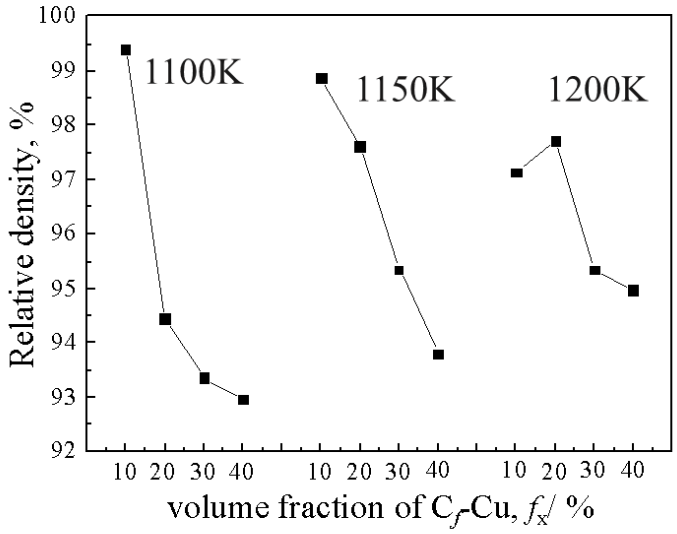

Figure 2-8 Relative density of composites at different sintering conditions with different C_f-Cu contents.

2.4.2 Phase of composites and Cu distribution

Figure 2-9 (a) shows the XRD patterns of the composites at different temperatures. At a sintering temperature higher than 1150K, ferrite disappears, ferrite reacts with carbon to form cementite and combines the ferrite to form a small amount of martensite. The carbon in cementite and ferrite originates from C_f, which indicates the destruction of C_f. Figure 2-9(b) shows the XRD patterns of the composites with different volume fractions of C_f-Cu. The ferrite still exists and the C_f is not destroyed. The Cu layer in the composite can still protect the C_f. In Figure 2-10, due to the lower sintering temperature and sintering time, Cu is closely distributed in the vicinity of C_f, and in the composite, C_f and Cu can still be regarded as a whole, C_f-Cu.

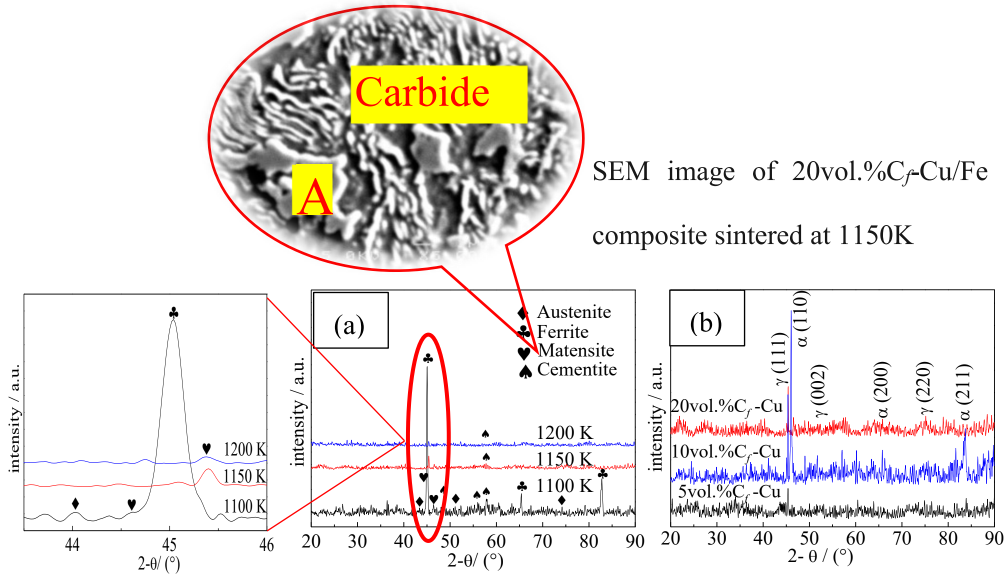

Figure 2-9 XRD of C_f-Cu/Fe composites with (a) different sintering temperatures and (b) different volume fractions of C_f-Cu.

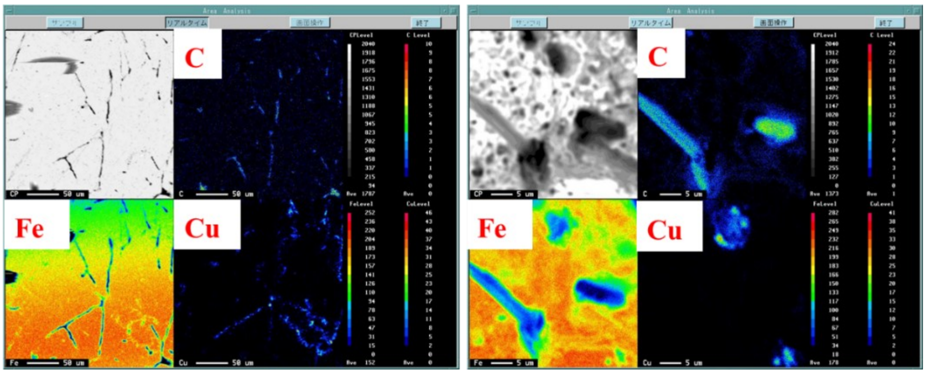

Figure 2-10 SEM image of 10vol.% C_f-Cu/Fe composite.

2.4.3 Mechanical properties and microstructure of composites

In this experiment, a hardness tester with a diamond indenter was used. Hardness indicates the ability of a composite to resist a diamond indenter. As shown in Figure 2-5, when the indenter acts on the surface of the composite, C_f-Cu can hinder the indentation of the indenter. As shown in Figure 2-11, when the C_f-Cu content does not exceed 20%, the hardness increases with the increase of the C_f-Cu content. When the volume fraction of C_f-Cu increases from 20% to 30%, the relative density of C_f-Cu/Fe composites decreases sharply. When the C_f-Cu content is large enough, the C_f-Cu overlaps with each other, and its hardness is much smaller than that of the matrix. When the C_f-Cu content exceeds 20%, the hardness decreases with the increase of the C_f-Cu content. The hardness of C_f-Cu/Fe reaches the maximum value when the volume fraction of C_f-Cu is 20%. Figure 2-9(a)shows that when the temperature exceeds 1100K, C_f-Cu is destroyed and a dense lamellar martensite is formed, whose hardness is much higher than that of the matrix, and the hardness of the composite increases. When the sintering temperature is 1150K, the hardness reaches the maximum value of 226HV.

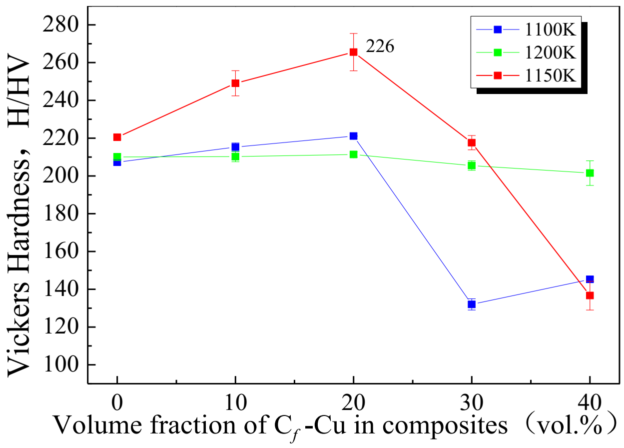

Figure 2-11 Vickers hardness of composites at different temperature with different C_f-Cu contents.

As shown in Figure 2-12, when the volume fraction of C_f-Cu does not exceed 20%, during the fracture process of the C_f-Cu/Fe composite, the fracture surface presents a river-like shape. With the addition of C_f-Cu, the hindering effect of the C_f-Cu on crack propagation and tensile fracture is enhanced, the orientation of C_f-Cu is not fixed, and the fracture surface is in the shape of an inclined step. When the composite is stretched and fractured, the ends of C_f-Cu deboned from the matrix and form dimples[21]. The 20vol.%C_f-Cu composite forms equiaxed dimples on the fracture surface, which is caused by the absorption of a large amount of energy under the uniform tensile force. The tensile strength of C_f-Cu/Fe increases with the increase of C_f-Cu content.

It can be seen from Figure 2-13 that when the C_f-Cu content in the composite exceeds 20%, a large amount of C_f-Cu has a greater probability of being distributed perpendicular to the tensile direction, and the fracture is caused by the interaction between C_f-Cu and iron. The fracture is determined by the mechanical meshing force between the iron substrates, which is much smaller than the metallic bonding between the iron substrates. The tensile strength of C_f-Cu/Fe composites decreases with the increase of C_f-Cu content. When the volume fraction of C_f-Cu is 20%, the tensile strength of the C_f-Cu/Fe composite reaches the maximum value of 679MPa, which is 9.5% higher than that of pure iron under the same conditions.

Within a certain range, the addition of C_f-Cu can not only improve the hardness of C_f-Cu/Fe composites but also improve the tensile strength of the materials and greatly enhance the mechanical properties of the materials[22].

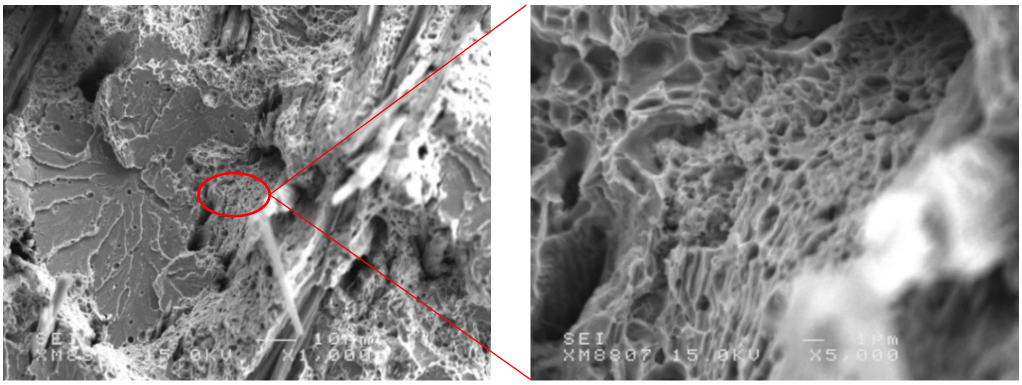

Figure 2-12 SEM image of 20vol.%C_f-Cu/Fe composite sintered at 1150K.

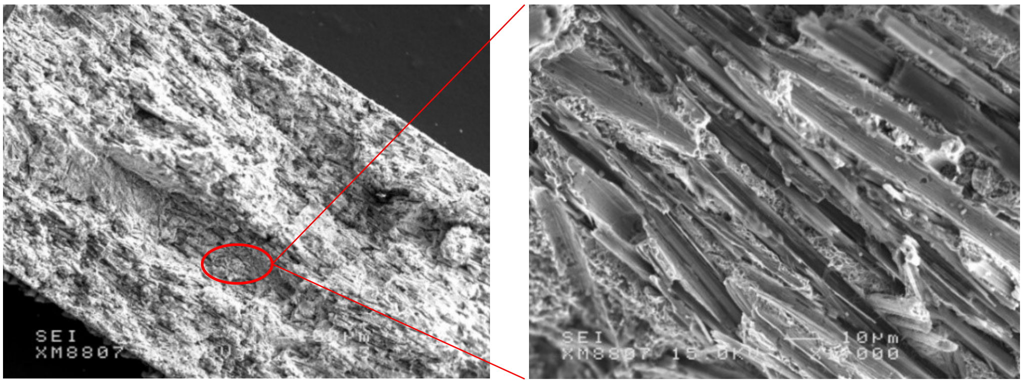

Figure 2-13 SEM image of 30vol.%C_f-Cu/Fe composite sintered at 1150K.

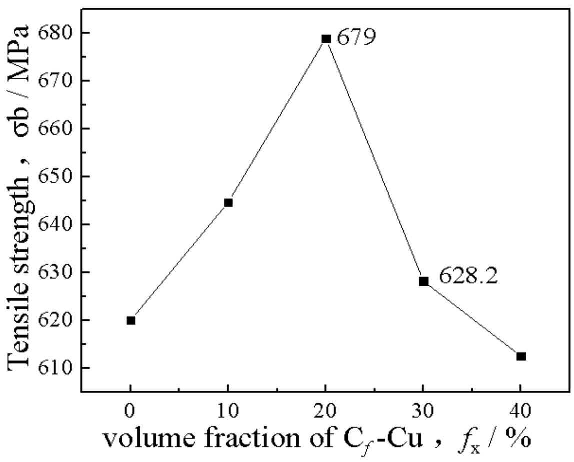

Figure 2-14 Tensile strength of composites with different C_f-Cu contents at 1150 K.

2.4.4 Thermal conductivity of C_f-Cu

As shown in Figure 2-15, the diameter of C_f-Cu, thickness of the Cu coating, and δ after electroless copper plating are 9.42 μm, 0.27 μm, and 0.54μm, respectively. The TC of Cu was 398 $Wm^{-1}K^{-1}$, and after correction for coating TC by the equation:

$$K_{Cf-Cu} = \frac{K_{Cf}K_{Cu}h}{K_{Cf}\delta + K_{Cu}(h-\delta)}$$

…… (2-7)

Where, $K_{Cf\text{-}Cu}$, K_{Cf}, K_{Cu} are the TC of C_f-Cu, C_f and Cu, respectively. h is the diameter of C_f-Cu. δ is the thickness of the Cu layer above and below of the C_f the axial TC of the C_f-Cu was 580 $Wm^{-1}K^{-1}$, and the radial TC was 5.3 $Wm^{-1}K^{-1}$.

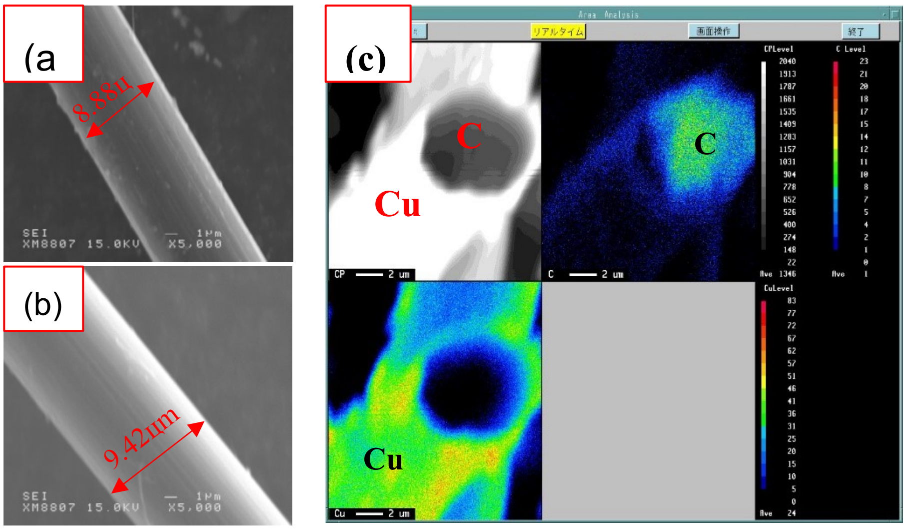

Figure 2-15 Schematic of (a)as-received C_f. (b) Cu plated C_f. (c) element distribution of C_f-Cu.

2.4.5 Thermal conductivity of the composites by steady state method

The TC of C_f-Cu/Fe composites with different sintering temperatures were measured under thermal steady state conditions, and the measurement positions are shown in Figure 2-16. SPS hot pressing was applied on the A plane and stretched in the direction perpendicular to the A and C planes. The TC of the C_f-Cu/Fe composite was measured on the C plane, and the measurement results were shown in Figure 2-17. Due to the scattering of phonons, a large amount of heat is dissipated. Compared with pure iron, the addition of C reduces the TC of pure iron by 20%. C_f-Cu is destroyed when sintered at temperatures above 1100K, and C_f-Cu cannot function as a thermal conduction channel. Under the same conditions, the TC of the C_f-Cu/Fe composites obtained by sintering at 1100K is larger. Most of the C_f-Cu in the 30vol.%C_f-Cu/Fe is parallel to the stretching direction and perpendicular to the heat flow direction. The radial TC (5.3) of C_f-Cu is much smaller than that of the iron (45), and its TC is less than TC of 20vol.% C_f-Cu/Fe. With the increase of C_f-Cu content, the C_f-Cu oriented parallel to the heat flow direction is more than the C_f-Cu oriented perpendicular to the heat flow direction, and the composite TC increases. With the increase of C_f-Cu content, the TC of C_f-Cu/Fe composites first increased (20vol.%C_f-Cu), then decreased (30vol.%C_f-Cu) and then increased (40vol.%C_f-Cu).

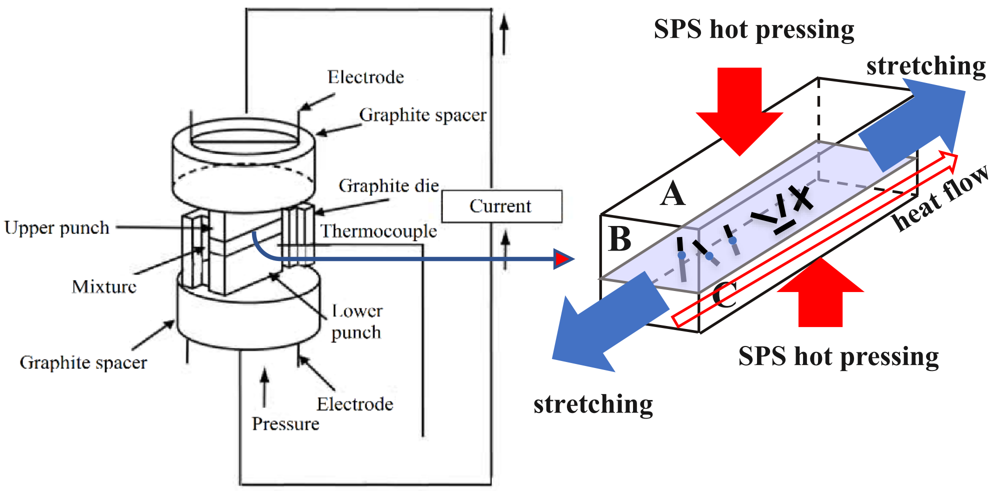

Figure 2-12 Schematic diagram of hot-pressing direction, stretching direction and measuring direction of TC of composites.

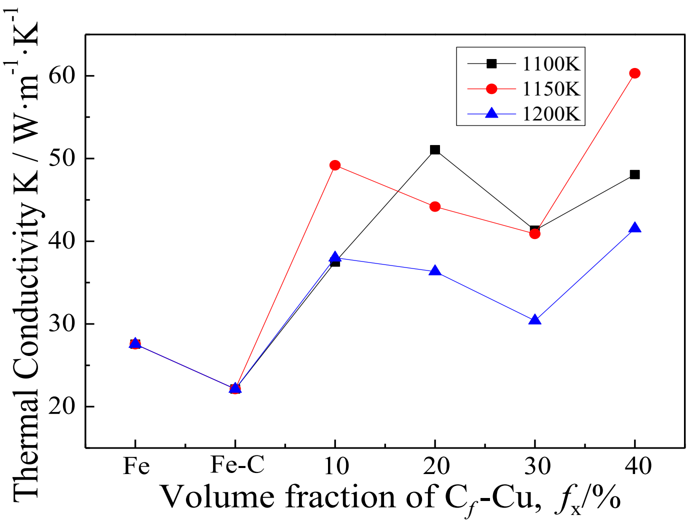

Figure 2-17 TC of composites with different C_f-Cu contents at various temperatures.

2.5 Summary

In this chapter, graphite with different volume fraction reinforced Cu matrix composite was prepared by spark plasma sintering. The relationship between thermal properties and microstructure of composites are discussed. To investigate the influence of the angle of graphite on thermal conductivity and thermal expansion, the thermal properties of graphite reinforce Cu matrix composite was calculated with a simulation code which can take account of the angle of graphite at cross-section face. The following conclusions are obtained.

(1) The relative densities of C_f-Cu/Fe composites decreased with the increase of C_f-Cu content, and the relative densities of all composites were higher than 93%. The sintering temperature hardly affects the relative density of the composites. When the sintering temperature is 1200K, the relative density deviation of C_f-Cu content to the composites is 1%.

(2) When the sintering temperature is higher than 1100K, ferrite disappears, Cf-Cu is destroyed by iron, and cementite or martensite is formed, which will improve the hardness of C_f-Cu/Fe composites. The Cu element is distributed around C_f.

(3) The hardness of C_f-Cu/Fe composites first increases and then decreases with the increase of the C_f-Cu content. When the sintering temperature is 1150K, the Cf-Cu is destroyed to form dense flaky martensite, and the hardness of the 20vol.% C_f-Cu/Fe composite is the highest, reaching 226HV. When the volume fraction of C_f-Cu in the C_f-Cu/Fe composite increases from 20% to 30%, the fracture mode changes. The tensile strength of the composites first increases and then decreases with the increase of C_f-Cu content. The tensile strength of the 20vol.%C_f-Cu/Fe composite reaches the maximum value of 679MPa, which is 9.5% higher than that of pure iron under the same conditions.

(4) Compared with pure iron, the addition of C reduces the TC of pure iron by 20%. With the increase of C_f-Cu content, the TC of C_f-Cu/Fe composites first increased (20vol.%C_f-Cu), then decreased (30vol.%C_f-Cu) and then increased (40vol.%C_f-Cu)

2.6 References

[1]Galán J, Samek L, Verleysen P, Verbeken K,Houbaert Y. Advanced high strength steels for automotive industry.Revista de Metalurgia. 2012;48(2):118-131.

[2]So H, Faßmann D, Hoffmann H, Golle R,Schaper M. An investigation of the blanking process of the quenchable boron alloyed steel 22MnB5 before and after hot stamping process.Journal of Materials Processing Technology. 2012;212(2):437-449.

[3]Lim W-S, Choi H-S, Ahn S-y,Kim B-M. Cooling channel design of hot stamping tools for uniform high-strength components in hot stamping process.The International Journal of Advanced Manufacturing Technology. 2013;70(5-8):1189-1203.

[4]Bok H-H, Lee M-G, Kim H-D,Moon M-B. Thermo-mechanical finite element analysis incorporating the temperature dependent stress-strain response of low alloy steel for practical application to the hot stamped part.Metals and Materials International. 2010;16(2):185-195.

[5]Tian T,Cole K D. Anisotropic thermal conductivity measurement of carbon-fiber/epoxy composite materials.International Journal of Heat and Mass Transfer. 2012;55(23-24):6530-6537.

[6]Zhang H, Wu K, Xiao G, Du Y,Tang G. Experimental study of the anisotropic thermal conductivity of 2D carbon-fiber/epoxy woven composites.Composite Structures. 2021;267(113870.

[7]Chantzis D, Liu X, Politis D J, El Fakir O, Chua T Y, Shi Z,Wang L. Review on additive manufacturing of tooling for hot stamping.The International Journal of Advanced Manufacturing Technology. 2020;109(1-2):87-107.

[8]Yao H, Sui X, Zhao Z, Xu Z, Chen L, Deng H, Liu Y,Qian X. Optimization of interfacial microstructure and mechanical properties of carbon fiber/epoxy composites via carbon nanotube sizing.Applied Surface Science. 2015;347(583-590.

[9]Sharma M, Mohan Rao I,Bijwe J. Influence of fiber orientation on abrasive wear of unidirectionally reinforced carbon fiber–polyetherimide composites.Tribology International. 2010;43(5-6):959-964.

[10]Shi C, Lei J, Zhou S, Dai X,Zhang L-C. Microstructure and mechanical properties of carbon fibers strengthened Ni-based coatings by laser cladding: The effect of carbon fiber contents.Journal of Alloys and Compounds. 2018;744(146-155.

[11]Xiong B, Wang Z, Wang C, Xiong Y,Cai C. Effects of short carbon fiber content on microstructure and mechanical property of short carbon fiber reinforced Nb/Nb5Si3 composites.Intermetallics. 2019;106(59-64.

[12]Tiwari S,Bijwe J. Surface Treatment of Carbon Fibers - A Review.Procedia Technology. 2014;14(505-512.

[13]Gao M, Gao P, Wang Y, Lei T,Ouyang C. Study on Metallurgically Prepared Copper-Coated Carbon Fibers Reinforced Aluminum Matrix Composites.Metals and Materials International. 2020;27(12):5425-5435.

[14]Fei J, Li H-J, Fu Y-W, Qi L-H,Zhang Y-L. Effect of phenolic resin content on performance of carbon fiber reinforced paper-based friction material.Wear. 2010;269(7-8):534-540.

[15]Gamstedt E K. Effects of debonding and fiber strength distribution on fatigue-damage propagation in carbon fiber-reinforced epoxy.Journal of Applied Polymer Science. 2000;76(4):457-474.

[16]Kumar K S S, Nair C P R,Ninan K N. Effect of fiber length and composition on mechanical properties of carbon fiber-reinforced polybenzoxazine.Polymers for Advanced Technologies. 2008;19(7):895-904.

[17]Zhou J, Zhong K, Zhao C, Meng H,Qi L. Effect of carbon nanotubes grown temperature on the fracture behavior of carbon fiber reinforced magnesium matrix composites: Interlaminar shear strength and tensile strength.Ceramics International. 2021;47(5):6597-6607.

[18]Wang J, Chen Y, Feng Y, Zhao G, Jian X, Huang Q, Yang L,Xu J. Influence of porosity on anisotropic thermal conductivity of SiC fiber reinforced SiC matrix composite: A microscopic modeling study.Ceramics International. 2020;46(18):28693-28700.

[19]Solórzano E, Reglero J A, Rodríguez-Pérez M A, Lehmhus D, Wichmann M,De

Saja J A. An experimental study on the thermal conductivity of aluminium foams by using the transient plane source method.International Journal of Heat and Mass Transfer. 2008;51(25-26):6259-6267.

[20]Sugio K, Yamada R, Choi Y B,Sasaki G. Effect of the Interfacial Thermal Resistance on Effective Thermal Conductivity of Al/SiC Particle-Dispersed Composites.Materials Science Forum. 2016;879(1889-1894.

[21]Liu N, Zhang Q, Zhang H, Cao F, Feng P, Zuo Y, Jiang Y, Tang W,Liang S. Experimental verification and numerical analysis on plastic deformation and mechanical properties of the in-situ TiB2 homogeneous composites and TiB2/Cu network composites prepared by powder metallurgy.Journal of Alloys and Compounds. 2022;920(165897.

[22]Sha J-j, L Z-z, Sha R-y, Zu Y-f, Dai J-x, Xian Y-q, Zhang W, Cui D,Yan C-l. Improved wettability and mechanical properties of metal coated carbon fiber-reinforced aluminum matrix composites by squeeze melt infiltration technique.Transactions of Nonferrous Metals Society of China. 2021;31(2):317-330.

Chapter 3

Effective thermal conductivity of C_f-Cu/Fe composites by 2D Image Analysis

3.1 Introduction

High-strength automotive parts manufactured by hot stamping technology have been investigated and attracted the interest of researchers[1-5]. Reducing fuel consumption, ensuring the safety and comfort of cars, improving production efficiency and prolonging the service life of hot stamping dies have become urgent issues for the prosperity and development of the automobile industry[3]. Hot stamping dies with high-strength and high-TC can accelerate heat conduction and obtain martensite during the hot stamping process, effectively reduce the weight of the car body, and meet the current development needs of the automotive industry[1,6-11].

In Chapter 2, the TC of C_f-Cu/Fe composites varies irregularly with C_f-Cu due to the uncontrollable orientation of C_f-Cu. In order to further improve the TC of C_f-Cu/Fe composites, it is necessary to control the orientation of the C_f-Cu. Many scholars have studied the method of controlling orientation of C_f. Matsuura. et al.[12,13] used the method of hot extrusion to orient C_f along the extrusion direction in the composite, which is mostly used in C_f-reinforced low-melting metal composite. Ma et al.[14] found that the orientation of C_f can be determined by the rapid freezing method, which is suitable for C_f-reinforced epoxy compounds. In this study, C_f-Cu can be rapidly aligned along the direction of heat flow by hot rolling, As shown in Figure 3-1. The A plane is the pressure surface in the SPS process, and the B plane is the side of the A plane. Plane B is the pressure surface during hot rolling, and Plane A is the side of Plane B.

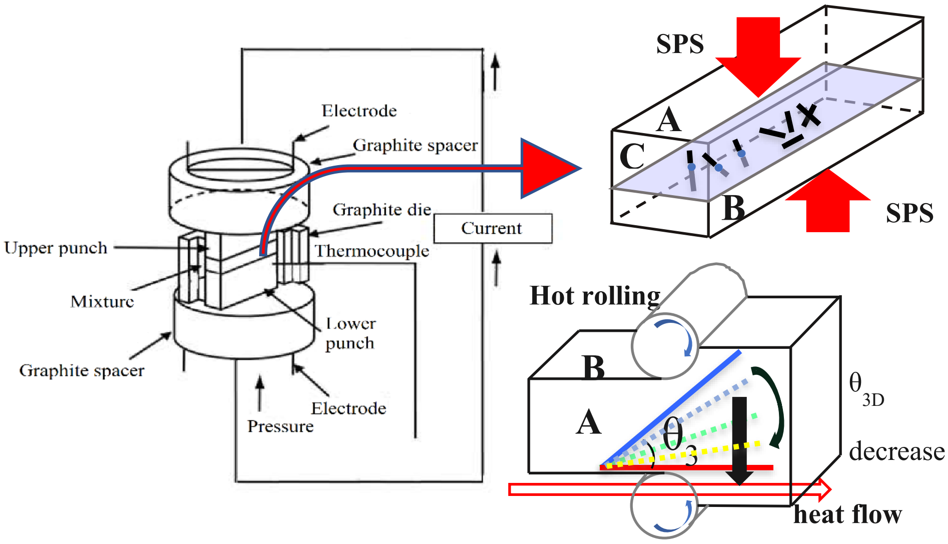

Figure 3-1 The schematic illustration of SPS and hot rolling.

Many experiments have been investigated to study the calculation of the effective TC of C_f-reinforced metal composites[15], and it was found that the established model cannot accurately predict the effective TC of C_f-reinforced metal composites for the following reasons: 1. Due to the high TC of anisotropy of C_f, the axial TC and radial TC of C_f are very different, and the orientation of C_f has a great influence on the TC of C_f reinforced composites. 2. The thermal resistance of the contact between C_f and other components in the composite will hinder heat conduction. 3. When C_f is connected end to end, a percolation model is formed, which will promote the heat conduction of C_f reinforced composites. 4. C_f is easily damaged during the preparation process, especially the coating of metal plated C_f is easily damaged. The length of C_f also affects the thermal conduction efficiency of C_f reinforced composites.

Previous calculations and predictions on the effective TC of C_f reinforced composites include mixing rules[16,17], percolation models[18,19], effective approximation theory[20], mathematical distribution models[21], and 3D simulations[22]. Wang et al.[23] used a 3D numerical method to reproduce a more realistic 3D distribution dispersed in the matrix phase by using a stochastic generation-growth approach to eliminate the overestimated fiber-to-fiber contacts in 2D simulations. The governing equations for energy transport in the 3D structure are then solved using an efficient lattice Boltzmann scheme. The calculated results are in good agreement with the experimental data. However, the real situation of C_f-Cu orientation in C_f-Cu/Fe composites is difficult to simulate and predict, which brings difficulties to the calculation and simulation of effective TC of C_f-Cu/Fe composites. The three-dimensional image simulation can reflect the real distribution of C_f-Cu inside the C_f-Cu/Fe composite, and the simulation results are in good agreement with the real measurement results[24]. The 3D image simulation is realized by ultra-high-resolution X-ray computed tomography images, which cost a lot of time and money and bring limitations to its wide application.

In addition, some scholars hope that these shortcomings can be avoided by replacing 3D image simulation with 2D image simulation. 2D image simulations were used to evaluate the C_f-Cu/Fe composite effective TC, saving both time and money. However, the 2D cross-section cannot provide the orientation information of C_f-Cu in the 3D space except the cross-section, the orientation of C_f-Cu on the two-dimensional cross-section cannot reflect its orientation in the 3D space. and the C_f-Cu on the two-dimensional cross-section. The included angle between C_f-Cu and the heat flow in the 2D cross-section is not greater than the included angle between C_f-Cu and the heat flow in 3D space.

In order to develop a method to calculate the effective TC of C_f-Cu/Fe composites by 2D image simulation, the relationship between the angle between C_f-Cu and heat flow in 2D cross-section and the angle between C_f-Cu and heat flow in 3D space was investigated. Moreover, the effect of the orientation of C_f-Cu on the TC of C_f-Cu/Fe composite material, the effect of rolling on the 20vol.%C_f-Cu/Fe composite TC, and the simulated TC by 2D image simulation and the measured TC by the steady-state method of the rolled 5-25vol.%C_f-Cu/Fe composite was investigated.

3.2 Experimental and calculation procedure

3.2.1 Experiments

In this study, Fe powder (FEE14PB, 100% in purity, Kojundo Chemical Laboratory Co., Ltd., Japan, 7.874 kg m^{-3}) were used, and the average diameter was 5~10 μm. The pitched-based C_f (K13C6U, Mitsubishi Chemical Co., Ltd., Japan, 2.18 Mg m^{-3}, 8.6 μm of average diameter) was shortcut into about 4.5 mm. C_f-Cu with a copper layer of 0.27 μm was obtained by electroless copper plating of chopped C_f to prevent C_f from contacting with the iron substrate and chemically reacting and being destroyed. C_f-Cu/Fe composite (die material) was fabricated by SPS. In order to distribute the axial direction of C_f-Cu in the composite along the direction of heat flow, hot rolling was used to change the orientation of C_f-Cu under the condition of rolling speed of 18r/min and compression rate of 50%. 3-1 shows the direction of SPS pressurization, hot pressing and thermal conductivity measurement. The relative density of the composites was measured by the Archimedes method. The ETC of the composites was measured at 300K by a steady-state thermal conductivity measurement device.

3.2.2 Calculation of thermal conductivity of matrix of composites

Heat conduction occurs because of the thermal movement of molecules and electrons from neighboring atoms. Fe contains many electrons, and the interatomic distance is small (10^{-10}m). The energy generated by thermal motion is small and the TC is high (54W m^{-1} K^{-1}). Since the molecular distance in the air is larger (10^{-9}m), the collision between molecules consumes more energy, and the TC is lower (0.03 W m^{-1} K^{-1}). Therefore, the voids in the composite significantly influence the TC, and therefore, the TC of the matrix must be corrected. The effective TC of the matrix changed with the porosity. The Bruggeman equation can be used to calculate the effective TC of a porous composite[25].

$$K_m = \frac{1}{4}\left[K_p(3V_p - 1) + K_{Fe}(3V_{Fe} - 1) + \left\{\left[K_p(3V_p - 1) + K_{Fe}(3V_{Fe} - 1)\right]^2 + 8K_pK_{Fe}\right\}^{1/2}\right]$$

······ (3-1)

K_{Fe} and K_p denote the TCs of the Fe matrix (54 $Wm^{-1}K^{-1}$) and air (0.03 $Wm^{-1}K^{-1}$), respectively. V_{Fe} and V_P represent the volume fraction of matrix and the porosity of composite, respectively.

3.2.3 Calculation of the orientation of C_f-Cu in 3D space

Figure 3-2 shows the rotation of C_f-Cu in 3D space. All the orientations of C_f-Cu can be regarded as C_f-Cu rotating along the M direction and N direction with the origin O (0,0,0) as the center. After rotation, the intersection line of C_f-Cu with the 2D cross section is an ellipse.

Figure 3-3 (a) shows the orientation of C_f-Cu in 3D space., the 2D cross-section is parallel to the X-O-Z plane, and the intersection line of C_f-Cu and the 2D cross-section is an ellipse. Figure 3-3(b) is a simplified schematic diagram of Figure3-3(a). θ_{2D} is the angle between C_f-Cu and the heat flow on the 2D cross-section. θ_{3D} is the angle between the C_f-Cu and the heat flow in 3D space. α is the angle between projection of C_f-Cu on X-O-Z plane and heat flow in 3D space. The intersection line of C_f-Cu with the 2D cross-section is an ellipse, which can be expressed as follows:

$$sin^2\theta_{3D}x^2 - \cos\theta_{3D}\sqrt{cos^2\theta_{2D} - cos^2\theta_{3D}}\, z^2 = r^2$$

$$R = \frac{b}{a} = \sin\theta_{2D}$$

······ (3-2)

Where, R is the ratio of the minor axis to the major axis of the ellipse, R=b/a. Orientation of C_f-Cu in 3D is related to the value of R. The θ_{3D} in 3D model is closely related to the α and R of C_f-Cu. Their relationship is given by the equation.

$$\cos\theta_{3D} = \cos\alpha * \cos\theta_{2D} = \cos\alpha * \sqrt{1-R^2} \qquad 0° \ll \alpha, \theta_{2D}, \theta_{3D} \ll 90°$$

······ (3-3)

In Figure 3-3(c), when C_f-Cu is parallel to the X-O-Z plane, the cross-section of C_f-Cu in X-O-Z planes is a rectangle. In Figure 3-3(d), α=0, and substituting α into Eq. (3-3), θ_{3D}=θ_{2D}.

Extract as many 2D cross-sections as possible from the 3D model, all cross-sections are parallel to the X-O-Z plane and obtain OM images of all cross-sections under an optical microscope. θ_{3D} can be obtained using Eqs. (3-1) and (3-2) by measuring and counting α and R on the OM image.

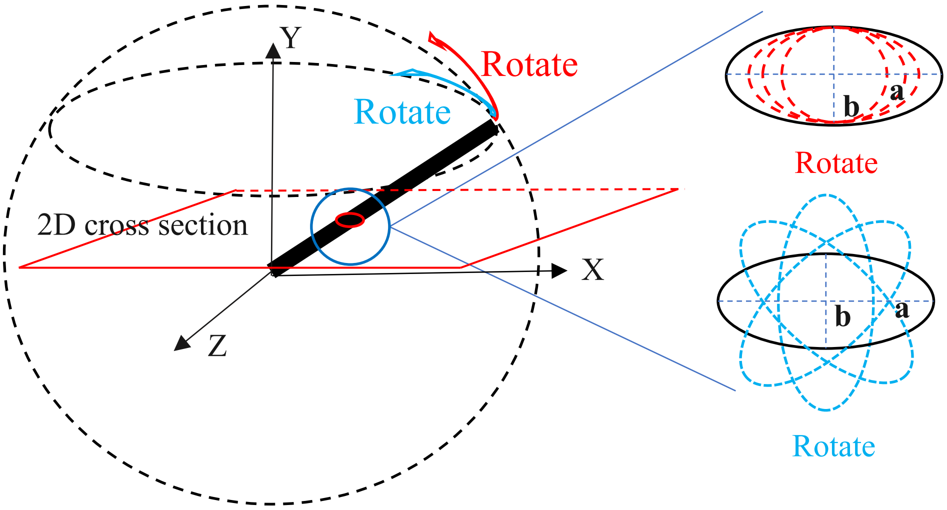

Figure 3-2 Rotation of C_f-Cu in the 3D model.

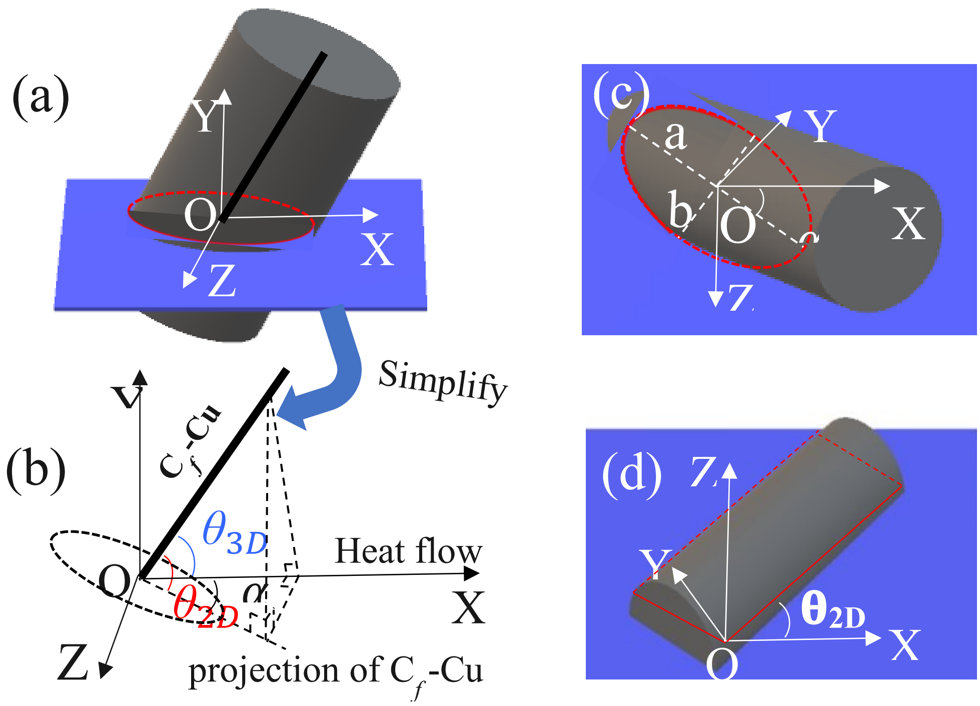

Figure 3-3 C_f-Cu in the 3D model. Simplify (a) to get (b), heat flow is X-axis, θ_{3D} is the angle between C_f-Cu and heat flow, α is the angle between the projection of C_f-Cu and heat flow, θ_{2D} is the angle between C_f-Cu and projection of C_f-Cu. (c) when C_f-Cu is not parallel to X-O-Z plane, the intersection line formed by C_f-Cu and the cross-section is an ellipse. (d) when C_f-Cu is parallel to X-O-Z plane, the intersection line formed by C_f-Cu and the cross-section is a rectangle.

3.2.4 Calculation of thermal conductivity of C_f-Cu

C_f is a highly anisotropic material with respect to the TC in two dimensions cross-sections. The heat flux was set along the X-axis, the effective TC of a C_f-Cu on X-axis (K_i) and Y-axis (K_j) can be expected as following equations[26,27].

$$K_i = K_x\left[1-\left(1-\frac{K_y}{K_x}\right)\sin^2\theta_{2D}\right] \qquad K_j = K_x\left[1-\left(1-\frac{K_y}{K_x}\right)\cos^2\theta_{2D}\right]$$

…… (3-4)

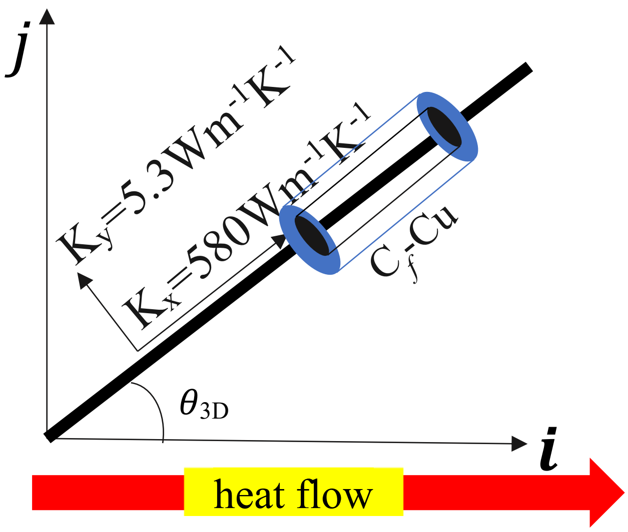

Figure 3-4 TC calculations of C_f-Cu in the direction of heat flow.

K_x and K_y are the TCs in the directions parallel and perpendicular to C_f-Cu, respectively. while K_i and K_j are the TCs of C_f-Cu in the directions parallel and perpendicular to the heat flow, respectively. The temperature distribution on the 2D section can be obtained by considering the K_i and K_j of each C_f-Cu.

3.2.5 2D image-based simulation method

The finite-volume method was used to calculate the 2D temperature distributions. The temperature of the elements can be calculated using the following equation[26,28]:

$$T_{x,y}^{n+1} = T_{x,y}^{n} + \frac{\Delta t}{\rho c}\left(\frac{q_{x+1,y}^{n} - q_{x-1,y}^{n} q_{x-1,y}}{\Delta x} + \frac{q_{x,y+1}^{n} - q_{x,y-1}^{n}}{\Delta y}\right)$$

…… (3-5)

Where x and y represent the coordinate position of the element, $T_{x,y}^{n}$ is the temperature of the element at coordinates (*x, y*), $T_{x,y}^{n+1}$ is the temperature of the element at coordinates (x, y) after a period Δt. ρ is the density, c is the specific heat. Δx and Δy represents the size of the elements on the x-axis and y-axis, respectively. $q_{x,y}^{n}$ represents the heat of the element at the coordinate (*x, y*). Figure 3(a) shows that when the heat of the coordinates (x, y) is transferred to the surroundings, the heat of element at the position near the coordinates (x, y) can be expressed by the following equation.

$$q_{x+1,y}^{n} = K_{x+\frac{1}{2},y}\left(\frac{T_{x+1,y}^{n}-T_{x,y}^{n}}{\Delta x}\right) \qquad q_{x-1,y}^{n} = K_{x-\frac{1}{2},y}\left(\frac{T_{x,y}^{n}-T_{x-1,y}^{n}}{\Delta y}\right)$$

$$q_{x,y+1}^{n} = K_{x,y+\frac{1}{2}}\left(\frac{T_{x,y+1}^{n}-T_{x,y}^{n}}{\Delta y}\right) \qquad q_{x,y-1}^{n} = K_{x,y-\frac{1}{2}}\left(\frac{T_{x,y}^{n}-T_{x,y-1}^{n}}{\Delta y}\right)$$

$$K_{x+\frac{1}{2},y} = \frac{2K_{x,y}K_{x+1,y}}{K_{x,y}+K_{x+1,y}} \qquad K_{x-\frac{1}{2},y} = \frac{2K_{x,y}K_{x-1,y}}{K_{x,y}+K_{x-1,y}}$$

$$K_{x,y+\frac{1}{2}} = \frac{2K_{x,y}K_{x,y+1}}{K_{x,y}+K_{x,y+1}} \qquad K_{x,y-\frac{1}{2}} = \frac{2K_{x,y}K_{x,y-1}}{K_{x,y}+K_{x,y-1}}$$

…… (3-6)

Where $K_{(x,y)}$ represents the TC of element at the coordinate (x, y). $K_{(x+1,y)}$, $K_{(x-1,y)}$, $K_{(x,y+1)}$ and $K_{(x,y-1)}$ represents the TC at the position near the coordinates (x, y). $K_{(x+1/2,y)}$, $K_{(x-1/2,y)}$, $K_{(x,y+1/2)}$ and $K_{(x,y-1/2)}$ represents the harmonic average of TC.

Due to thermal expansion and contraction in the composite preparation process, voids are generated. The different materials such as Fe, Cu, C_f and air in the composite contact each other and cause heat loss during the heat conduction process. Therefore, the influence of interface thermal resistance must be considered. The interface heat transfer coefficient is h. The heat at the contact interface of different materials can be obtained by the following equation.

$$q_{x+1,y}^{n} = h\left(T_{x+1,y}^{n} - T_{x,y}^{n}\right) \quad q_{x-1,y}^{n} = h\left(T_{x,y}^{n} - T_{x-1,y}^{n}\right)$$

$$q_{x,y+1}^{n} = h\left(T_{x,y+1}^{n} - T_{x,y}^{n}\right) \quad q_{x,y-1}^{n} = h\left(T_{x,y}^{n} - T_{x,y-1}^{n}\right)$$

…… (3-7)

The heat equation given by the Laplace operator is used as the basis of the simulation program. The temperature of the element can be calculated by using this equation. The schematic diagram of the simulation model is shown in Figure 3-5, the simulation model includes two heat sources and composites. Both the top surface and the bottom surface correspond to the periodic boundary of heat conduction, while the left and right sides correspond to the adiabatic boundary to prevent thermal diffusion. The composite part is based on the microstructure of the sample. Therefore, the size ($N_x \times N_y$) of all samples is 960×1280 elements. The size of the left and right heat sources is 5×1280 elements (NL = NR = 5 elements). The size of each element is 1.18×10^{-6} m. The heat source on the left is set to 303K, and the heat source on the right is set to 293K, keeping the temperature of the left and right heat sources constant. The temperature of the remaining elements is iterated until the temperature change is less than 10^{-13} K, and the steady-state temperature distribution in the thermal equilibrium state is obtained. The simulated effective TC value of C_f-Cu/Fe, $K_{Simulated}$, in the equilibrium state, the temperature distribution is as follows[26,27,29]:

$$K_{Simulated} = \frac{K_m \triangle T_{12} N_x}{\triangle T_{LR} + N_L \triangle T_{12} - N_x \triangle T_{12}} \quad \cdots\cdots (3\text{-}8)$$

K_m is the TC of the C_f-Cu/Fe composite compounded with different C_f-Cu content, ΔT_{LR} is the temperature difference between the left and right sides, and ΔT_{12} is the average temperature difference between the first column and the second column. N_L and N_R are the number of elements on the left and right heat sources, respectively. N_x is the number of elements along the corresponding direction.

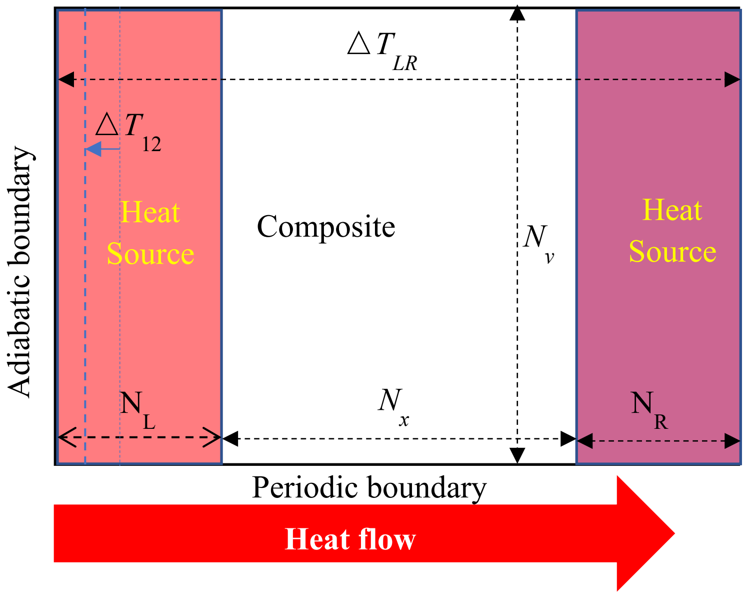

Figure 3-5 Simulation model for the effective TC calculation of C_f-Cu/Fe composite.

3.3 Results and discussion

3.3.1 Porosity of composites and thermal conductivity of the matrix

The porosity of C_f-Cu/Fe composite and the matrix TC correction results are list in Table 3-1. The porosity of the composite and TC of matrix both increase with the increase of the C_f-Cu content. When the volume fraction of C_f-Cu is lower than 20%, the porosity does not exceed 2.5%, and there are very few voids in the composite. These voids have little effect on the TC of matrix. When the volume fraction of C_f-Cu exceeds 20%, the porosity increases to 6.8%, and there are many voids in the composite. The effect of air on its internal heat conduction hindering effect increases significantly and the TC of the matrix decreases to 48.5 $Wm^{-1}K^{-1}$.

Table 3-1 Volume fraction of voids in the C_f-Cu/Fe composite and the corresponding TC of the matrix, V_p and K_m denote the Volume fraction of voids and TC of matrix, respectively.

volume fraction of C_f-Cu, f_v / %	0	5	10	15	20	25
V_p (%)	0.4	0.8	1.3	1.7	2.5	6.8
K_m / W m^{-1} K^{-1}	54	53.67	52.95	52.62	51.98	48.5

3.3.2 Orientation of C_f-Cu in 3D matrix

Figure 3-6 shows plane B of the rolled C_f-Cu/Fe composite, a frequency histogram was obtained by counting the occurrence frequencies of α and R of C_f-Cu in various directions. The statistical results α and R corresponding to the 2D cross-section, θ_{3D} can be obtained by Eq (3-3). The statistical results of θ_{2D}, correspond to the case shown in Figure 3-7, in the plane A of the rolled C_f-Cu/Fe composite, where $\alpha=0$, $\theta_{3D}=\theta_{2D}$. This indicates that hot rolling promoted the arrangement of C_f-Cu along the heat flow.

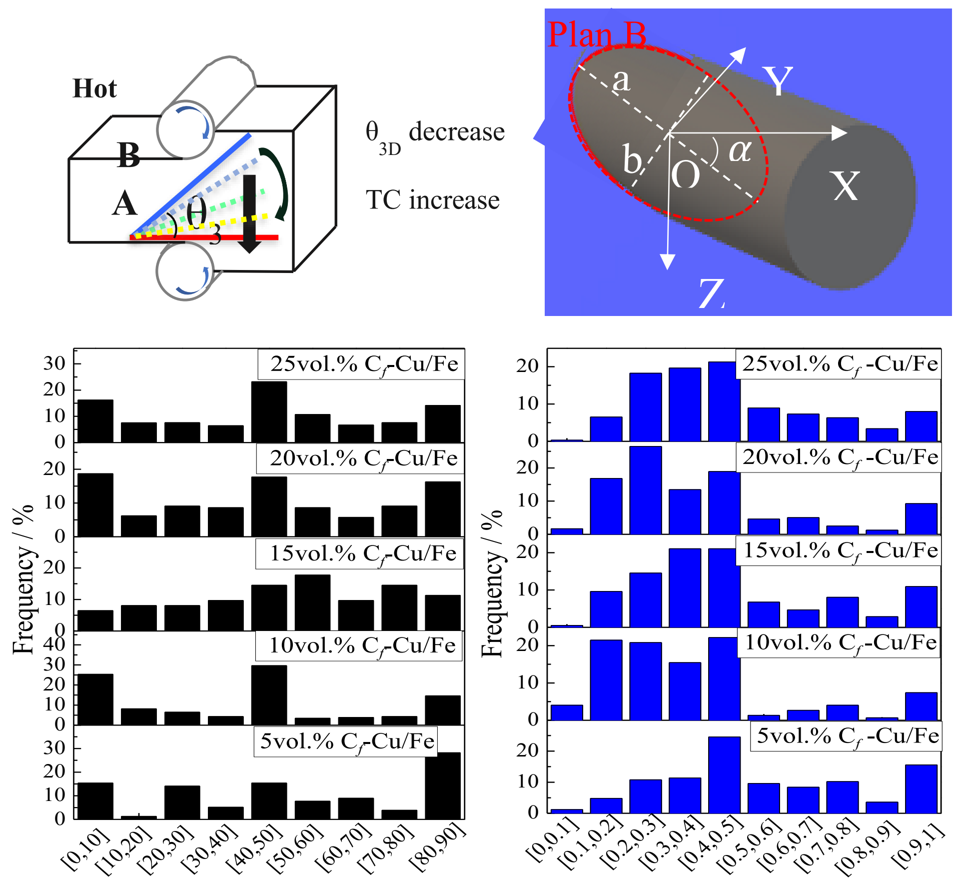

Figure 3-6 Frequency histograms of α and R in the B plane for rolled C_f-Cu/Fe composites with different C_f-Cu contents.

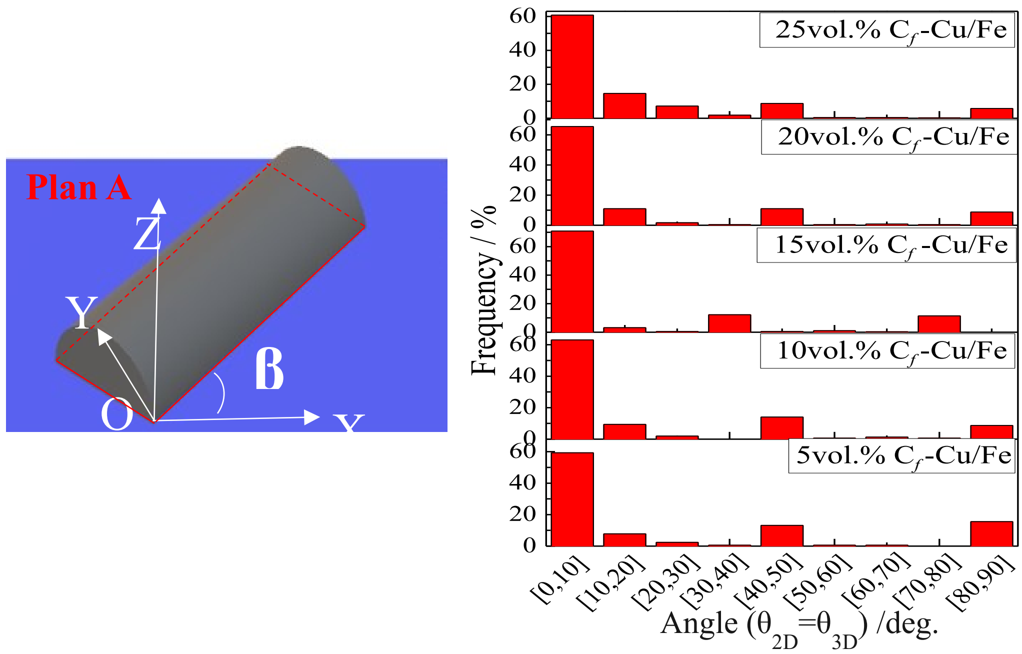

Figure 3-7 Frequency histograms of θ_{2D} in the A plane for rolled C_f-Cu/Fe composites with different C_f-Cu contents.

3.3.3 Effect of orientation of C_f-Cu on the TC of composites

The TC of C_f-Cu in the axial and radial directions are 580 $Wm^{-1}K^{-1}$ and 5.3 $Wm^{-1}K^{-1}$, respectively. Substituting this result into equation (3-4), obtain the influence of θ_{3D} on the TC of C_f-Cu in the direction of heat flow, as shown in Figure 3-8. Obviously, the effective TC gradually decreases as θ_{3D} increases. Regardless of the effect of voids on the TC of the matrix, K_m=54 $Wm^{-1}K^{-1}$, when θ_{3D} is 73.08°, K_{Fe} and K_i have the same value. when θ_{3D} was less than 73.08°, K_i is greater than K_{Fe}, and the TC of C_f-Cu in the direction of heat flow was higher than that of the pure Fe, C_f-Cu can improve the TC of composite, and vice versa. The same principle, considering the effect of voids on the TC of the matrix, $K_m \neq 54$ $Wm^{-1}K^{-1}$, The corrected results of K_m for C_f-Cu/Fe with different volume fractions are listed in Table 3-1. C_f-Cu/Fe with different volume fractions have different θ_{3D}. (x vol.% C_f-Cu/Fe, x=5, θ_{3D}=73.14°. x=10, θ_{3D}=73.26°. x=15, θ_{3D}=73.32°. x=20, θ_{3D}=73.44°. x=25, θ_{3D}=74.09°). Figure 3-7 shows that most of C_f-Cu has an angle less than 73° with the direction of heat flow, which indicates that most of the C_f-Cu can be used as a heat conduction channel to effectively improve the TC of the composite.

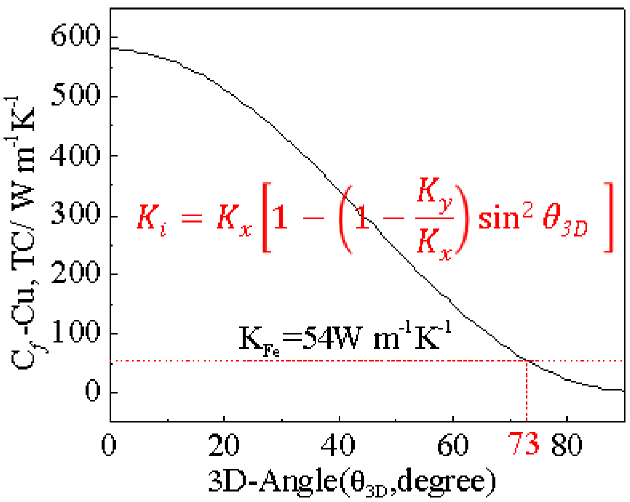

Figure 3-8 Relationship between θ_{3D} and the effective TC of C_f in the direction of heat flow.

3.3.4 Effect of hot rolling on the TC of composites

Figure 3-9(a) shows that the frequency distribution of θ_{3D} of 25vol.%C_f-Cu/Fe have been counted and plotted. There are still a few C_f-Cu perpendicular to the heat flow after hot rolling, θ_{3D} =90°, because of the cross-connect and folding of C_f-Cu during sintering and rolling. Figure 3-9(b) shows that during the rolling process, C_f-Cu folds, and crosslinks. Figure 3-9(c) shows the real state of C_f-Cu in the composite after rolling. This causing part of the C_f-Cu to bend, while some C_f-Cu intersect and obstruct each other. This accounts for the large θ_{3D} value in the composites after rolling. The rolling process promoted the arrangement of C_f-Cu along the direction of heat flow, which effectively increased the TC of the composite. This was also observed in the study of Yang[27]. During SPS and hot rolling, the composite gradually became dense, the height and θ_{3D} decreases, and TC increased. After hot rolling, the TC of the composite increased from 47.18 W m^{-1} K^{-1} to 68.89 W m^{-1} K^{-1}.

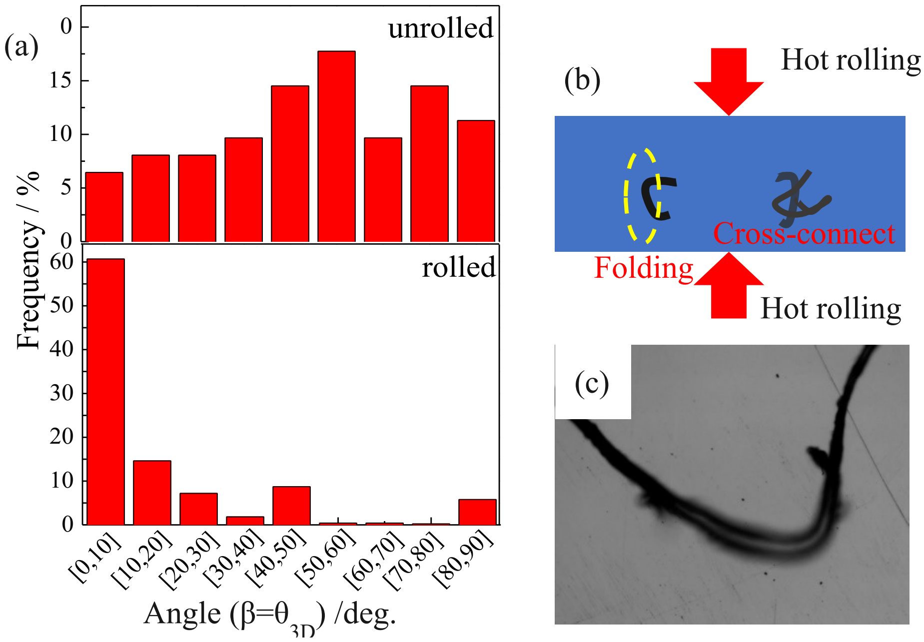

Figure 3-9 (a) Orientation of C_f-Cu in the 20vol.%C_f-Cu/Fe composite before and after rolling. (b) Large values of θ_{3D} which exist because the C_f-Cu fold over and cross each other. (c) Folding of C_f-Cu in the rolled composite.

3.3.5 Temperature distribution of A/B plane of composites

The effective TC in the direction of the heat flow of each element (C_f-Cu and Fe matrix) was calculated and an effective TC map of the elements on the 2D section was obtained in the steady state. Figure 3-10 shows the map of effective TC of elements on the 2D section of composites with different volume fractions on the A/B plane. On the A plane, most of the C_f-Cu is parallel to the heat flow, C_f-Cu exhibits a high TC, and θ_{3D} is primarily distributed at a smaller angle, which is consistent with the result shown in Figure.3-7. In the 2D cross-section simulation diagram, assuming that the right direction is the direction of heat flow, the matrix of the composite is blue, C_f-Cu exhibited high TC, and the C_f-Cu is marked in red, θ_{3D}=0°. As θ_{3D} increases, the color of C_f-Cu gradually changes from red to blue, indicating a decrease in TC. C_f-Cu is evenly distributed in the Fe matrix. On the B plane, C_f-Cu is uniformly and freely distributed in the composite because C_f-Cu was not aligned. Its distribution of C_f-Cu is similar to the cross-section of an unrolled composite.

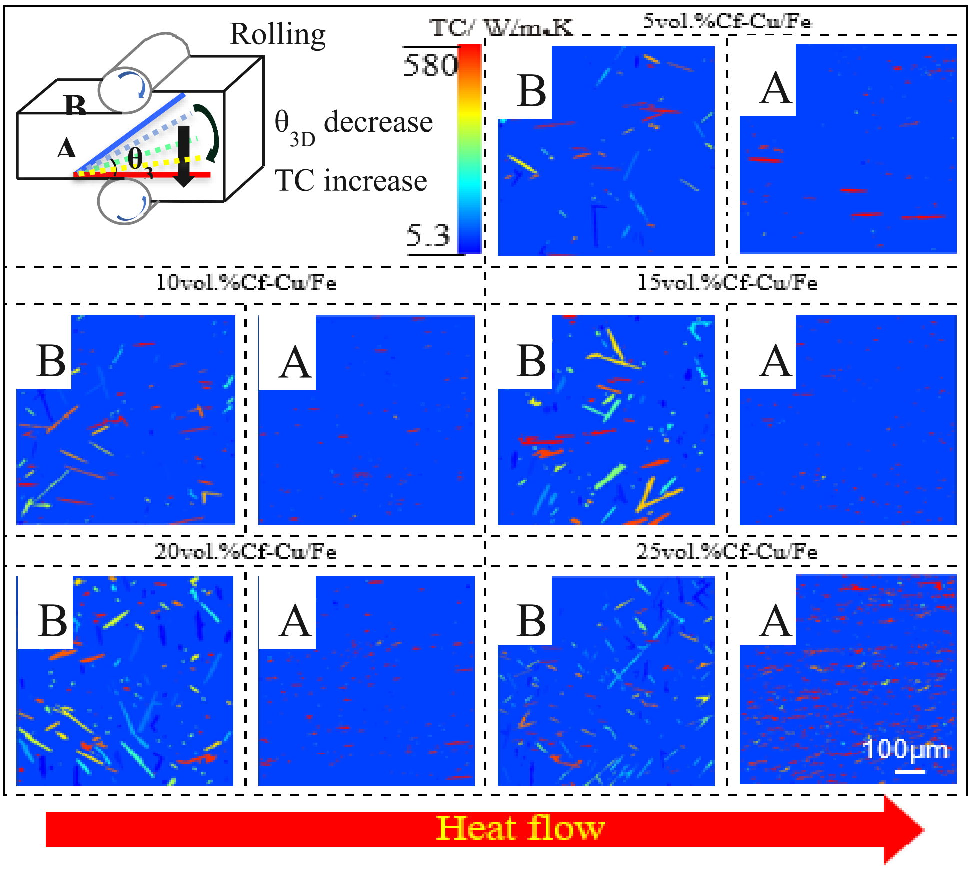

Figure 3-10 Effective TC diagrams of the elements (C_f-Cu and Fe matrix) on the 2D crosse-section of composites with different volume fractions of C_f-Cu.

3.3.6 Measured and simulated thermal conductivity

Figure 3-11 shows the results for the measurements of TC on the A plane before and after rolling and the simulated TC on the A/B plane of rolled composites with different volume fractions of C_f-Cu. On the A plane, after rolling, the simulated value is larger than the measured value owing to experimental error, and displays the same trend as the measured value, with a small deviation of 3% to 4%. When the volume fraction of C_f-Cu is lower 20%, the simulated and measured values increase with increasing C_f-Cu content. When the volume fraction of C_f-Cu exceeds 20%, both decrease with the increase in C_f-Cu content; in addition, the porosity increases sharply (shown in Tab.3-1) and the TC decreases. Its hindering effect on TC was greater than the effect of increased C_f-Cu content on the improvement of TC. When the volume fraction of C_f-Cu is 20%, the simulated and measured values attain their maximum values simultaneously, which are 71.02 $Wm^{-1}K^{-1}$ and 68.89 $Wm^{-1}K^{-1}$, respectively. Before rolling, the measured TC increased with the C_f-Cu content. C_f-Cu acted as a heat conduction channel to increase the TC of the composites. Because $\theta_{2D}\neq 0$(the angle between C_f-Cu and the projection of C_f-Cu), the measured TC before and after rolling had large deviations of 40%- 60%.

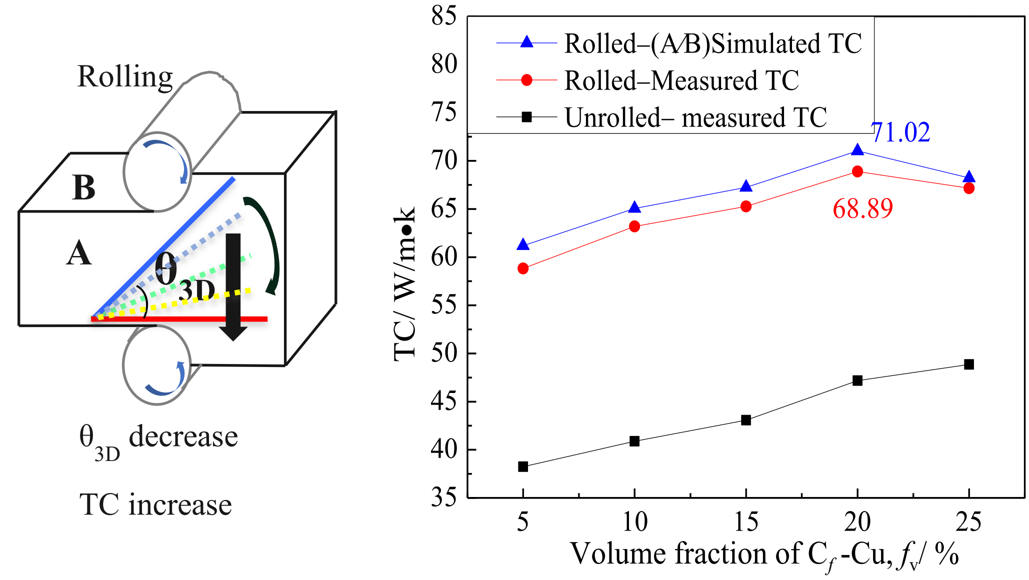

Figure 3-11 Simulated and measured TC of C_f-Cu/Fe composites with different volume fractions of C_f-Cu on the A/B plane.

3.4 Summary

In this chapter, 5 (10, 15, 20, 25) vol.% C_f-Cu/Fe composites were prepared by SPS. The porosity and TC of the C_f-Cu/Fe composites before and after being rolled with different C_f-Cu content were measured, and the TC of the matrix was calculated. The TCs of the composites were also simulated by 2D image simulation. The conclusions drawn in this chapter are summarized as follow. Our conclusions are listed below:

(1) The TC of the matrix of C_f-Cu/Fe composites decreased with the increasing C_f-Cu content. When the volume fraction of C_f-Cu exceeds 20%, the porosity was higher than 2.5%, and the TC dropped to 48.5 W m^{-1} K^{-1}.

(2) The ETC of each element (C_f-Cu and Fe matrix) in the 2D section can be obtained by counting the orientation and frequency of α and R of C_f-Cu on the 2D cross section of C_f-Cu/Fe composites, which was used to calculate theθ_{3D}.

(3) Rolling treatment can effectively control the orientation of C_f-Cu, and almost all the axial direction of C_f-Cu are oriented along the direction of heat flow. When $\theta<73°$, C_f-Cu can increase the TC of the C_f-Cu/Fe composite.

(4) On the A plane, the simulated value is consistent with the measured value, with deviations between 3%-4%. When the volume fraction of C_f-Cu was 20%, the simulated and measured values attained their maximum value of 68.89 Wm^{-1}K^{-1} and 71.02 Wm^{-1} K^{-1}, respectively. Owing to the rolling treatment, the measured TCs before and after rolling exhibit a large deviation of 40% to 60%.

3.5 References

[1]Naderi M, Ketabchi M, Abbasi M,Bleck W. Analysis of microstructure and mechanical properties of different high strength carbon steels after hot stamping.Journal of Materials Processing Technology. 2011;211(6):1117-1125.

[2]Bao L, Liu W J, Wang B, Li H, You X, Zhou Q, Liu M,Gao S. Experimental investigation on partition controllable induction heating-hot stamping process of high-strength boron alloyed steel plates with designable temperature patterns.Journal of Materials Research and Technology. 2020;9(6):13963-13976.

[3]Chantzis D, Liu X, Politis D J, El Fakir O, Chua T Y, Shi Z,Wang L. Review on additive manufacturing of tooling for hot stamping.The International Journal of Advanced Manufacturing Technology. 2020;109(1-2):87-107.

[4]Mori K, Akita K,Abe Y. Springback behaviour in bending of ultra-high-strength steel sheets using CNC servo press.International Journal of Machine Tools and Manufacture. 2007;47(2):321-325.

[5]Jing C, Ye D, Zhao J, Lin T, Wu C,Lei Q. Effect of hot stamping and quenching & partitioning process on microstructure and mechanical properties of ultra-high strength steel.Materials Research Express. 2021;8(3):036506.

[6]Liu H, Jin X, Dong H,Shi J. Martensitic microstructural transformations from the hot stamping, quenching and partitioning process.Materials Characterization. 2011;62(2):223-227.

[7]Zhang P, Zhu L, Xi C,Luo J. Study on Phase Transformation in Hot Stamping Process of USIBOR® 1500 High-Strength Steel.Metals. 2019;9(10):1119.

[8]Karbasian H,Tekkaya A E. A review on hot stamping.Journal of Materials Processing Technology. 2010;210(15):2103-2118.

[9]Chang Y, Li G, Wang C, Li X,Dong H. Effect of Quenching and Partitioning with Hot Stamping on Martensite Transformation and Mechanical Properties of AHSS.Journal of Materials Engineering and Performance. 2015;24(8):3194-3200.

[10]Muro M, Artola G, Gorriño A,Angulo C. Effect of the Martensitic Transformation

on the Stamping Force and Cycle Time of Hot Stamping Parts.Metals. 2018;8(6):385.

[11]Shen Y, Song Y, Hua L,Lu J. Influence of Plastic Deformation on Martensitic Transformation During Hot Stamping of Complex Structure Auto Parts.Journal of Materials Engineering and Performance. 2017;26(4):1830-1838.

[12]Kontani H, Tokunaga T, Ohno M, Sasaki K, Matsuura K. Fabrication of unidirectionally orientated carbon fiber reinforced cu-based composites by hot extrusion and evaluation of their thermal properties.Journal of the Japan Institute of Metals and Materials. 2018; 82(5): 125-129.

[13]Tokunaga T, Takahashi K, Ohno M, Sasaki K, Imanishi T,Matsuura K. Fabrication of Carbon Fiber Oriented Al-Based Composites by Hot Extrusion and Evaluation of Their Thermal Conductivity.Journal of the Japan Institute of Metals. 2016;80(10):640-645.

[14]Ma J, Shang T, Ren L, Yao Y, Zhang T, Xie J, Zhang B, Zeng X, Sun R, Xu J-B,Wong C-P. Through-plane assembly of carbon fibers into 3D skeleton achieving enhanced thermal conductivity of a thermal interface material.Chemical Engineering Journal. 2020;380(122550.

[15] Pietrak K, Wiśniewski T S. A review of models for effective thermal conductivity of composite materials.Journal of Power Technologies, 2015; 95(1).

[16]Wang J, Chen Y, Feng Y, Zhao G, Jian X, Huang Q, Yang L,Xu J. Influence of porosity on anisotropic thermal conductivity of SiC fiber reinforced SiC matrix composite: A microscopic modeling study.Ceramics International. 2020;46(18):28693-28700.

[17]Jopek H, Strek T. Optimization of the effective thermal conductivity of a composite.Convection and Conduction Heat Transfer. 2011;197-214.

[18]Zhang G, Xia Y, Wang H, et al. A percolation model of thermal conductivity for filled polymer composites.Journal of composite materials. 2010;44(8):963-970.

[19]Gao L, Zhou X, Ding Y. Effective thermal and electrical conductivity of carbon nanotube composites.Chemical Physics Letters. 2007; 434(4-6): 297-300.

[20]Xue Q Z. Model for the effective thermal conductivity of carbon nanotube composites.Nanotechnology. 2006;17(6):1655-1660.

[21]Wang M, He J, Yu J, et al. Lattice Boltzmann modeling of the effective thermal conductivity for fibrous materials.International Journal of Thermal Sciences. 2007; 46(9): 848-855.

[22]She W, Zhang Y,Jones M R. Three-dimensional numerical modeling and simulation of the thermal properties of foamed concrete.Construction and Building Materials. 2014;50(421-431.

[23]Wang M, Kang Q,Pan N. Thermal conductivity enhancement of carbon fiber composites.Applied Thermal Engineering. 2009;29(2-3):418-421.

[24]Naderi S,Zhang M. A novel framework for modelling the 3D mesostructure of steel fibre reinforced concrete.Computers & Structures. 2020;234(106251.

[25]Landauer R. The electrical resistance of binary metallic mixtures.Journal of applied physics, 1952;23(7): 779-784.

[26]Zhao Y, Sugio K, Choi Y, Gen S, Xu Z,Yu J. Effect of Anisotropic Thermal Conductivity of Graphite Flakes and Interfacial Thermal Resistance on the Effective Thermal Conductivity of Graphite Flakes/Aluminum Composites.Materials Transactions. 2021;62(1):98-104.

[27]Yang L, Miyoshi Y, Sugio K, Choi Y, Matsugi K,Sasaki G. Effect of graphite orientation distribution on thermal conductivity of Cu matrix composite.Materials Chemistry and Physics. 2021;257(123702.

[28]Sugio K, Choi Y-B,Sasaki G. Effect of the Interfacial Thermal Resistance on the Effective Thermal Conductivity of Aluminum Matrix Composites.Materials Transactions. 2016;57(5):582-589.

[29]Sugio K, Choi Y-B,Sasaki G. Effect of the Interfacial Thermal Resistance on the Effective Thermal Conductivity.Materials Transactions. 2016;57(5):582-589.

Chapter 4

Influencing factors and degrees of thermal conductivity of C_f-Cu/Fe composites

4.1 Introduction

Improving the TC of hot stamping dies can not only improve production efficiency and obtain high-strength auto parts through rapid heat conduction, but also reduce die cracking and increase die service life[1,2]. Considering the scattering effect of impurity atoms on phonon heat conduction[3-5], pure iron is used as the matrix. C_f has high TC in the axial direction and can be used as a heat conduction channel to improve the TC of the composite[6-8].

The 3 chapter has introduced that the orientation of C_f-Cu in 5-25vol.%C_f-Cu/Fe composite has a significant impact on the TC, C_f-Cu can be arranged along the heat flow direction by hot rolling. Improving the TC of the composite by controlling the C_f, which has been confirmed in many literatures. Matsuura. et al.[9,10] used the method of hot extrusion to orient C_f along the extrusion direction in the composite. Ma et al.[11] found that the orientation of C_f can be determined according to the designed direction by the rapid freezing method(Freeze drying at 225K and 27 Pa for 50 hours). Meanwhile, the hindering effect of C_f-Cu content and voids on heat conduction was also investigated.

However, in C_f-reinforced metal composite systems, factors affecting heat conduction are not limited to voids and content and orientation of C_f, but other factors, such as type, structure and aspect ratio of C_f, synergistic effect (network structure) and temperature will affect the heat conduction of C_f-reinforced metal composite. The precursors of C_f are mainly include polyacrylonitrile (PAN) and pitch[12], and the higher the degree of orientation and crystallinity of crystallites in C_f, the higher of the TC[13]. PAN-based C_f have excellent mechanical properties, while pitch-based C_f forms a structure similar to graphite single crystals during post-processing, which is beneficial to heat conduction[14]. Inoue et.al.[15] used PAN-based C_f (T300) and pitch-based C_f (K223HG) to reinforce ZrB2-SiC-ZrC (ZSC) composites. The TC of K223HG-reinforced composites is higher than that of T300-reinforced composites, and PAN-based C_f-reinforced composites has a lower density and better mechanical properties.

The length of C_f will affect the thermal conductivity of the composite material [83]. the longer C_f in the composite with high C_f content is easier to form heat conduction channels and the promotion of heat transfer[16], and the shorter C_f in the composite with low C_f content are easily dispersed to form oriented structures that facilitate thermal diffusion[17].

The TC of the void is about 0.03 W·m^{-1}K^{-1}. In the composite, the TC of pure iron is 54 W·m^{-1}K^{-1}, and the axial and radial TC of C_f-Cu are 580 W·m^{-1}K^{-1}, respectively. 1 and 5.3 W·m^{-1}K^{-1}. The voids of the C_f-Cu/Fe composites seriously hinder the TC. Wang et al.[18] summarized the calculation model of the TC of the void-containing composites. The equations of the voids and TC of the material can be Expressed as:

$$\frac{K_{Effective}}{K_m} = (1-\omega)^n = \left(1 - \frac{V_p}{1-V_f}\right)^n$$

$\cdots\cdots$ (2-1)

where, ω is the relative matrix porosity, $K_{Effective}$ and K_m are the ETC of the corrected material and the TC of the matrix, respectively. For different theoretical models, N has different values. n = 1.5, 1.65-1.85 and 1.55 for the Bruggeman model, Scaling relation and Progelhoff model, respectively. Solórzano[19] believed that n is a geometric factor of pores, which is related to the shape, connectivity and topology. Choosing a suitable processing method can simplify the operation and save money.

A lot of ideal models have been established in the related research of heat conduction. However, these models are very different from the actual situation, and the heat transfer in the actual situation is more complicated. Void, orientation, and content of C_f are all factors that hinder the TC of composites. The interface thermal resistance obtained by many models cannot represent the real thermal resistance of the material. In this paper, powder metallurgy technology was used to prepare Copper plated carbon fiber (C_f-Cu) reinforced iron matrix composites with different volume fractions, the Bregman equation was used to correct the TC of the iron matrix containing voids. The composite TC (K_{ROM} and K_{EMA}) under the layer-in-parallel (ROM)[20] and the effective medium approximation (EMA) models were calculated. The simulated TC ($K_{simulated}$)

was obtained by simulating the thermal distribution of the elements on the 2D section by the finite element volume method. The measured TC of the composite was measured by the steady-state method. We consider the difference between calculated and measured TC as a heat conduction hindering factor, and Figure 4-1 shows various factors that affect heat conduction in the real composite. The influence degree of contact thermal resistance (R_{123}), voids(R_4), orientation and aspect ratio of C_f-Cu(R_5) and experimental error on the TC of C_f-Cu/Fe composites was investigated by comparing the calculated TC by mixing rules and effective approximation theory, the simulated TC by 2D image simulation and the measured TC by the steady-state method.

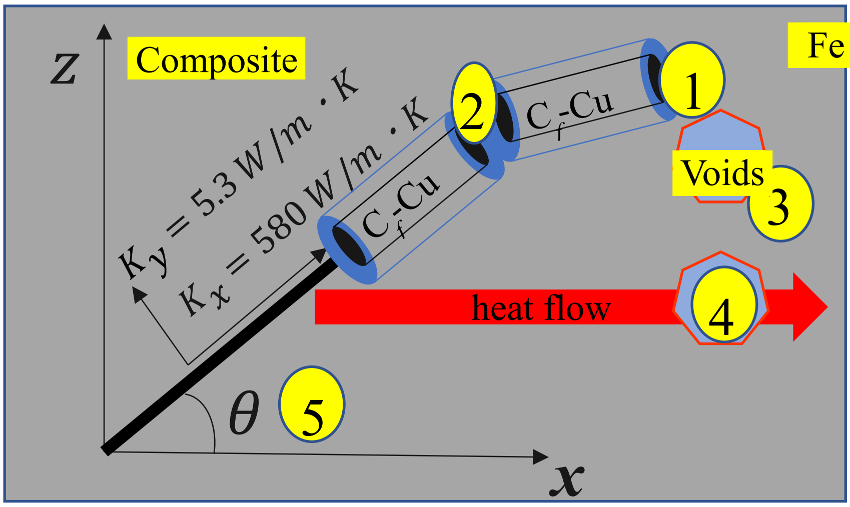

Figure 4-1 Factors that hinder the heat conduction of composites. Contact thermal resistance, $R_{123}=R_1+R_2+R_3$, voids and Fe in contact with each other. voids, R_4. orientation and aspect ratio of C_f-Cu, R_5。

4.2 Experimental and calculation procedure

4.2.1 Experiments

In this study, Fe powder (FEE14PB, 100% in purity, Kojundo Chemical Laboratory Co., Ltd., Japan, 7.874 kg m^{-3}) were used, and the average diameter was 5~10 µm. The pitched-based C_f (K13C6U, Mitsubishi Chemical Co., Ltd., Japan, 2.18 kg m^{-3}, 8.6 µm of average diameter) was shortcut into about 4.5 mm. C_f-Cu with a copper layer of 0.27 µm was obtained by electroless copper plating of chopped C_f to prevent C_f from contacting with the iron substrate and chemically reacting and being destroyed. C_f-Cu/Fe composite (die material) was fabricated by SPS. In order to distribute the axial direction of C_f-Cu in the composite along the direction of heat flow, hot rolling was used to change the orientation of C_f-Cu under the condition of rolling speed of 18r/min and compression rate of 50%. Figure 4-2 shows the direction of SPS pressurization, hot pressing and thermal conductivity measurement. The relative density of the composites was measured by the Archimedes method. The ETC of the composites was measured at 300K by a steady-state thermal conductivity measurement device.

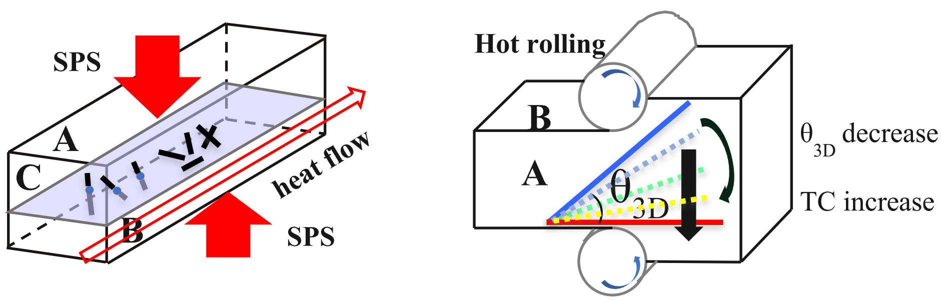

Figure 4-2 The direction of SPS pressing, hot pressing and thermal conductivity measurement of the composite.

4.2.2 Numerical methods

The copper prevents the C_f from contacting and reacting with the iron. This reaction will destroy the continuity of the C_f and increase the interface thermal resistance. gap is formed between the copper layer and the iron, air hinders heat conduction, and TC of the matrix needs to be corrected. The Bruggeman equation can be used to calculate the effective TC of the composite with pores.

$$K_m = \frac{1}{4}\left[K_p(3V_p - 1) + K_{Fe}(3V_{Fe} - 1) + \left\{\left[K_p(3V_p - 1) + K_{Fe}(3V_{Fe} - 1)\right]^2 + 8K_pK_{Fe}\right\}^{1/2}\right]$$

...... (2-2)

K_{Fe} and K_p are the TC of iron (54 W m^{-1} K^{-1}) and air (0.03 W m^{-1} K^{-1}), respectively. V_{Fe} and V_p are the volume fraction of iron and air, respectively.

When studying a certain property of composite, a relatively simple method is to set a layer-in-parallel (ROM) model, which is shown in Figure 4-3(a). If all C_f-Cu is a long fiber horizontally distributed in the composite, ignoring all internal and external influencing factors, only the composition ratio of the components is used to determine the TC of the composite. The TC of the composite can be expressed by equation.

$$K_C = K_{Cf-Cu} \times V_{Cf-Cu} + K_m \times (1 - V_{Cf-Cu})$$

...... (2-3)

Where K_C, $K_{Cf\text{-}Cu}$ and K_m are the TC of composite, C_f and matrix, respectively. $V_{Cf\text{-}Cu}$ is the volume fraction of C_f-Cu in the composite. Considering the effect of the internal thermal resistance and on the TC of the composite, the effective TC of C_f-Cu (K_{Cf-Cu}^{eff}) can be modified by the equation:

$$K_{Cf-Cu}^{eff} = \frac{K_{Cf-Cu}}{1 + \frac{2K_{Cf-Cu}}{hd}}$$

...... (2-4)

Where, h is the thermal conductivity coefficient, 6.4×10^7W$m^{-2}$$K^{-1}$, which is the reciprocal of ITR.

$$K_C = \frac{K_{Cf-Cu}}{1 + \frac{2K_{Cf-Cu}}{hd}} \times V_{Cf-Cu} + K_m \times (1 - V_{Cf-Cu})$$

...... (2-5)

All C_f-Cu is set as one long fiber in the ROM model, but the C_f-Cu may be interrupted during the preparation of the composite, which increases the contact interface of C_f-Cu. Therefore, the aspect ratio and content of C_f-Cu need to be considered when building the model. Nan et al. introduced a method for predicting the ETC of particle-reinforced composites with ITR while studying the relationship between particle shape and contact thermal resistance. The method is based on the analysis method of effective medium, combined with the basic concept of Kapitsa contact thermal resistance to establish a mathematical model and calculated the ETC of the composite according to the EMA model, which can be used in this study. Figure 4-3(b) shows that all the C_f-Cu is oriented in the x-direction, the C_f-Cu and the matrix are regarded as a unit, and many composite units form a composite, the heat flow direction is the x-axis. The EMA model considers the geometrical factor and h to evaluate the ETC of composites, and the equation can be expressed as[9,10]:

$$K_{EMA} = K_m \left(\frac{1 + V_{Cf-Cu} \dfrac{K_X^C - K_m}{K_m + L_x(K_X^C - K_m)} (2L_x)}{1 - V_{Cf-Cu} \dfrac{K_X^C - K_m}{K_m + L_x(K_X^C - K_m)} (1 - 2L_x)} \right)$$

$$L_x = 1 - \frac{P^2}{P^2 - 1} - \frac{P}{(P^2 - 1)^{3/2}} \cosh^{-1} P, \qquad P = \frac{L}{d} = 573.2$$

…… (2-6)

Where, Lx is the shape parameter of C_f-Cu, L is the length of C_f-Cu, 5400 μm. d is the diameter of C_f-Cu, which is 9.42 μm. P is the aspect ratio of C_f-Cu. K_X^C is the TC of C_f-Cu in the x direction, which can be determined by the following equation.

$$K_X^C = \frac{L \cdot K_{Cf-Cu}}{L + 2R_{EMA} K_{Cf-Cu}}$$

…… (2-7)

The TC of C_f-Cu, $K_{Cf\text{-}Cu}$, is 580 W m^{-1} K^{-1}

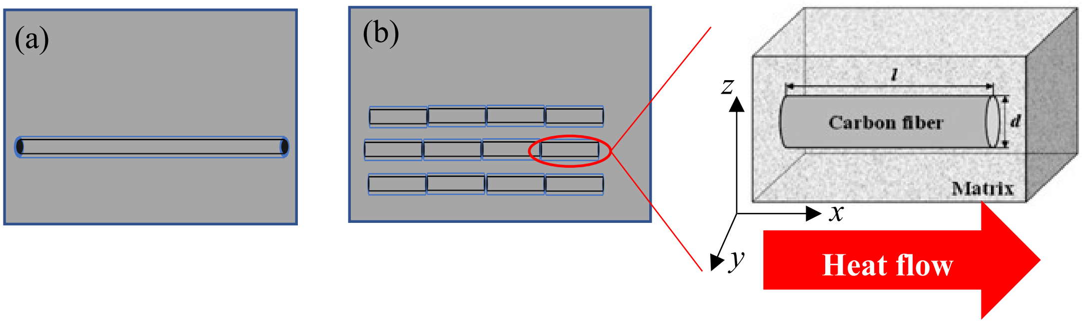

Figure 4-3 Models of C_f-Cu/Fe composite (a) ROM model (b) EMA model.

Using finite element analysis to calculate the simulated TC by 2D image simulation. The measured TC was obtained by the steady state method.

4.3 Results and discussions

4.3.1 Thermal conductivity and resistance under the ROM model

The matrix TC correction results for the C_f-Cu /Fe composite and its porosity are presented in Table 4-1. As C_f-Cu content increased, the porosity of the composite increased, but the matrix TC decreased. When the volume fraction of C_f-Cu does not exceed 20%, the porosity does not exceed 2.5%, the K_m shows negative growth for every 5% increase in the volume fraction of C_f-Cu, and the growth rate is from -0.63 to - 1.36%. the voids have little effect on the TC of matrix. As the volume fraction of C_f-Cu exceeds 20%, the porosity increases to 6.8%. There are many voids in the composite, which hinders heat conduction significantly, resulting in TC of the matrix dropping to 48.5 W m^{-1} K^{-1}.

In the ROM model, regardless of the aspect ratio or orientation of C_f-Cu, the TC of the composite. The TC of the composite can be determined by equation 2-5. When ignoring the effect of voids, the calculated TC is K_{ROM}. When considering voids, the calculated TC is K_{ROM}'. When the volume fraction of C_f-Cu does not exceed 20%, the growth rates of K_{ROM}, K_{ROM}', and $K_{Measured}$ for every 5% increase in the volume fraction of C_f-Cu were between 19.79-48.7%, 19-32%, and 3.3-8.94%, respectively. When the volume fraction of C_f-Cu exceeds 20%, the growth rate of K_{ROM}' is reduced to 12.35%. $K_{measured}$ showed negative growth, with a growth rate of -2.58%, decreasing to 67.16 $Wm^{-1}K^{-1}$. Through equations 2-5, the thermal resistance, R_6, was calculated when K_{ROM} is equal to $K_{measured}$, and the thermal resistance, R_7, was calculated when K_{ROM}' is equal to $K_{measured}$, the results were listed in Table 4-2, about 10^{-8} K m^2 W^{-1}. With the increase of C_f-Cu content, the axial TC of C_f-Cu is much higher than that of the matrix, and the TC gradually increases. However, with the increase of the contact interface, R_6 increases from 2.31×10^{-8} to 3.6×10^{-8} Km^2W^{-1} and R_7 increases from 2.08×10^{-8} to 3.01×10^{-8} Km^2W^{-1}. The hindering effect of voids on heat conduction is included in R_6, so R_6 is slightly larger than R_7. Since the voids increase with the increase of the C_f-Cu content, the growth rate of the contact thermal resistance also increases. When the volume fraction of C_f-Cu increases from 15% to 20%, there is almost no increase in R_6 and R_7, and the effect of increasing C_f-Cu on increasing and decreasing the TC of the composites cancels each other out.

Table 4-1. Volume fraction of voids (V_p), TC of matrix (K_m), TC of composites for ROM models (K_{ROM} and K_{ROM}') and the measured TC($K_{measured}$) in the composite with different volume fraction of C_f-Cu under the ROM model.

volume fraction of C_f-Cu, f_v / %	0	5	10	15	20	25
V_p (%)	0.4	0.8	1.3	1.7	2.5	6.8
K_m / W m^{-1} K^{-1}	54	53.67	52.95	52.62	51.98	48.5
K_{ROM} / Wm^{-1}K^{-1}	54	80.3	106.6	132.9	159.2	185.5
K_{ROM}' / W m^{-1} K^{-1}	53.67	79.99	106.06	131.71	157.6	181.37
$K_{measured}$ / W m^{-1} K^{-1}	54	58.83	63.2	65.27	68.89	67.16

Table 4-2 Heat transfer coefficient (h_6 and h_7) and thermal resistance (R_6 and R_7) of composites with different volume fraction of C_f-Cu under the ROM model, R=1/h.

volume fraction of C_f-Cu, f_v / %	0	5	10	15	20
h_6/W m^{-2} k^{-1} (×10^{7})	4.32	4.14	3.53	3.50	2.77
R_6/m^2 KW^{-1} (×10^{-8})	2.31	2.41	2.83	2.85	3.60
h_7/W m^{-2} k^{-1} (×10^{7})	4.81	4.51	3.81	3.79	3.32
R_7/m^2 KW^{-1} (×10^{-8})	2.08	2.22	2.63	2.64	3.01

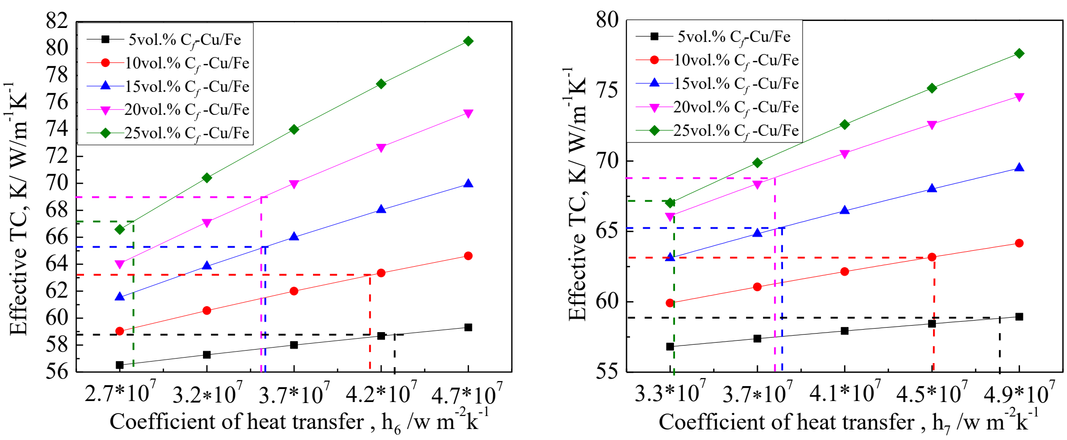

4.3.2 Thermal conductivity and resistance under the EMA model

In the EMA model, regardless of the influence of C_f-Cu orientation on TC, the internal thermal resistance is assumed to be 6.4×10^{-8} Km^2W^{-1}. The values of TC (K_{EMA}) ignoring voids, TC (K_{EMA}') of the composites with voids being considered, and measured TC ($K_{measured}$) are listed in Table 4-3. $K_{measured}$' is smaller than K_{ROM}' and still much larger than $K_{measured}$. Through equations 2-6 and 2-7, the thermal resistance, R_8, was calculated when K_{EMA} is equal to $K_{measured}$. The thermal resistance, R_9, was calculated when K_{EMA}' is equal to $K_{measured}$, the results are listed in Table 4-4, which is about 10^{-7} Km^2W^{-1}. The calculation and the changing laws of TC and thermal resistance are the same as those of the ROM model. R_8 is always larger than R_9 because of the impediment of TC heat conduction by voids in R_8. For every 5% increase in the volume fraction of C_f-Cu (from 5 vol. % to 25 vol. %), the growth rates of R_8 were 14.06%, 16.44%, 0.59%, and 24.56%, and the growth rates of R_9 were 5.86%, 16.97%, 0.315% and 13.52%, respectively. With the increase of C_f-Cu, the contact thermal resistance and the negatively oriented C_f-Cu increase, which leads to the decrease of TC. and the positive oriented C_f-Cu increases, which leads to the increase of TC. When the volume fraction of C_f-Cu increases from 15% to 20%, there is almost no increase in R_8 and R_9, and the two influencing factors cancel each other out. When the volume fraction of C_f-Cu increases from 20% to 25%, the growth rates of R_9 is smaller than that of R_8, and the voids have little effect on the TC of the composites.

Table 4-3 TC of composites with different volume fraction of C_f-Cu for EMA models (K_{EMA} and K_{EMA}'), and the measured TC ($K_{measured}$).

volume fraction of C_f-Cu, f_v / %	0	5	10	15	20	25
V_p (%)	0.4	0.8	1.3	1.7	2.5	6.8
K_{EMA} / $Wm^{-1}K^{-1}$	54	71.35	88.37	105.05	121.41	137.47
K_{EMA}' / W m^{-1} K^{-1}	53.67	70.74	87.44	103.89	119.80	133.34
$K_{measured}$ / W m^{-1} K^{-1}	54	58.83	63.2	65.27	68.89	67.16

Table 4-4 Heat thermal resistance (R_8 and R_9) of composites with different volume fraction of C_f-Cu under the EMA model.

volume fraction of C_f-Cu, f_v / %	0	5	10	15	20
R_8/m^2 KW^{-1}(×10^{-7})	2.31	2.41	2.83	2.85	3.60
R_9/m^2 KW^{-1}(×10^{-7})	2.08	2.22	2.63	2.64	3.01

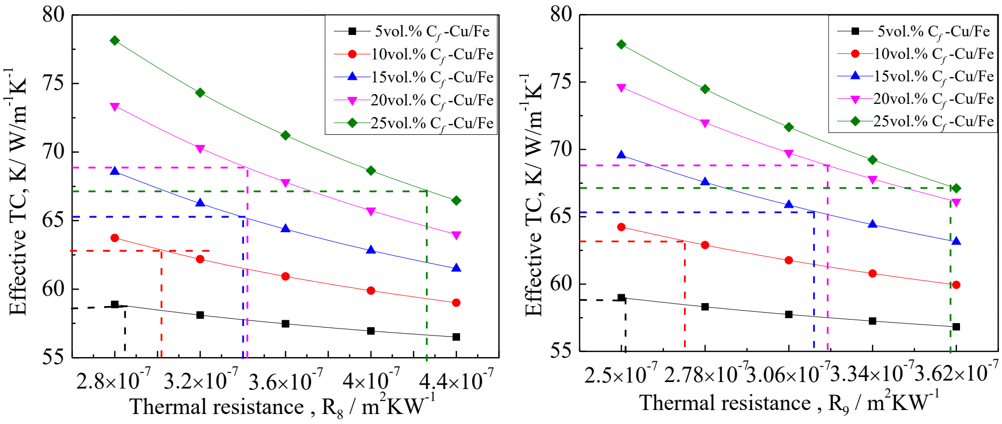

In the EMA model, the internal thermal resistance is assumed to be a constant value of 6.4×10^{-8}, and the TCs of C_f-Cu composites with different aspect ratios are calculated. Figure 4-4 (a) and (b) shows an optical microscope image of C_f-Cu. The composite fragments were completely dissolved in HCl (wt.38%), the resulting mixture was filtered to obtain C_f-Cu, and the length of C_f-Cu was counted under an optical microscope. According to statistics, the average length of C_f-Cu is 110 μm, which is less than the original length (4.5 mm). Figure 4-4 shows that a large amount of C_f-Cu was destroyed during the sintering and rolling process. The copper layer fell off the carbon fiber due to mixing friction and coating stress, causing the C_f to directly contact the iron matrix and cause damage. Many C_f-Cu cross-linked and squeezed and broke, which greatly hinders heat conduction. Figure 4-5 shows the variation law of C_f-Cu content and the TC corresponding to different C_f-Cu contents at initial length (4500 μm) and actual length (110 μm), which is infinitely close to a straight line. The diameter of C_f-Cu is a fixed value, 9.42 μm. The aspect ratio of C_f-Cu is the ratio of length to diameter. The larger the aspect ratio of C_f-Cu, the faster the TC increases with the C_f-

Cu content. The measured TC is placed in the Figure 4-5, and the $K_{measured}$ value appears near the TC line corresponding to the C_f-Cu length of 225 μm. The actual TC of the composite is equivalent to the TC obtained by connecting two C_f-Cu end-to-end.

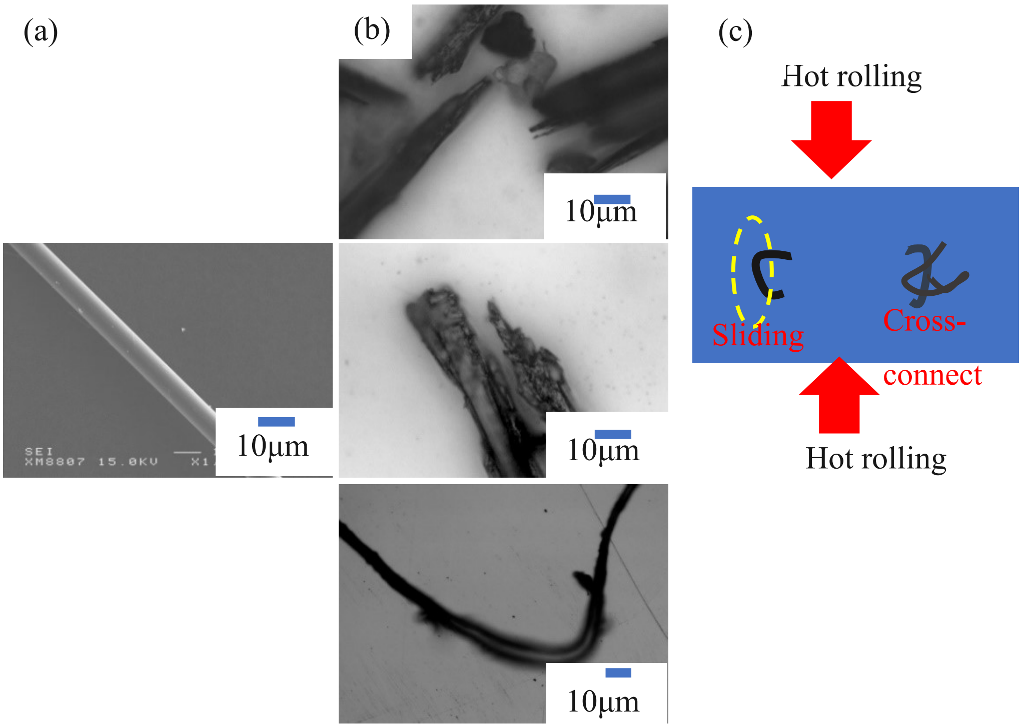

Figure 4-4 Optical micrograph of (a)obtained C_f-Cu and (b) after rolling C_f -Cu. (c) Folding of C_f-Cu in the rolled composite.

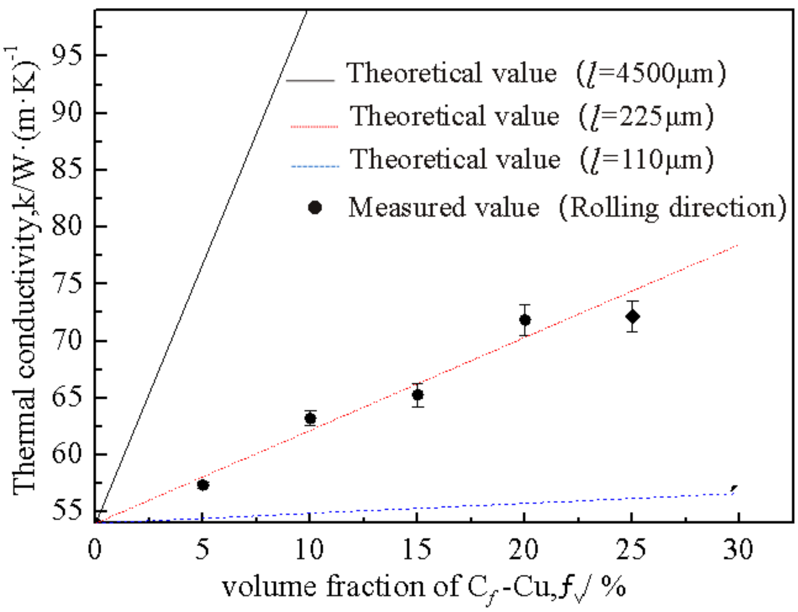

Figure 4-5 Relationship between TC of composite with different aspect ratios of C_f-Cu under the EMA model and volume fraction of C_f-Cu.

4.3.3 The simulated thermal conductivity by finite element volume method

The (A/B plane) simulated TC and measured TC of the rolled composite, and the measured TC of the unrolled composite have been investigated in Chapter 3. Figure 4-6 shows the results for the measurements of TC on the A plane before and after rolling and the simulated TC on the A/B plane of rolled composites with different volume fractions of C_f-Cu.

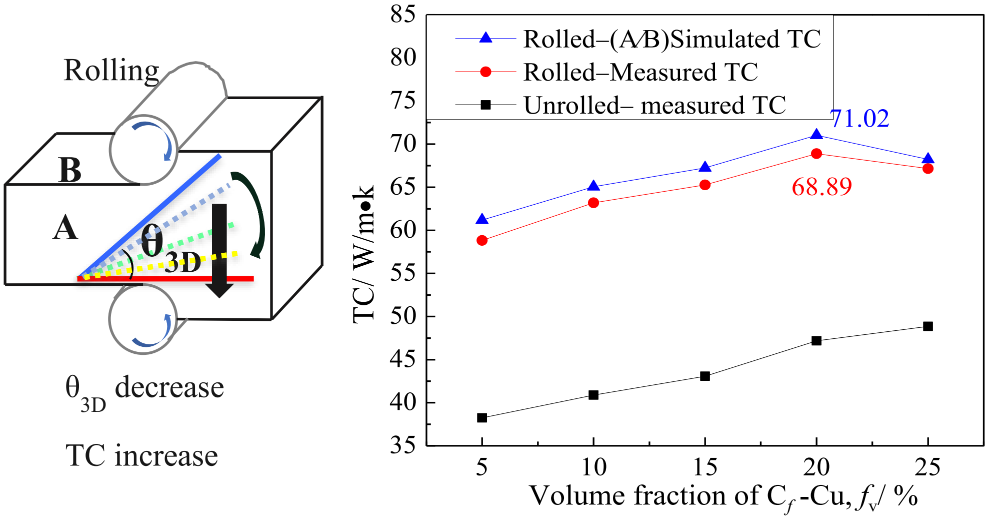

Figure 4-6 Simulated and measured TC of C_f-Cu/Fe composites with different volume fractions of C_f-Cu on the A/B plane.

4.3.4 The influencing factors and degree of thermal conductivity

The deviation of K_{ROM} and K_{ROM}' is caused by voids in the composites. The deviation of K_{ROM}' and K_{EMA}' is caused by the aspect ratio of C_f-Cu. The deviation of K_{EMA}' and $K_{simulated}$ is caused by the orientation of C_f-Cu. The deviation of $K_{simulated}$ and $K_{measured}$ is caused by experimental error. The results of K_{ROM}, K_{ROM}', K_{EMA}', $K_{simulated}$ and $K_{measured}$ are listed in Table 4-5. The effects of voids, C_f-Cu aspect ratio, C_f-Cu orientation, and experimental error on the TC of the composites are listed in Table 4-6. The main factors hindering thermal conduction are the aspect ratio and orientation of C_f-Cu. With the increase of C_f-Cu content, the effect of aspect ratio on TC increases from 40.586% to 43.08%, and the effect of C_f-Cu orientation on TC decreases from 44.53% to 55.02%. When the volume fraction of C_f-Cu is 20%, the hindering effect of the two on TC is offset by the promoting effect of C_f-Cu on TC, so $K_{simulated}$ and $K_{measured}$

achieve the maximum value.

Table 4-5 TC of composites with different volume fraction of C_f-Cu for ROM models (K_{ROM} and K_{ROM}'), EMA models (K_{EMA}'), simulated TC ($K_{simulated}$)and the measured TC ($K_{measured}$).

	volume fraction of C_f-Cu, f_v / %	5	10	15	20	25
Voids	K_{ROM} / $Wm^{-1}K^{-1}$	80.3	106.6	132.9	159.2	185.5
Aspect ratio of C_f-Cu	K_{ROM}' / $W\ m^{-1}\ K^{-1}$	79.99	106.06	131.71	157.6	181.37
Orientation of C_f-Cu	K_{EMA}' / $W\ m^{-1}\ K^{-1}$	70.74	87.44	103.89	119.80	133.34
Experiment error	$K_{simulated}$/ $W\ m^{-1}\ K^{-1}$	61.08	65.06	67.24	71.02	68.23
	$K_{measured}$ / $W\ m^{-1}\ K^{-1}$	58.83	63.2	65.27	68.89	67.16

Table 4-6 The degree of influence of various thermal resistances on the TC of composites with different volume fraction of C_f-Cu.

	volume fraction of C_f-Cu, f_v / %	5	10	15	20	25
Influence coefficient (%)	Voids	1.44	1.244	1.76	1.772	3.49
	Aspect ratio of C_f-Cu	43.08	42.9	41.135	41.8558	40.586
	Orientation of C_f-Cu	44.53	51.57	54.192	54.014	55.02
	Experiment error	10.95	4.28	2.93	2.3585	0.904

4.4 Summary

In this chapter, 5 (10, 15, 20, 25) vol.% C_f-Cu/Fe composites were prepared by SPS. In composites, the TC of the matrix has been corrected by the Bruggeman equation. The TC of the C_f-Cu/Fe composites before and after being rolled with different C_f-Cu content were measured, and the TC of the matrix was calculated. The TCs of the composites were also simulated by 2D image simulation. The conclusions drawn in this chapter are summarized as follow. Our conclusions are listed below.

(1) The TC of the matrix of C_f-Cu/Fe composites decreased with the increasing C_f-Cu content. When the volume fraction of C_f-Cu exceeds 20%, the porosity increases to 6.8%, and the TC of matrix dropped to 48.5 W m^{-1} K^{-1}.

(2) When the volume fraction of C_f-Cu is less than 20%, the thermal resistance hardly increases, and the contact thermal resistance and the negatively oriented C_f-Cu decrease the TC less than the positively oriented C_f-Cu increases the TC.

(3) When the volume fraction of C_f-Cu exceeds 20%, the growth rate of thermal resistance is obviously small, and the reduction effect of contact thermal resistance and negatively oriented C_f-Cu on TC dominates.

(4) The main factors hindering thermal conduction are the aspect ratio and orientation of C_f-Cu. When the volume fraction of C_f-Cu is 20%, the contact thermal resistance and the negatively oriented C_f-Cu decrease the TC is offset the positively oriented C_f-Cu increases the TC, so $K_{simulated}$ and $K_{measured}$ achieve the maximum value.

4.5 References

[1]Lim W-S, Choi H-S, Ahn S-y,Kim B-M. Cooling channel design of hot stamping tools for uniform high-strength components in hot stamping process.The International Journal of Advanced Manufacturing Technology. 2013;70(5-8):1189-1203.

[2]Bok H-H, Lee M-G, Kim H-D,Moon M-B. Thermo-mechanical finite element analysis incorporating the temperature dependent stress-strain response of low alloy steel for practical application to the hot stamped part.Metals and Materials International. 2010;16(2):185-195.

[3]Rahman M H, Chowdhury E H, Bin Shahadat M R,Islam M M. Engineered defects to modulate the phonon thermal conductivity of Silicene: A nonequilibrium molecular dynamics study.Computational Materials Science. 2021;191(110338.

[4]Yang B, Li D, Yang H, Wang J,Yang P. Thermal conductivity enhancement of defective graphene nanoribbons.International Communications in Heat and Mass Transfer. 2020;117(104735.

[5]Lee S, Yang F, Suh J, Yang S, Lee Y, Li G, Sung Choe H, Suslu A, Chen Y, Ko C, Park J, Liu K, Li J, Hippalgaonkar K, Urban J J, Tongay S,Wu J. Anisotropic in-plane thermal conductivity of black phosphorus nanoribbons at temperatures higher than 100 K.Nat Commun. 2015;6(8573.

[6]Huang D, Tan R, Liu L, Ye C, Zhu S, Fan Z, Zhang P, Wu H, Han F, Liu H,Liu J. Preparation and properties of the three-dimensional highly thermal conductive carbon/carbon-silicon carbide composite using the mesophase-pitch-based carbon fibers and pyrocarbon as thermal diffusion channels.Journal of the European Ceramic Society. 2021;41(8):4438-4446.

[7]Cao L, Wang J, Liu Y, Zhang Y, Liu B, Cao Y,Zhang Q. Effect of heat transfer channels on thermal conductivity of silicon carbide composites reinforced with pitch-based carbon fibers.Journal of the European Ceramic Society. 2022;42(2):420-431.

[8]Hou X, Chen Y, Dai W, Wang Z, Li H, Lin C-T, Nishimura K, Jiang N,Yu J. Highly thermal conductive polymer composites via constructing micro-phragmites communis

structured carbon fibers.Chemical Engineering Journal. 2019;375(121921.

[9]Kontani H, Tokunaga T, Ohno M, et al. Fabrication of unidirectionally orientated carbon fiber reinforced cu-based composites by hot extrusion and evaluation of their thermal properties.Journal of the Japan Institute of Metals and Materials, 2018; 82(5): 125-129.

[10]Tokunaga T, Takahashi K, Ohno M, Sasaki K, Imanishi T,Matsuura K. Fabrication of Carbon Fiber Oriented Al-Based Composites by Hot Extrusion and Evaluation of Their Thermal Conductivity.Journal of the Japan Institute of Metals. 2016;80(10):640-645.

[11]Ma J, Shang T, Ren L, Yao Y, Zhang T, Xie J, Zhang B, Zeng X, Sun R, Xu J-B,Wong C-P. Through-plane assembly of carbon fibers into 3D skeleton achieving enhanced thermal conductivity of a thermal interface material.Chemical Engineering Journal. 2020;380(122550.

[12]Khayyam H, Jazar R N, Nunna S, Golkarnarenji G, Badii K, Fakhrhoseini S M, Kumar S,Naebe M. PAN precursor fabrication, applications and thermal stabilization process in carbon fiber production: Experimental and mathematical modelling.Progress in Materials Science. 2020;107(100575.

[13]Gallego N C, Edie D D. Structure–property relationships for high thermal conductivity carbon fibers.Composites Part A: Applied Science and Manufacturing, 2001;32(8):1031-1038.

[14]Lee H-M, Lee B-H, Kim J-H, An K-H, Park S-J,Kim B-J. Determination of the optimum porosity for 2-CEES adsorption by activated carbon fiber from various precursors.Carbon Letters. 2019;29(6):649-654.

[15]Inoue R, Arai Y, Kubota Y, Goto K,Kogo Y. Development of short- and continuous carbon fiber-reinforced ZrB2-SiC-ZrC matrix composites for thermal protection systems.Ceramics International. 2018;44(13):15859-15867.

[16]Xu H H K, Eichmiller F C, Barndt P R. Effects of fiber length and volume fraction on the reinforcement of calcium phosphate cement.Journal of Materials Science:

Materials in Medicine. 2001;12(1):57-65.

[17]Lee G W, Lee J I, Sang-Soo L, et al. Comparisons of thermal properties between inorganic filler and acid-treated multiwall nanotube/polymer composites.Journal of materials science, 2005;40(5):1259-1263.

[18]Wang J, Chen Y, Feng Y, Zhao G, Jian X, Huang Q, Yang L,Xu J. Influence of porosity on anisotropic thermal conductivity of SiC fiber reinforced SiC matrix composite: A microscopic modeling study.Ceramics International. 2020;46(18):28693-28700.

[19]Solórzano E, Reglero J A, Rodríguez-Pérez M A, Lehmhus D, Wichmann M,De Saja J A. An experimental study on the thermal conductivity of aluminium foams by using the transient plane source method.International Journal of Heat and Mass Transfer. 2008;51(25-26):6259-6267.

[20]Truong H V, Zinsmeister G E. Experimental study of heat transfer in layered composites.International Journal of Heat and Mass Transfer. 1978; 21(7): 905-909.

Chapter 5

Thermal conductivity of C_f-Cu dispersed SKD61(40CrMoV5) composites

5.1 Introduction

R Die casting is a casting method that presses molten alloys such as aluminum alloys and zinc alloys into precision dies to rapidly cycle and mass-produce castings with excellent surface and high precision[1]. In Japan, this casting method is actively used, especially in the automotive industry. In recent years, the production of die castings has increased significantly, but the rapid heating and cooling of die castings in the production of die steels creates thermal stresses, which can lead to shortened die life[2,3]. It can improve heat transfer by increasing the thermal conductivity (TC) of the die, reducing the local thermal stress in the production process, and improving the lives of the die.

In Chapters 2 and 3, the heat conduction and the hindering factors of heat conduction in copper coated carbon fiber (C_f -Cu) reinforced iron matrix composites have been investigated. In Japan, hot stamping dies are usually based on SKD61 (40CrMoV5), and other reinforcements are added to improve the mechanical and thermal properties of composite. In fact, die materials with high TC have been developed within the compositional standard range of SKD61(40CrMoV5) for dies. The representative DHA-Thermo[4] from Daido steel Co. has a higher TC (37.1 $W \cdot m^{-1} \cdot K^{-1}$ at room temperature), nearly twice that of conventional dies. However, the TC has reached its limit within the composition range of the JIS standard. To break this limit, the development of composites for dies with high TC can be considered. At present, composite for dies has attracted much attention[5,6]. The carbide-reinforced traditional hot work die steel developed by Rovalma Co. in Spain has a TC above 42 $W \cdot m^{-1} \cdot K^{-1}$). Since its composition is different from traditional tool steel, there are many problems in practical application.

In this chapter, a die material with excellent mechanical properties and thermal conductivity was developed by adding C_f -Cu with high TC in the axial direction to the SKD61(40CrMoV5) alloy die[7-12]. C_f-Cu reinforced composites with high TC, but when C_f are sintered with steel, carbon reacts with iron to form solid solutions or carbides. Therefore, to develop a die with both the above characteristics, electroless copper plating on the surface of C_f hinders the contact between carbon and iron, and SPS makes the orientation of C_f-Cu tend to be consistent to obtain a metal matrix with dense, excellent mechanical properties and high thermal conductivity[13-15]. Generally, copper can be used to promote composite densification during the sintering of steel powders[16-18]. Under the normal sintering temperature and die use temperature, iron and copper will not form solid solutions, which can maintain the characteristics of steel. Copper is an austenite stabilizing element[19-22]. Heat treatment is required for die steel to adjust the hardness and evaluate the mechanical properties. By controlling the direction of C_f-Cu, controlling the direction of heat conduction of the die[15,23-25]. Improve the TC in some special parts of the die to develop unique die materials.

5.2 Experimental and calculation procedure

5.2.1 Experimental procedure

As raw materials, SKD61(40CrMoV5) powder (Mitsubishi Steel Corporation) with an average particle size of 70 μm and pitch-based carbon fiber K13C6U (about 10 μm in diameter, Mitsubishi Chemical Corporation) was used. Table 5-1 shows the chemical composition of SKD61(40CrMoV5). The TC of C_f-Cu along the fiber direction and the radial direction of fiber are 580W/m·K. and 20W/m·K, respectively. In the procedure of electroless copper plating, remove organics from C_f surfaces with acetone, nitric acid (10wt.%) was used for roughening treatment, tin chloride solution ($SnCl_2 \cdot 2H_20$+HCl) for sensitization treatment, palladium chloride solution ($PdCl_2$+HCl) for activation treatment. In the electroless copper plating solution (OPC-750 electroless copper plating M, Okuno Chemical Industries Co., Ltd.), the C_f was treated for 2 hours. These treatments are all carried out under the condition of ultrasonic waves. 3vol.% and 5vol.% of electroless copper plated C_f reinforced SKD61(40CrMoV5) composite were fabricated SPS. The composite was prepared by SPS under the sintering conditions of vacuum less than 10^{-2}Pa, pressure 15MPa, sintering temperature 1173K, and holding time 1.5ks. The SKD61(40CrMoV5) alloy without C_f-Cu was fabricated under the same conditions. The density was measured by the Archimedes method. To clarify the relationship between the orientation of C_f-Cu and the direction of sintering pressure, the microstructure was observed by scanning electron microscopy (SEM) and element distribution was determined by EPMA. To search for the relationship between the content of C_f-Cu and TC, TC was measured by steady-state method.

Table 5-1 Chemical composition of SKD61 powder used in this study.

	C	Si	Mn	P	S
SKD61(40CrMoV5)	0.39	1.11	0.38	0.01	0.01
powder/ Wt.%	Ni	Cr	Mo	V	Fe
	0.07	4.67	1.16	1.04	Bal.

5.2.2 Spark plasma sintering of C_f-Cu/SKD61(40CrMoV5) composite

When the axial of carbon fiber is completely parallel to the effective TC measurement direction, the effective TC of the C_f-Cu/SKD61(40CrMoV5) composites is calculated by the rule of mixture. The C_f-Cu are unidirectionally oriented, the evaluation of effective TC in the fiber direction in composites by the rule of mixture follows the equation[26-29].

$$U_C = U_f \times V_f + U_{Cu} \times V_{Cu} + V_m\left(1 - V_f - V_{Cu}\right) \times U_m$$

…… (5-1)

Among them, U_c, U_f, U_{Cu} and U_m are the TC of composite, axial of C_f, copper and SKD61(40CrMoV5) matrix. V_f, V_{Cu} and V_m are the volume fractions of C_f, copper and SKD61(40CrMoV5) matrix. In addition, the modified equation[30] were used to calculate the effective TC of SKD61(40CrMoV5) matrix with voids.

$$K_{eff} = \frac{1}{4}\left[K_p\left(3V_p - 1\right) + K_S(3V_S - 1) + \left\{\left[K_p\left(3V_p - 1\right) + K_S(3V_S - 1)\right]^2 + 8K_pK_S\right\}^{1/2}\right]$$

…… (5-2)

where K_p and K_S are the TC of the void and SKD61(40CrMoV5) matrix. V_p and V_S are the volume fractions of voids and SKD61(40CrMoV5) matrix. In addition, if the C_f-Cu is not parallel to the measurement direction of TC, its TC will decrease. Considering the orientation of C_f-Cu, the formula for the effective TC along the measurement direction of TC when the angle between the C_f-Cu and heat flow is θ is shown below[31-33].

$$K_{\parallel} = K_a\left[1 - \left(1 - \frac{K_c}{K_a}\right) sin^2\theta\right]$$

…… (5-3)

where $K_{//}$ is the TC along the measurement direction of TC when the C_f-Cu is tilted by θ. K_a is the axial TC of the C_f-Cu (580 $Wm^{-1}K^{-1}$) and K_c is the radial TC of the C_f-Cu (20 $Wm^{-1}K^{-1}$).

5.3 Results and discussions

5.3.1 Observation of C_f-Cu and C_f-Cu/SKD61(40CrMoV5) composites

The C_f-Cu was embedded in the resin and observed by EPMA. The result was shown in Figure 5-1, and Figure 5-1(a) is the cross-sectional image of the C_f-Cu. There is a uniform copper layer of about 2 μm around the C_f with a diameter of 10 μm. The line analysis results of copper and carbon in the red line range in the figure are shown in Figure 5-1(b). The copper element was detected in the part of the white line, indicating that the copper was uniformly formed around the C_f.

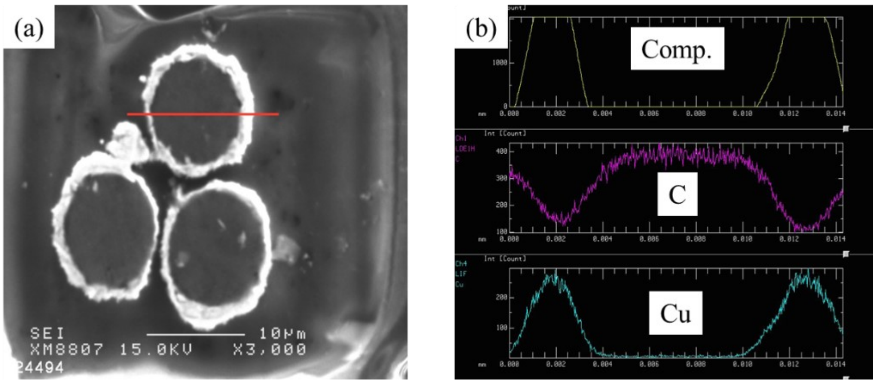

Figure 5-1 (a) Microstructure and (b) EPMA line analysis of C and Cu elements in the C_f-Cu.

Figure 5-2 shows the microstructure of 3vol.% C_f-Cu reinforced SKD61 (40CrMoV5) composites observed by an optical microscope. In the preparation process of the composite, the C_f-Cu are arranged along the direction perpendicular to the pressure during spark plasma sintering, and the C_f-Cu are arranged anisotropically. As shown in Figure 5-2(a), the directions perpendicular to the pressing direction are the X-axis and the Y-axis, and the pressing direction is the Z-axis. Figure 5-2(b) and 2(c) show the microstructures in the X-Z plane and the Y-Z plane, respectively. On the X-Z plane, the C_f-Cu were not observed in the upper and lower parts of the figure but are concentrated in the central part and parallel each other. On the Y-Z plane, the C_f-Cu has a circular cross-section, and the C_f-Cu gather to form fiber bundles. The average particle size of the SKD61 (40CrMoV5) powder used in this study is 70 μm, which is larger than the diameter(10μm) of C_f-Cu, so it is considered the C_f-Cu can agglomerate during pressure sintering.

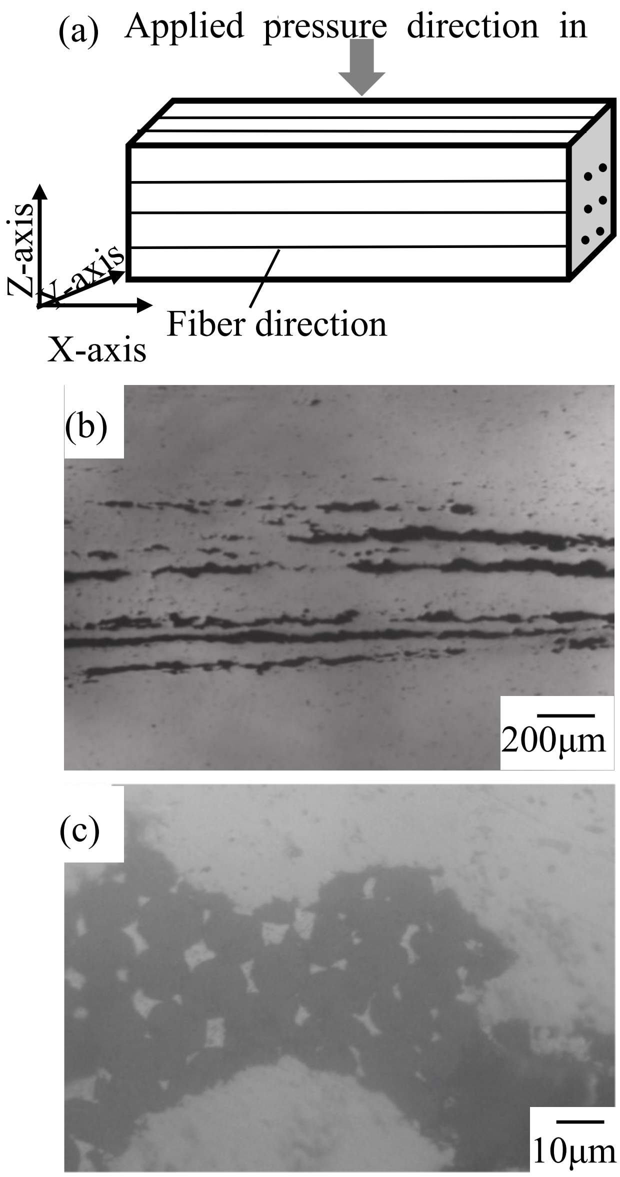

Figure 5-2 Fiber distribution in 3vol.% Cu plated carbon fiber/ SKD61 composites for each direction. (a) schematics and definition of observation plane. (b) microstructure of X-Z plane, and (c) microstructure of Y-Z plane.

Figure 5-3 is EPMA mapping of the 3vol.% C_f-Cu reinforced SKD61(40CrMoV5) alloy composite and the EPMA image of the distribution of copper, iron, and carbon elements. By observing the Y-Z plane of the sample, it is found that there is a layer of copper around the C_f, which is surrounded by iron elements. After the composite was prepared by spark plasma sintering, the copper layer was distributed around the C_f, and the copper layer hinders the direct contact between the iron and C_f.

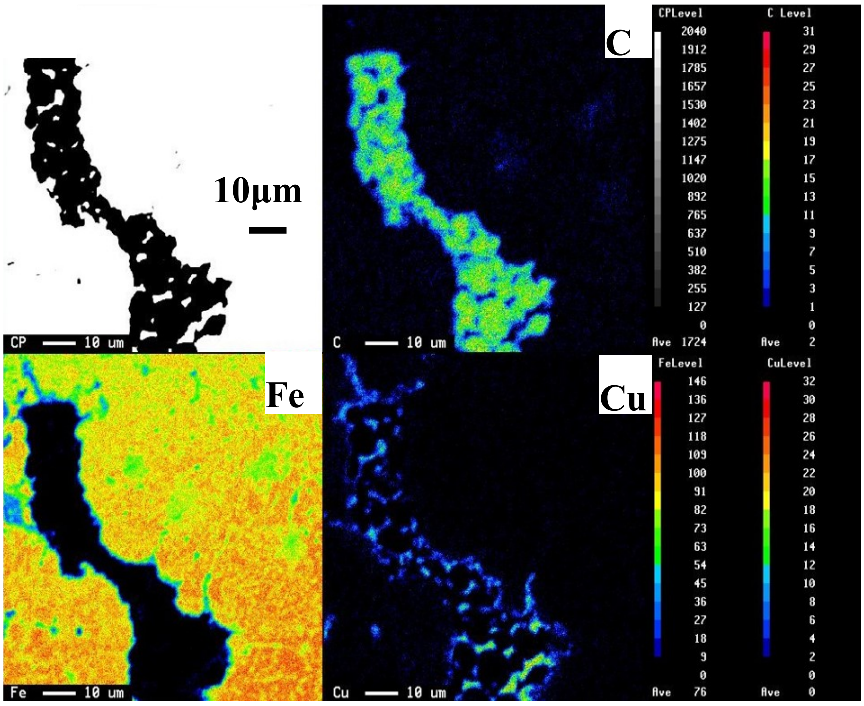

Figure 5-3 EPMA mapping of carbon (C), iron (Fe) and copper (Cu) elements for 3 vol.% Cu plated carbon fiber/ SKD6I composites.

Table 5-2 shows the relative densities of SKD61(40CrMoV5) alloys and C_f-Cu reinforced SKD61 (40CrMoV5) composites fabricated by spark plasma sintering. The relative density is the ratio of measured density obtained by Archimedes method and the theoretical density of the composite calculated by mixture rule. The relative density of pure SKD61(40CrMoV5) alloy is as high as 98.1%. The relative densities of the composites with a C_f-Cu content of 3vol.% and 5vol.% are 97.7% and 98.3%, respectively, which are comparable to pure SKD61(40CrMoV5) alloy. The metal matrix composites were prepared by the SPS, the reinforcement and the matrix will not promote the sintering and densification, the relative density of the composite will decrease with the increase of the reinforcement. However, the results showed that the density did not decrease significantly, which is considered as the copper on the surface of C_f promote the densification of the composites. In solid sintering, the main causes of densification are atomic motion due to viscous flow, plastic flow, evaporative agglomeration, volume diffusion, particle diffusion, and surface diffusion[34-36]. Copper is almost insoluble in iron, the main reason why copper promotes sintering densification is that higher plasticity of copper and fluidity compared with SKD61(40CrMoV5) powder. In the case of adding copper, it can be sintered by SPS below the melting point. Copper atoms are easier to evaporation, diffuse, and agglomerate.

Table 5-2 Relative density of monolithic SKD6l block and composite prepared by spark plasma sintering.

	C	Si	Mn	P	S
SKD61(40CrMoV5)	0.39	1.11	0.38	0.01	0.01
powder/ Wt.%	Ni	Cr	Mo	V	Fe
	54	53.67	52.95	52.62	51.98

5.3.2 Thermal conductivity of C_f-Cu/SKD61(40CrMoV5) composites

Figure 5-4 shows the orientation distribution of C_f-Cu in the 3vol.% C_f-Cu reinforced SKD61(40CrMoV5) alloy composite in the X-Z and X-Y planes shown in Figure 5-2(a). As shown in Figure 5-4, the X-axis direction is 90°, it shows the distribution of the deviation of the angle between the X-axis and the axial of C_f-Cu. On the X-Y plane, the mean angle is 84.32° with a standard deviation of 34.39. On the X-Z plane, the mean angle is 88.42° with a standard deviation of 39.29. In most cases, C_f-Cu are aligned in two planes along the X-axis.

Considering the influence factors of void, orientation of C_f-Cu and the rule of mixture, the theoretical TC of the composite was evaluated by the rule of mixture. Figure 5-5 shows the measured TC and theoretical TC of 3 vol.% and 5vol.%C_f-Cu reinforced SKD61(40CrMoV5) composites. According to the experimental results, the TC increases with the increase of C_f-Cu content. It is found that the TC of SKD61(40CrMoV5) steel can be improved by adding C_f-Cu. In particular, the TC of 5vol.%C_f-Cu/SKD61(40CrMoV5) composite is 42 $Wm^{-1}\cdot K^{-1}$, which is significantly higher than that of pure SKD61(40CrMoV5) alloy (22 $Wm^{-1}K^{-1}$). The experimental results are lower than the theoretical value. The TC of plating copper is lower than that of conventional copper, and the acid oxide film remaining on the surface of steel powder during spark plasma sintering increases the thermal resistance between the SKD61(40CrMoV5) steel particles. Carbon and copper diffused into the contact face between SKD61(40CrMoV5) and C_f-Cu, strain at the interface also made the experimental result lower than theoretical TC.

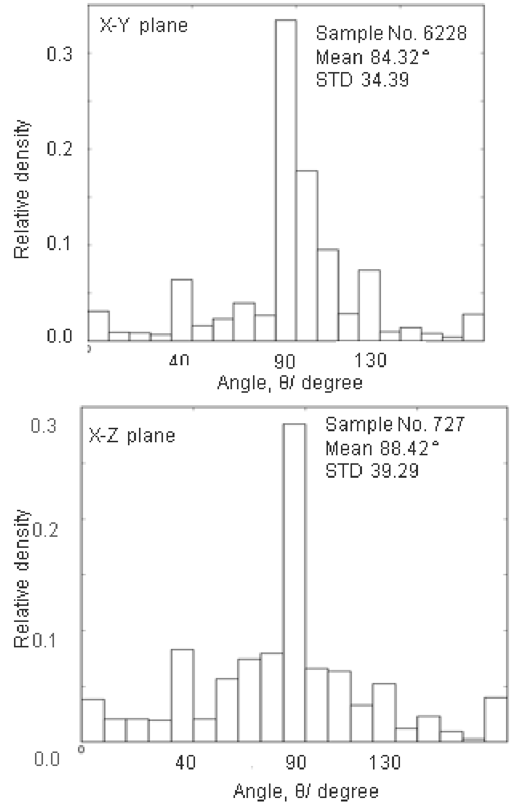

Figure 5-4 Angle distribution of the difference between C_f-Cu direction and X-axis in 3vol.% C_f-Cu dispersed SKD61 alloy composites shown in Figure 5-2(a). 90 degrees shows the X-axis direction.

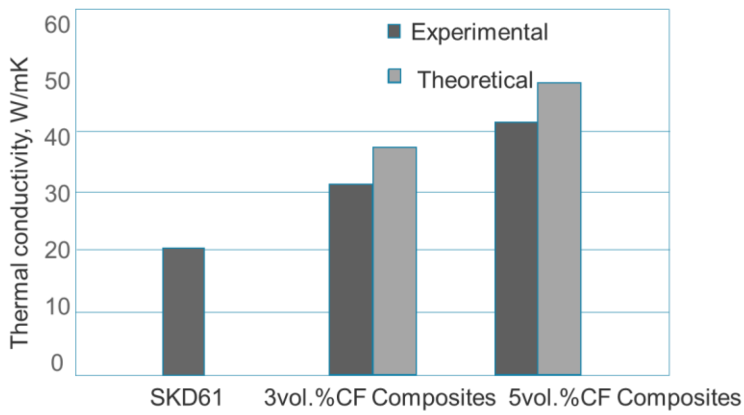

Figure 5-5 Experimental results and theoretical value of thermal conductivity for SKD61 block and C_f-Cu dispersed SKD6I matrix composites.

5.4 Summary

In this chapter, to improve the thermal conductivity of hot tool steel (SKD61(40CrMoV5) alloy), the oriented C_f-Cu reinforced SKD61(40CrMoV5) alloy composite was fabricated by the spark plasma sintering. The TC of the matrix of the void-containing composite was corrected by the Bregman equation, the orientation of C_f-Cu in the composite was considered, and the theoretical TC of the composite was calculated, and the measured TC was obtained by the steady-state method. The results obtained are as follows.

(1) The relative density of the C_f-Cu /SKD61(40CrMoV5) composite was similar to that of pure SKD61(40CrMoV5) alloy. The copper layer on the surface of C_f can promotes sintering densification and hinder the direct contact between SKD61(40CrMoV5) alloy and C_f and prevent the chemical reaction between iron and carbon fiber.

(2) The C_f-Cu reinforced SKD61(40CrMoV5) composite exhibited higher TC than single SKD61(40CrMoV5), and its TC increased with the increase of C_f-Cu content. The 5 vol% C_f-Cu /SKD61(40CrMoV5) composite has a high TC of 42 $Wm^{-1}K^{-1}$.

5.5 References

[1]McKie M G. Research and Development of a Sustainable Technology Improvement Model for the Foundry Industry. Doctoral Dissertation, Teesside University, Middlesbrough, England, 10.13140/RG. 2.2. 23201.25443, 2015.

[2]Schwam D, Wallace J, Birceanu S. Die materials for critical applications and increased production rates. Case Western Reserve University/Dept of Materials Science and Engineering (US), 2002.

[3]Mellouli D, Haddar N, Köster A,Ayedi H F. Hardness effect on thermal fatigue damage of hot-working tool steel.Engineering Failure Analysis. 2014;45:85-95.

[4] Kono M, Inoue K. Development of high thermal conductivity steel "DHA-Thermo" for die casting dies. Materia, 2009, 48(1):32-34.

[5]Karbasian H,Tekkaya A E. A review on hot stamping.Journal of Materials Processing Technology. 2010;210(15):2103-2118.

[6]Chantzis D, Liu X, Politis D J, El Fakir O, Chua T Y, Shi Z,Wang L. Review on additive manufacturing of tooling for hot stamping.The International Journal of Advanced Manufacturing Technology. 2020;109(1-2):87-107.

[7]Wang M, Kang Q,Pan N. Thermal conductivity enhancement of carbon fiber composites.Applied Thermal Engineering. 2009;29(2-3):418-421.

[8]Hou X, Chen Y, Dai W, Wang Z, Li H, Lin C-T, Nishimura K, Jiang N,Yu J. Highly thermal conductive polymer composites via constructing micro-phragmites communis structured carbon fibers.Chemical Engineering Journal. 2019;375(121921.

[9]Wei J, Liao M, Ma A, Chen Y, Duan Z, Hou X, Li M, Jiang N,Yu J. Enhanced thermal conductivity of polydimethylsiloxane composites with carbon fiber.Composites Communications. 2020;17:141-146.

[10]Chen S, Feng Y, Qin M, Ji T,Feng W. Improving thermal conductivity in the through-thickness direction of carbon fibre/SiC composites by growing vertically aligned carbon nanotubes.Carbon. 2017;116:84-93.

[11]Mazov I, Burmistrov I, Il'inykh I, Stepashkin A, Kuznetsov D,Issi J-P. Anisotropic

thermal conductivity of polypropylene composites filled with carbon fibers and multiwall carbon nanotubes.Polymer Composites. 2015;36(11):1951-1957.

[12]Hamada Y, Otsu W, Fukai J, Morozumi Y,Miyatake O. Anisotropic heat transfer in composites based on high-thermal conductive carbon fibers.Energy. 2005;30(2-4):221-233.

[13]Shirvanimoghaddam K, Hamim S U, Karbalaei Akbari M, Fakhrhoseini S M, Khayyam H, Pakseresht A H, Ghasali E, Zabet M, Munir K S, Jia S, Davim J P,Naebe M. Carbon fiber reinforced metal matrix composites: Fabrication processes and properties.Composites Part A: Applied Science and Manufacturing. 2017;92(70-96.

[14]Sciti D, Galizia P, Reimer T, Schoberth A, Gutiérrez-Gonzalez C F, Silvestroni L, Vinci A,Zoli L. Properties of large scale ultra-high temperature ceramic matrix composites made by filament winding and spark plasma sintering.Composites Part B: Engineering. 2021;216(108839.

[15]Zhu C, Su Y, Wang X, Sun H, Ouyang Q,Zhang D. Process optimization, microstructure characterization and thermal properties of mesophase pitch-based carbon fiber reinforced aluminum matrix composites fabricated by vacuum hot pressing.Composites Part B: Engineering. 2021;215(108746.

[16]Johnson J L, German R M. Role of solid-state skeletal sintering during processing of Mo-Cu composites.Metallurgical and Materials Transactions A. 2001;32(3): 605-613.

[17]Yan A, Wang Z, Yang T, Wang Y,Ma Z. Sintering densification behaviors and microstructural evolvement of W-Cu-Ni composite fabricated by selective laser sintering.The International Journal of Advanced Manufacturing Technology. 2016;90(1-4):657-666.

[18]Wang D, Dong X, Zhou P, Sun A,Duan B. The sintering behavior of ultra-fine Mo–Cu composite powders and the sintering properties of the composite compacts.International Journal of Refractory Metals and Hard Materials. 2014;42(240-245.

[19]Bhambroo R, Roychowdhury S, Kain V,Raja V S. Effect of reverted austenite on

mechanical properties of precipitation hardenable 17-4 stainlesssteel.Materials Science and Engineering: A. 2013;568(127-133.

[20]Zhou W H, Guo H, Xie Z J, Shang C J,Misra R D K. Copper precipitation and its impact on mechanical properties in a low carbon microalloyed steel processed by a three-step heat treatment.Materials & Design. 2014;63(42-49.

[21]Bihari B, Kumar R, Singh A K. Effect on the mechanical properties of gray cast iron with variation of copper and molybdenum as alloying elements.International Journal of Engineering Research. 2014;3(5).

[22]Harvig H, Kirchner G, Hillert M. On the ferrite-austenite equilibrium in the Fe-Cu system.Metallurgical and Materials Transactions B. 1972;3(1):329-332.

[23]Spoerk M, Savandaiah C, Arbeiter F, Traxler G, Cardon L, Holzer C,Sapkota J. Anisotropic properties of oriented short carbon fibre filled polypropylene parts fabricated by extrusion-based additive manufacturing.Composites Part A: Applied Science and Manufacturing. 2018;113(95-104.

[24]Shofner M L, RodríGuez-MacíAs F J, Vaidyanathan R,Barrera E V. Single wall nanotube and vapor grown carbon fiber reinforced polymers processed by extrusion freeform fabrication.Composites Part A: Applied Science and Manufacturing. 2003;34(12):1207-1217.

[25]Shim H B, Seo M K, Park S J. Thermal conductivity and mechanical properties of various cross-section types carbon fiber-reinforced composites.Journal of materials science. 2002; 37(9):1881-1885.

[26]Yu S, Park K, Lee J-W, Hong S M, Park C, Han T H,Koo C M. Enhanced thermal conductivity of epoxy/Cu-plated carbon fiber fabric composites.Macromolecular Research. 2017;25(6):559-564.

[27]Pardini L C,Gregori M L. Modeling elastic and thermal properties of 2.5D carbon fiber C/SiC hybrid matrix composites by homogenization method.Journal of Aerospace Technology and Management. 2010;2(2):183-194.

[28]Bard S, Schonl F, Demleitner M,Altstadt V. Influence of Fiber Volume Content on Thermal Conductivity in Transverse and Fiber Direction of Carbon Fiber-Reinforced

Epoxy Laminates.Materials (Basel). 2019;12(7):

[29] Korab J, Štefánik P, Kavecký Š, et al. Thermal conductivity of unidirectional copper matrix carbon fibre composites.Composites Part A: Applied Science and Manufacturing. 2002;33(4): 577-581.

[30]Nait-Ali B, Haberko K, Vesteghem H, Absi J,Smith D S. Thermal conductivity of highly porous zirconia.Journal of the European Ceramic Society. 2006;26(16):3567-3574.

[31]Kelly B T. Physics of graphite. 1981;

[32]Zhao Y, Sugio K, Choi Y, Gen S, Xu Z,Yu J. Effect of Anisotropic Thermal Conductivity of Graphite Flakes and Interfacial Thermal Resistance on the Effective Thermal Conductivity of Graphite Flakes/Aluminum Composites.Materials Transactions. 2021;62(1):98-104.

[33]Yang L, Miyoshi Y, Sugio K, Choi Y, Matsugi K,Sasaki G. Effect of graphite orientation distribution on thermal conductivity of Cu matrix composite.Materials Chemistry and Physics. 2021;257(123702.

[34]German R M. Thermodynamics of sintering.Sintering of advanced materials. Woodhead Publishing. 2010;3-32.

[35]Kang S J L. Liquid phase sintering. 2010;110-129.

[36]Nzihou A, Adhikari B, Pfeffer R. Effect of metal chlorides on the sintering and densification of hydroxyapatite adsorbent.Industrial & engineering chemistry research. 2005;44(6):1787-1794.

Chapter 6

Conclusions, discussion and future work

6.1 Background and objective of this study

Global warming, melting glaciers, and reduction of CO_2 emissions have become major global issues. Among them, CO_2 emissions from transportation are second only to electricity, and about 90% of CO_2 emissions from transportation come from vehicles[1]. With the advancement of science and technology and the rapid development of the automobile industry for more than 100 years, automobiles have become the most commonly used means of transportation for people to travel, and the global automobile production is also increasing day by day. After continuous research and exploration, scholars have found that the lightweight of automobiles can not only improve the fuel efficiency of automobiles and reduce CO_2 emissions, but also improve the safety and comfort of automobiles[2,3]. For every 10 percent reduction in vehicle weight, fuel efficiency can increase by nearly 2.5 percent[4,5]. Cars are reduced in weight by using thinner and stronger parts. In order to perfectly match the strength and density of automotive parts, molds are required that can produce (ultra)high-strength automotive parts. The traditional cold stamping process not only causes the indenter to bond with the parts in the process of preparing auto parts, reducing production efficiency, but also shortens the life of the die due to excessive stamping pressure, which puts forward high requirements on stamping equipment. According to the principle of metal softening at high temperature, the cold stamping of auto parts is replaced by hot stamping. Especially in the production process of steel auto parts with a strength exceeding 1000MPa[6], the workpiece needs to be cooled rapidly under external ambient temperature and pressure to obtain martensite, and only hot stamping can be used.

A production system is evaluated by the production cycle, production cost, product quality produced, and system flexibility. In the hot stamping process, the heating and cooling time of the workpiece accounts for one-third of the production cycle. Improving the TC of the hot stamping die can shorten the production cycle, improve production efficiency, reduce thermal stress, and increase the service life of the die. SKD61(40CrMoV5) has become the most commonly used mold in Japan because of its uniform distribution of small spherical carbides, good hardenability, strong resistance to high-temperature tempering softening, high-temperature impact resistance, excellent thermal fatigue resistance, and high-temperature melting loss resistance. Material. DHA1 produced by DAIDO STEEL, SKD61(40CrMoV5), TC at room temperature is 28.5 $Wm^{-1}K^{-1}$. In order to further improve production efficiency, DAIDO STEEL has produced DHA-HS1. Compared with SKD61, the TC of DHA-HS1 can reach 36 $Wm^{-1}K^{-1}$, which is 1.5 times that of SKD61(40CrMoV5). DHA-HS1 has high softening resistance, which is 10 times that of SKD61 (40CrMoV5) for workpieces under the same conditions. The lower the temperature, the harder it is to cool down. Under the same cooling condition, the temperature of the workpiece processed by DHA-HS1 is 30K lower than that of the SKD61(40CrMoV5) mold. It is suitable for the integrated molding of (ultra) high-strength auto parts. The DHA-HS1 mold achieves high TC as a whole through reasonable matching of various components in the composite and sintering to obtain the phase with high TC. With the continuous discovery of new materials, especially two-dimensional anisotropic carbon materials, which have an excellent TC in the axial direction, such as carbon fibers, carbon nanotubes, etc. These two-dimensional materials provide a new possibility for improving the TC of composites by establishing thermal conduction channels in composites. The preparation process of carbon nanotubes is complicated, especially because the purification is difficult, it is not friendly to the environment, and the cost of industrialization is high, so it is only used in small-scale laboratory applications. The TC of C_f is highly anisotropic, and the orientation of C_f in the composite can be controlled by simple rolling, and the manufacturing is simple. At present, C_f has been able to be produced industrially on a large scale at a low cost. This paper is to add C_f with high TC to SKD61 to improve the TC of the composite, improve the production efficiency of the mold, and prolong the service life of the mold.

The purpose of this thesis is to improve the TC of C_f-Cu reinforced SKD61 (40CrMoV5) composites and improve the production efficiency of dies by exploring the mechanism of mechanical and thermal properties of C_f-Cu reinforced iron composites.SKD61(40CrMoV5) alloy contains many chemical elements, these impurity atoms (except Fe) will cause lattice distortion of iron, and destroy the continuity and stability of heat conduction, making the internal heat conduction mechanism of composites complicated and difficult to understand. In order to clarify the mechanism of C_f-Cu improving the TC of SKD61 (40CrMoV5) alloy, this thesis is first based on pure iron (regardless of the scattering effect of impurity atoms on phonons), with C_f-Cu as the reinforcement, and composite was fabricated by spark plasma sintering. Due to the requirements of the mechanical properties of the die, the mechanical properties of the C_f-Cu/Fe composites were studied, (Chapter 2). To evaluate C_f-Cu/Fe composite TC rapidly and accurately, the relationship of the orientation of Cf-Cu in 2D cross-section and 3D space by establishing a mathematical model was determined, and the 2D image analysis was used (Chapter 3). Based on the research in Chapter 3, various factors on the TC of C_f-Cu/Fe composites were investigated by comparing the TC obtained from ROM and EMA models, finite element simulation calculations, and steady-state method measurements (Chapter 4). Based on the study of the effects of C_f-Cu on the mechanical properties of C_f-Cu/Fe composites (Chapter 2), evaluating TC of C_f-Cu/Fe composites by 2D image simulation (Chapter 3) and investigating of factors influencing the TC of C_f-Cu/Fe composites (Chapter 4), in order to improve the TC of SKD611 (40CrMoV5) alloy, the TC of C_f-Cu reinforced SKD611 (40CrMoV5) alloy were investigated (Chapter 5).

6.2 Conclusions of this study

C_f-Cu/Fe and C_f-Cu/SKD611 (40CrMoV5) were fabricated by SPS. The mechanical properties and TC of C_f-Cu/Fe were investigated. The effective TC of C_f-Cu/Fe was evaluated by 2D image analysis, and the factors affecting the TC of the composites and the degree of influence were investigated. The TC of C_f-Cu/SKD611(40CrMoV5) composite was explored. This thesis can draw the following conclusions:

1. In chapter 2, 0-40vol.%C_f-Cu/Fe composites were fabricated by spark plasma sintering (SPS). The relative density of C_f-Cu/Fe composites decreased with the increase of C_f-Cu content, and the relative density of composites was higher than 93%. The sintering temperature hardly affects the relative density of the composites. When the sintering temperature is higher than 1100K, ferrite disappears, and C_f-Cu is destroyed by iron to form cementite or martensite, which improves the hardness of C_f-Cu/Fe composite. Cu elements are distributed around C_f. The hardness of C_f-Cu/Fe composites increases first and then decreases with the increase of C_f-Cu content. When the sintering temperature is 1150K, C_f-Cu is destroyed to form dense flake martensite, and the hardness of 20vol.%C_f-Cu/Fe composite is the highest, reaching 226HV. The fracture mode changes when the volume fraction of C_f-Cu in the C_f-Cu/Fe composite increases from 20% to 30%. With the increase of C_f-Cu content, the tensile strength of the composites first increased and then decreased. The tensile strength of the 20vol.%C_f-Cu/Fe composite reaches a maximum of 679MPa, which is 9.5% higher than that of pure iron under the same conditions. Due to the scattering effect of impurity atoms on phonons, the TC of C_f-Cu/Fe composites decreased by 20% when carbon was added to pure iron. The orientation of C_f-Cu in the composite cannot be determined, the TC of the C_f-Cu/Fe composite changes irregularly with the increase of C_f-Cu content.
2. In chapter 3, 5 (10, 15, 20, 25) vol.% C_f-Cu/Fe composites were prepared by SPS. Most of the C_f-Cu are aligned along the direction of heat flow by hot rolling. The TC of the matrix of C_f-Cu/Fe composites decreased with the increasing C_f-Cu

content. When the volume fraction of C_f-Cu exceeds 20%, the porosity was higher than 2.5%, and the TC dropped to 48.5 W m-1 K-1. The ETC of each element (C_f-Cu and iron matrix) in the 2D cross-section can be obtained by counting the angle between the projection of C_f-Cu on the 2D cross-section and the heat flow (θ_{2D}) and the aspect ratio of the ellipse which was formed by the intersection of C_f-Cu and the 2D cross-section, which was used to calculate the angle between the C_f-Cu and the heat flow (θ_{3D}). Calculation of effective TC of composite materials by finite element simulation. Rolling treatment can effectively control the orientation of C_f-Cu, and almost all the axial directions of C_f-Cu are oriented along the direction of heat flow. When $\theta<73°$, C_f-Cu can increase the TC of the C_f-Cu/Fe composite. On the A plane, the simulated TC is consistent with the measured TC, with deviations between 3%-4%. When the volume fraction of C_f-Cu was 20%, the simulated and measured values attained their maximum value of 68.89 $W\text{m}^{-1}\text{K}^{-1}$ and 71.02 $W\text{m}^{-1}$ K^{-1}, respectively. Owing to the rolling treatment, the measured TCs before and after rolling exhibit a large deviation of 40% to 60%.

3. In chapter 4, 5 (10, 15, 20, 25) vol.% C_f-Cu/Fe composites were prepared by SPS. Most of the C_f-Cu are aligned along the direction of heat flow by hot rolling. The TC of the matrix of C_f-Cu/Fe composites decreased with the increasing C_f-Cu content. When the volume fraction of C_f-Cu exceeds 20%, the porosity increases to 6.8%, and the TC of matrix dropped to 48.5 W m-1 K-1. When the volume fraction of C_f-Cu is less than 20%, the thermal resistance hardly increases, and the contact thermal resistance and the negatively oriented C_f-Cu decrease the TC less than the positively oriented C_f-Cu increases the TC. When the volume fraction of C_f-Cu exceeds 20%, the growth rate of thermal resistance is obviously small, and the reduction effect of contact thermal resistance and negatively oriented C_f-Cu on TC dominates. The main factors hindering TC are the aspect ratio and orientation of C_f-Cu. When the volume fraction of C_f-Cu is 20%, the contact thermal resistance and the negatively oriented C_f-Cu decrease the TC is offset the positively oriented

C_f-Cu increases the TC, so simulated and measured TC achieve the maximum value.

4. In chapter 5, To improve the TC of hot tool steel SKD61(40CrMoV5) alloy, the oriented C_f-Cu reinforced SKD61(40CrMoV5) alloy composite was fabricated by the SPS. The TC of the matrix of the void-containing composite was corrected by the Bregman equation, the orientation of C_f-Cu in the composite was considered, the theoretical TC of the composite was calculated, and the measured TC was obtained by the steady-state method. The relative density of the C_f-Cu /SKD61(40CrMoV5) composite was similar to that of pure SKD61(40CrMoV5) alloy. The copper layer on the surface of C_f can promote sintering densification and hinder the direct contact between SKD61(40CrMoV5) alloy and C_f and prevent the chemical reaction between iron and C_f. The C_f-Cu reinforced SKD61(40CrMoV5) composite exhibited higher TC than single SKD61(40CrMoV5), and its TC increased with the increase of C_f-Cu content. The 5 vol% C_f-Cu /SKD61(40CrMoV5) composite has a high TC of 42 $W \cdot m^{-1}K^{-1}$.

6.3 Discuss the details of this study

We all know that there are many factors affecting the TC of C_f-Cu/Fe. This study has carried out a detailed study on these influencing factors and has made outstanding contributions to the study of the TC of C_f-Cu dispersed iron-based composites.

6.3.1 Sintering temperature

In Chapter 2, we have discussed the effect of sintering temperature on the formation of phase during the preparation of C_f-Cu/Fe composites. As shown in Figure 6-1, when the temperature is higher than 1100K, iron-carbon compounds exist in the composite. C_f is surrounded by Cu, and it is impossible for C to enter the iron matrix. The formation of iron-carbon compounds can only because of the destruction of the copper layer on the surface of C_f-Cu. C_f is in contact with the pure iron and occurs a chemical reaction, and C_f will also be destroyed by the chemical reaction. In this experiment, the sintering temperature should be strictly controlled not higher than 1100K. The content of C_f-Cu has little effect on the phase composition.

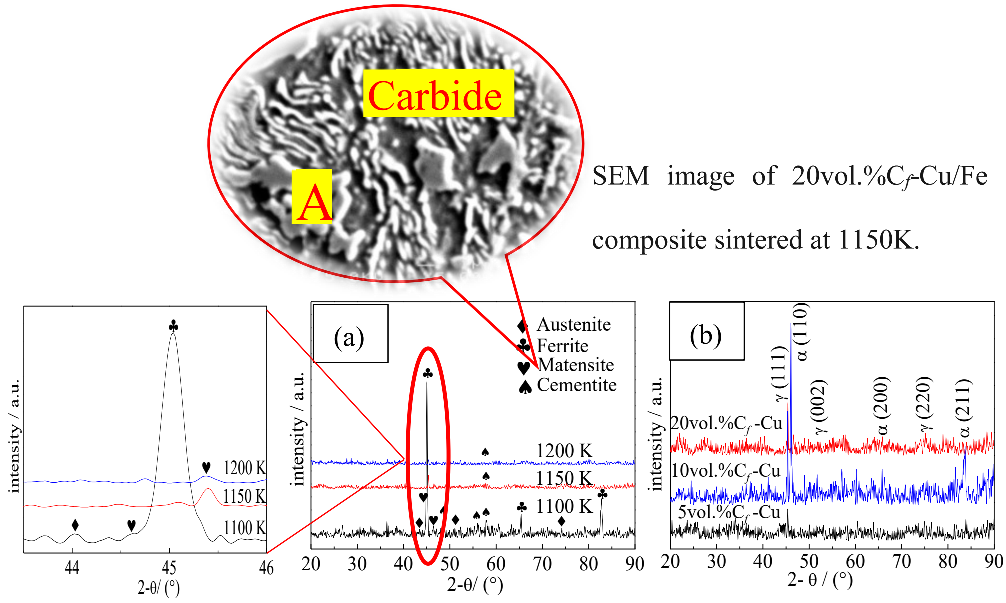

Figure 6-1 XRD of C_f-Cu/Fe composites with (a) different sintering temperatures and (b) different volume fractions of C_f-Cu.

6.3.2 Orientation of C_f-Cu

In this study, K13C6U produced by Mitsubishi Chemical was used. Its tensile strength is about 3.6Gpa, and its shape is a linear cylinder. The mechanical properties of C_f-Cu/Fe are closely related to the orientation of C_f-Cu. As shown in Figure 6-2, when the diamond indenter acts in the radial direction of C_f-Cu, C_f-Cu hinders the indenter from pressing in, and the formed rhombus is small (D is small). According to a formula 6-1, the value of hardness increases.

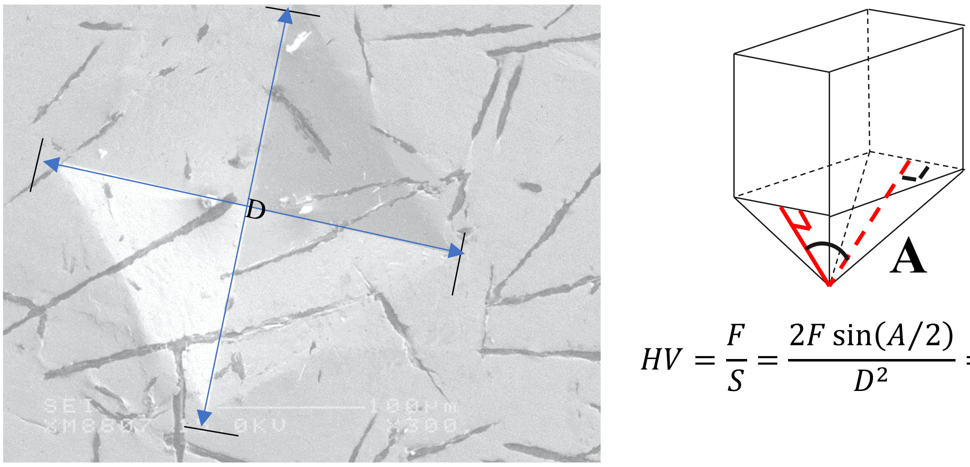

$$HV = \frac{F}{S} = \frac{2F\sin(A/2)}{D^2} = \frac{1.854F}{D^2} \quad \cdots\cdots \text{(6-1)}$$

Fig.6-2 Schematic diagram of hardness tester forming a diamond on composite.

However, when the content of C_f-Cu is too large, C_f-Cu crosslinks to form voids, the relative density of the composite decreases sharply (Figure 6-3), and the hardness decreases (Figure 6-4).

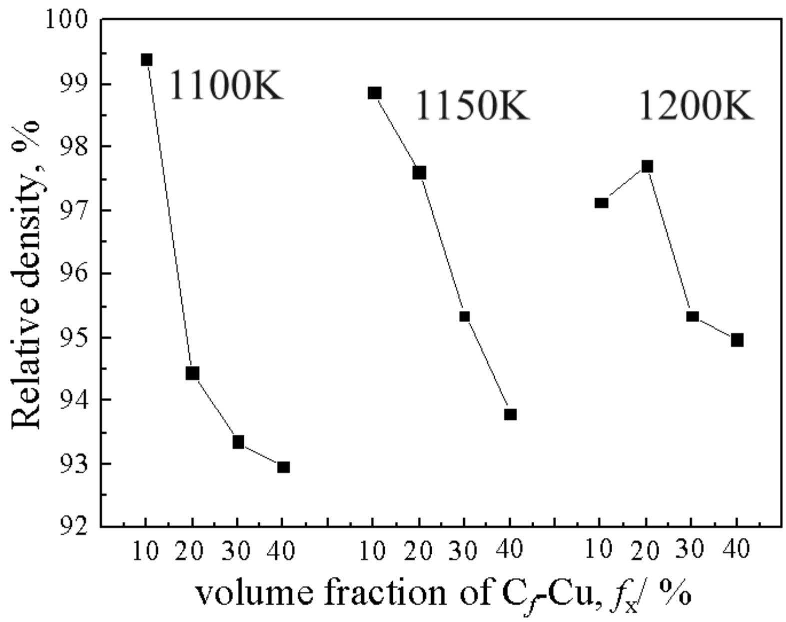

Figure 6-3 Relative density of composites at different sintering conditions with different C_f-Cu contents.

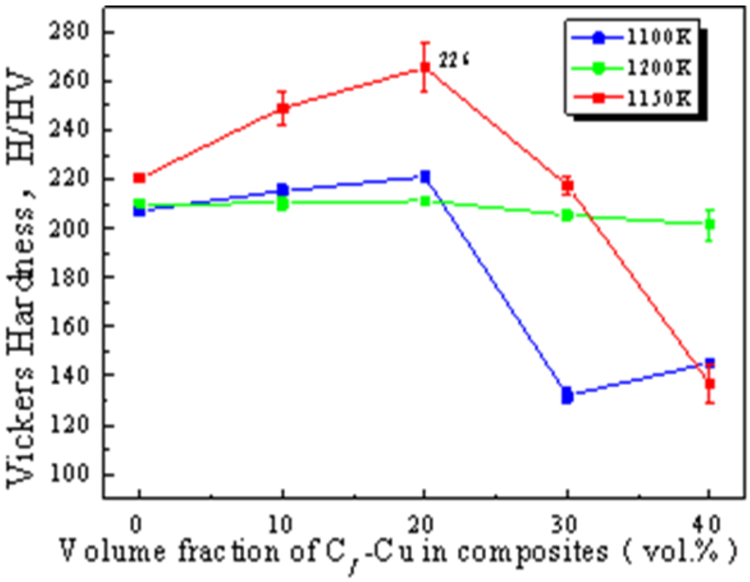

Figure 6-4 Vickers hardness of composites at different temperature with different C_f-Cu contents.

As shown in Figure 6-5, during the fracture process of the composite, C_f-Cu is pulled out, forming dimples, and the Cu coating is peeled off. The existence of C_f-Cu hinders the stretching of the composite, and the tensile strength increases with the increase of C_f -Cu content increases (Figure 6-6). With the increase of C_f-Cu content, the probability of C_f-Cu being arranged on the same plane increases, and Fe and Cu do not react to form a weak bonding interface, breaking will occur on this plane easily, and the tensile strength is drastically reduced (Figure 6-7).

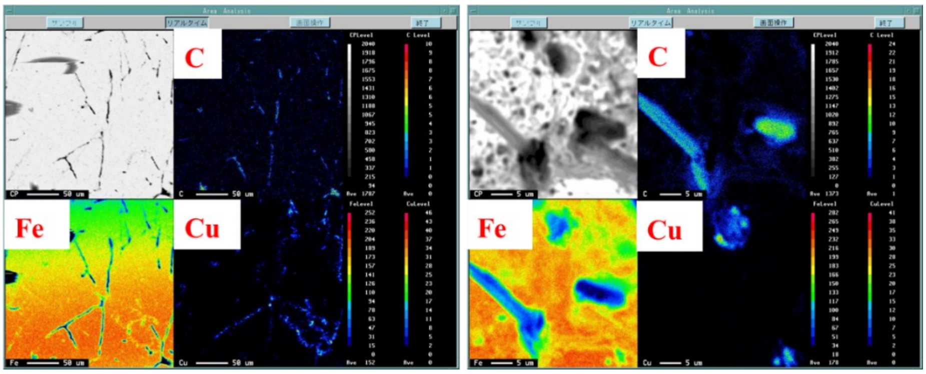

Figure 6-5 SEM image of 10vol.% C_f-Cu/Fe composite.

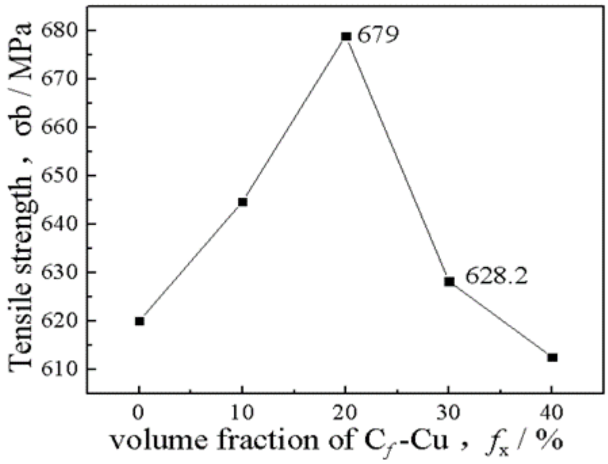

Figure 6-6 Tensile strength of composites with different C_f-Cu contents at 1150 K.

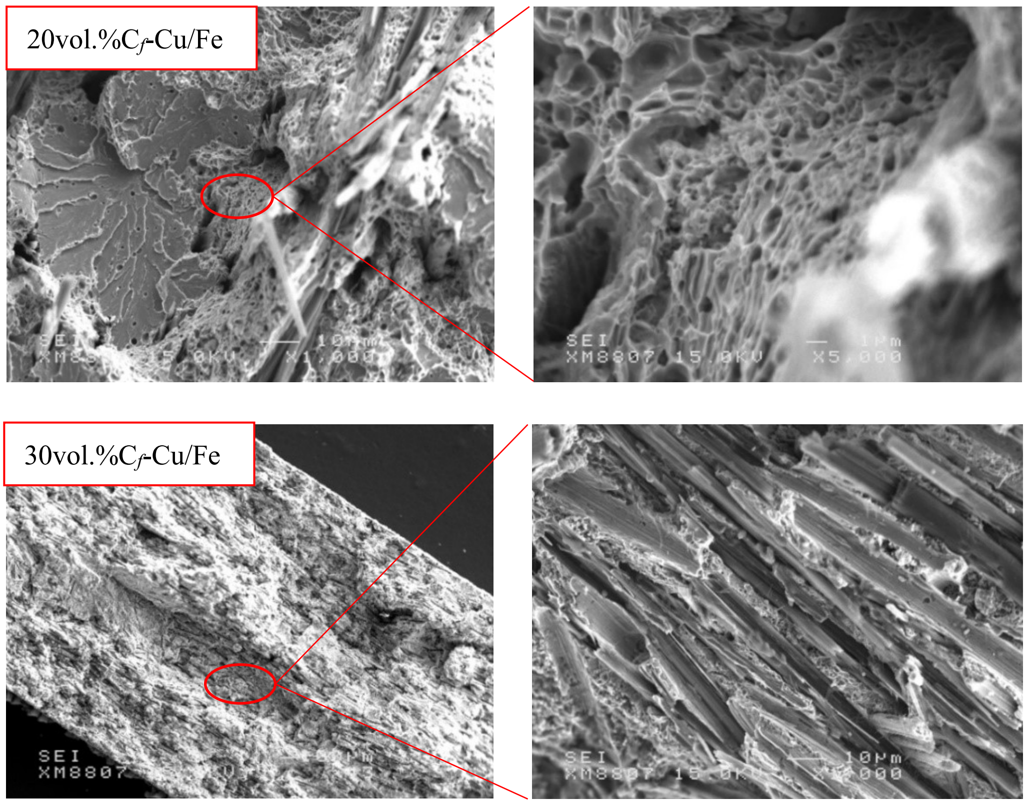

Figure 6-7 SEM image of (20)30vol.%C_f-Cu/Fe composite sintered at 1150K.

Currently, there are very few related studies on C_f to improve TC of composites while maintaining excellent mechanical properties. Most of the research focuses on improving the TC of organic materials by adding C_f[7], and there are also composite materials formed by Cf-enhanced high-TC metals, and these composite materials have very low requirements on mechanical properties.

The TC of C_f-Cu is highly anisotropic, its axial TC is 580$Wm^{-1}K^{-1}$, the radial TC is 5 $Wm^{-1}K^{-1}$, and the TC of pure iron is 54 $Wm^{-1}K^{-1}$, which is in between both of them, so the orientation of C_f-Cu has a great influence on the TC of the composites. The heat flux was set along the X-axis, the effective TC of a C_f-Cu on X-axis (K_i) and Y-axis (K_j) can be expected as following equations[8,9].

$$K_i = K_x\left[1-\left(1-\frac{K_y}{K_x}\right)\sin^2\theta_{3D}\right] \qquad K_j = K_x\left[1-\left(1-\frac{K_y}{K_x}\right)\cos^2\theta_{3D}\right] \qquad \cdots\cdots (6\text{-}2)$$

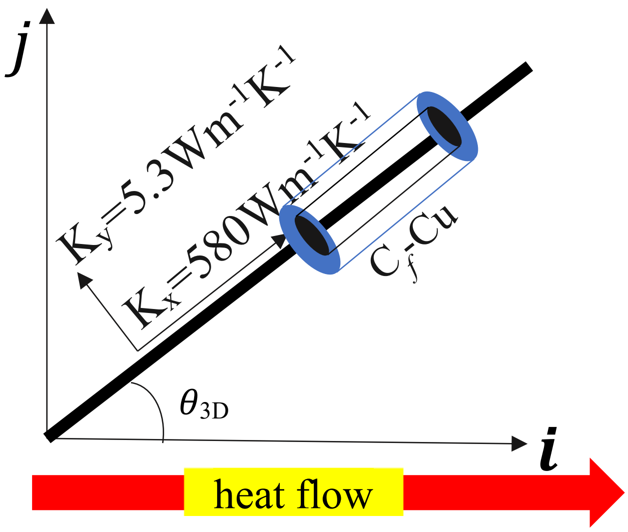

Figure 6-8 TC calculations of C_f-Cu in the direction of heat flow.

Substituting this result into equation (6-2), obtain the influence of θ_{3D} on the TC of C_f-Cu in the direction of heat flow, as shown in Figure 6-9.

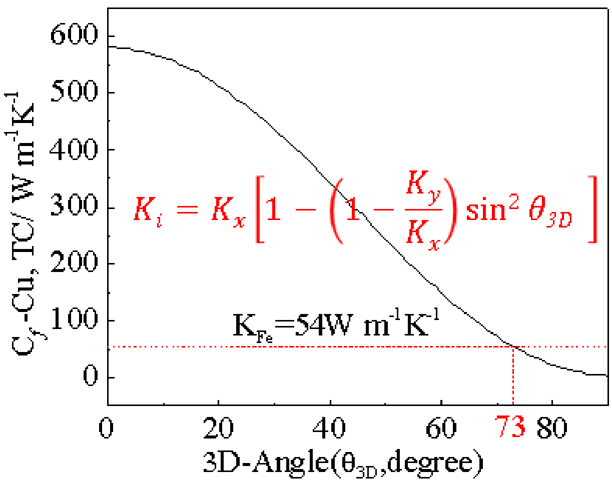

Figure 6-9 Relationship between θ_{3D} and the effective TC of C_f in the direction of heat flow.

When the TC of C_f-Cu on the x-axis is equal to that of the matrix, C_f-Cu neither increases nor decreases the TC of the composite, and the angle between C_f-Cu and the X-axis is the critical angle. In this study, ignoring the effect of voids, the critical included angle of C_f-Cu reinforced pure iron is 73°. Similar curves can also be obtained in the research of Zhao[8] and Yang[9], in which Zhao studied graphite dispersed Al matrix composites, and the critical angle is 61°. While yang studied graphite-reinforced Cu, and the critical angle is 56.6°. Both of them want to fabricate electronic packaging composites with high TC, and the reinforcement are graphite, which has low hardness. As shown in Figure 6-10, the composites were manufactured by SPS, and they believe that SPS will distribute graphite along the horizontal direction (plane parallel to the direction of pressure) during the SPS process.

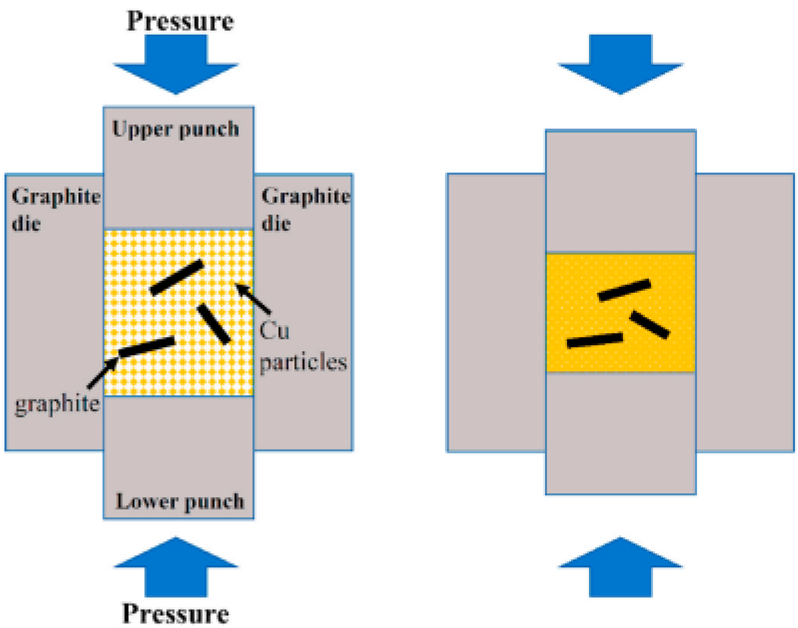

Figure.6-10. Schematic illustration showing processing of graphite reinforced Cu matrix composite by spark plasma sintering (left: before sintering; right: after sintering).

As shown in Figure 6-11, after SPS sintering, the reinforcements are distributed on the A plane, and the orientation is irregular, and the effect of the reinforcements on the TC of the composites is not obvious. To increase the TC of the composite as much as possible, the reinforcement must be oriented in the horizontal direction. The B plane also needs to orient the reinforcement so that the axis of the reinforcement will be aligned with the TC measurement direction. In this study, C_f-Cu was used as the reinforcement, which can withstand large compressive stress. In order to further orient the C_f-Cu, the composites were rolled on the B plane. The average volume of C_f-Cu can improve the TC of the composite material is 1Wm^{-1}K^{-1}.

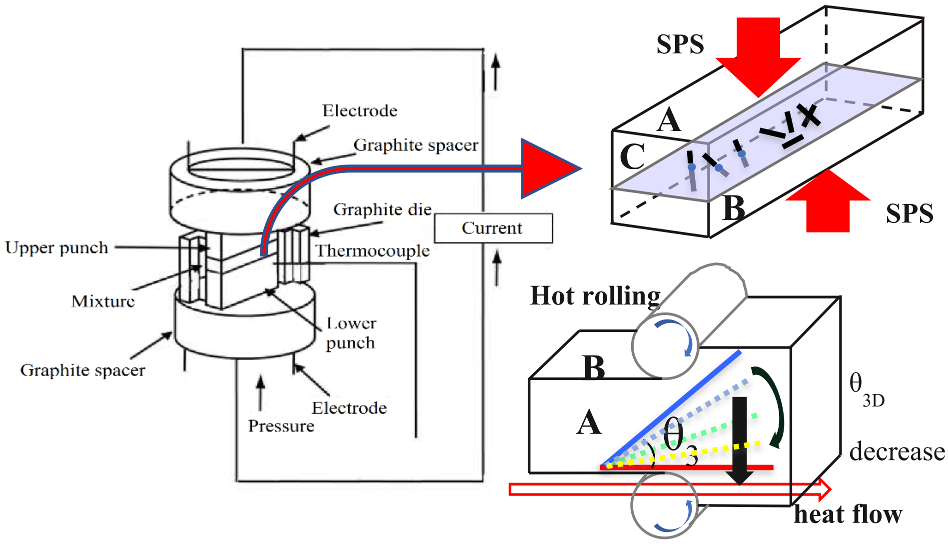

Figure 6-11 The schematic illustration of SPS and hot rolling

6.3.3 Aspect ratio of C_f-Cu

The aspect ratio of C_f-Cu refers to the ratio of the length and diameter of C_f-Cu. When the diameter is constant, the smaller the aspect ratio, the smaller the length, which will increase the contact thermal resistance and reduce the TC of the composite. According to the interpretation of the effective approximate model, the aspect ratio is different, and the corresponding composite materials have different change rates with C_f-Cu (different slopes in the figure). Matsuura et al.[10,11] have done a lot of research on Cf-reinforced metal matrix composites. As shown in Figure 6-12, the initial length of Cf selected in the Cf-reinforced Al matrix composite is 370 μm, the length after hot extrusion is 20 μm, and the length corresponding to the thermal conductivity calculated by the effective approximate model is 120 μm. The equivalent Cf can be seen as the joint effect of six actual Cf end to end. As shown in Figure 6-13, the initial length of C_f selected in the C_f-reinforced Cu-based composite material is 150 μm, the length after hot extrusion is 45 μm, and the length corresponding to the thermal conductivity calculated by the effective approximate model is 94 μm. The equivalent C_f can be seen

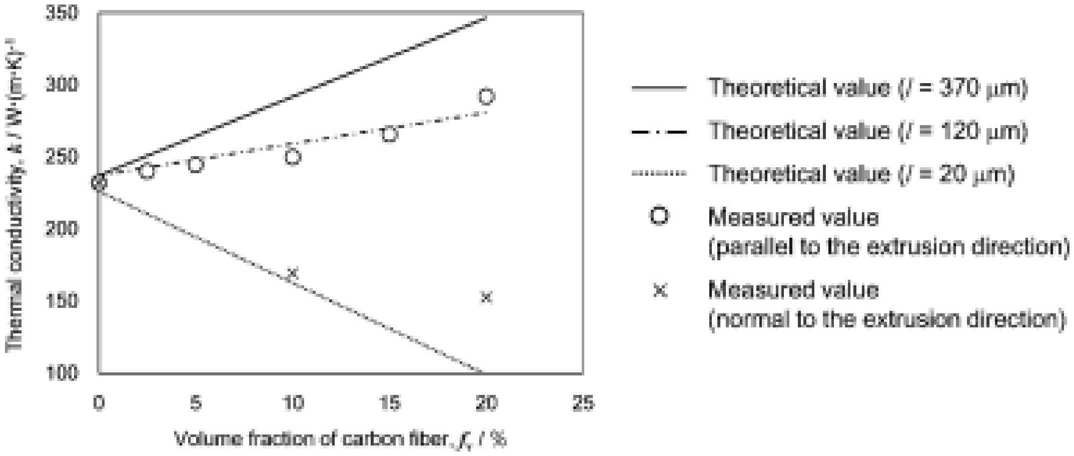

as the joint effect of two actual C_f end to end.

Figure 6-12 Relation between thermal conductivity of extruded C_f/Al composite and the volume fraction of carbon fiber.

Figure. 6-13 Relation between thermal conductivity of extruded C_f/Cu composites and the volume fraction of C_f.

In this research, as shown in Figure 6-14, the initial length of Cf-Cu in this study is 4500 μm, the length after hot extrusion is 110 μm, and the length corresponding to TC calculated by the effective approximate model is 225 μm.

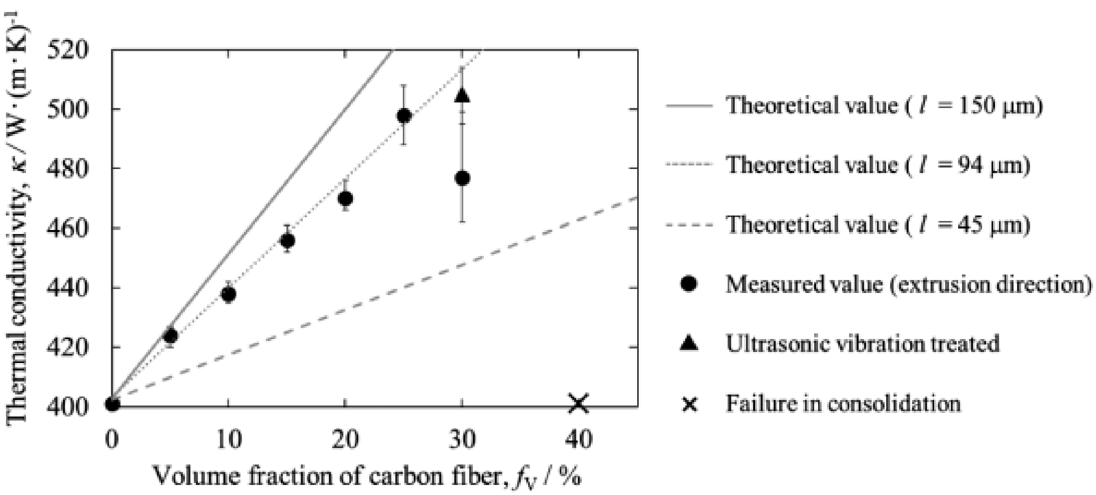

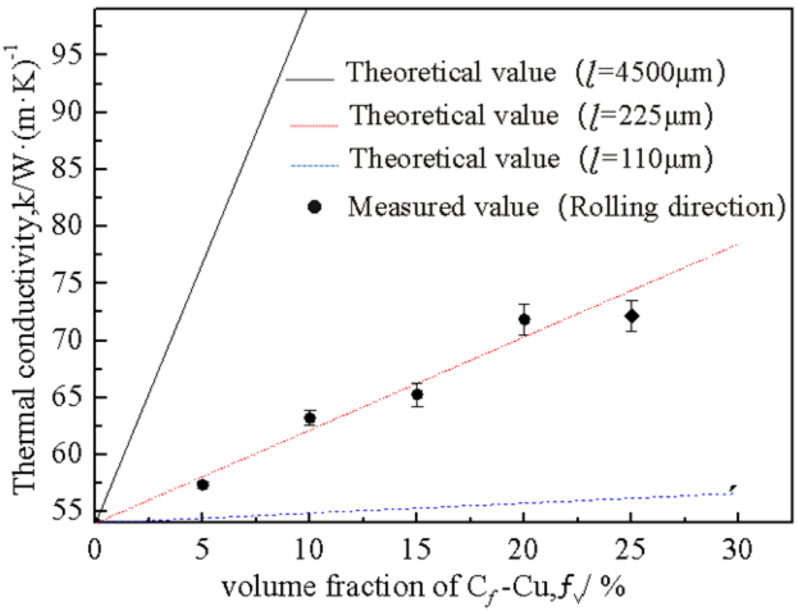

Figure 6-14 Relationship between TC of composite with different aspect ratios of C_f-Cu under the EMA model and volume fraction of C_f-Cu.

6.3.4 Quantitative analysis of the influence weight of thermal conductivity

With the continuous improvement of composite measurement technology, in order to predict the TC of composites more accurately, scholars have continuously explored and established a series of calculation models. The calculation methods of these models ignore different factors, and we can use the TC calculated by different models to roughly evaluate the weight of various neglected factors affecting composites. By reading a lot of literature and found that scholars generally only do qualitative research, and only focus on the influence of certain factors on the TC of composites, such as the influence of the content and orientation of reinforcement on TC. Few scholars have paid attention to the influence weight of various factors that hinder heat conduction in composites on TC. But in the actual production process, by focusing on the main influencing factors and ignoring the secondary factors, high-quality products can be produced at the lowest cost.

6.4 Highlights and limitations

The highlight of this study is to analyze and establish the model of C_f-Cu in three-dimensional space, and to find the relationship between the orientation of Cf-Cu on the two-dimensional section (θ_{2D}) and the orientation of C_f-Cu in three-dimensional space(θ_{3D}) through mathematical calculations. Using the method of two-dimensional image analysis to evaluate the TC of the composite, can quickly and accurately obtain the TC of the composite. By comparing the TC obtained from different TC calculation models, the weight of various heat conduction hindering factors is explored. This calculation method is currently being used for the first time, which is of great experimental value and has positive guiding significance for actual production. The TC of the 5vol.%C_f-Cu dispersed SKD61 alloy in this study reaches 42 $Wm^{-1}K^{-1}$, which is 68% higher than that of SKD61 alloy and 17% higher than that of DHA-HS1.

This study also has limitations. This thesis mainly focuses on the composite of C_f-Cu dispersed pure iron, and mainly studied the mechanism of reinforcement improving the mechanical properties and TC of the composite, providing a new evaluation method of TC. The experimental results of this study are far from the performance of similar products currently on the market. By various models for calculating TC, the percentage of the different factors on TC was evaluated. Although this evaluation method is novel, it still cannot fully reflect various factors, such as the copper layer on the surface of the C_f not being considered, the cracking of the composite due to the high content of C_f-Cu during the rolling process, the copper layer was peeled off or the C_f-Cu is broken. In real social production, in order to improve the mechanical of the mold, it is necessary to add other trace elements, which can react with iron to form compounds and affect the TC of composites. Theoretically, the TC of ferrite in the structure of steel is the highest, about 70-80 $Wm^{-1}K^{-1}$, the TC of tempered martensite is 35 $Wm^{-1}K^{-1}$, and the thermal conductivity of cementite is the lowest 7 $Wm^{-1}K^{-1}$. At present, the effect of the phase composition of composites still cannot be calculated quantitatively, C_f-Cu has an effect on improving the TC of the SKD61 composite, but compared to the theoretical value, the improvement is not very obvious.

6.5 Future work

This study is only the most basic research work on the influence of C_f-Cu on the mechanical properties and TC of pure iron. Under real working conditions, other elements in the composite react with pure iron to form compounds. The effect of these compounds on improving the mechanical properties and TC needs to be further studied. The future research direction is to gradually increase other trace elements (contained by SKD61) except for iron on the basis of pure iron, and gradually study the influence of various added trace elements on the mechanical properties and TC of composites. For example, by adding carbon as a matrix on the pure iron, the iron-carbon compound formed by the reaction of iron and carbon can not only strengthen the mechanical properties of the composite but also have a TC much higher than that of pure iron. In addition to the effect of adding carbon on the performance of composites, other elements, such as nickel, chromium, etc., can improve the performance of composites. It is also possible to explore the influence of various factors on the performance of composites. Adding trace elements will improve the mechanical properties of composites and reduce the TC of composites. According to different actual production conditions, a variety of formulations of hot stamping die composites are designed.

Although the two-dimensional image analysis method can intuitively, quickly, and accurately reflect the TC of the composite, the image analysis method can only obtain the TC when the heat flow passes through a certain plane, which has some difference from the TC of other planes parallel to the identified plane in the composite. The evaluation method of composite TC needs to be further improved, such as the use of three-dimensional modeling and three-dimensional structural analysis. Three-dimensional structural analysis methods can be used, but this method is expensive and time-consuming. Therefore, the method of three-dimensional structure analysis to evaluate the TC of composite materials needs further study.

6.6 References

[1]Mori K, Bariani P F, Behrens B A, Brosius A, Bruschi S, Maeno T, Merklein M,Yanagimoto J. Hot stamping of ultra-high strength steel parts.CIRP Annals. 2017;66(2):755-777.

[2]Merklein M,Lechler J. Investigation of the thermo-mechanical properties of hot stamping steels.Journal of Materials Processing Technology. 2006;177(1-3):452-455.

[3]Mori K, Maki S,Tanaka Y. Warm and Hot Stamping of Ultra High Tensile Strength Steel Sheets Using Resistance Heating.CIRP Annals. 2005;54(1):209-212.

[4]Kiani M, Gandikota I, Rais-Rohani M,Motoyama K. Design of lightweight magnesium car body structure under crash and vibration constraints.Journal of Magnesium and Alloys. 2014;2(2):99-108.

[5]Tong C, Rong Q, Yardley V A, Li X, Luo J, Zhu G,Shi Z. New Developments and Future Trends in Low-Temperature Hot Stamping Technologies: A Review.Metals. 2020;10(12):1652.

[6]Lim W-S, Choi H-S, Ahn S-y,Kim B-M. Cooling channel design of hot stamping tools for uniform high-strength components in hot stamping process.The International Journal of Advanced Manufacturing Technology. 2013;70(5-8):1189-1203.

[7]Lee E, Cho C H, Hwang S H, Kim M G, Han J W, Lee H,Lee J H. Improving the Vertical Thermal Conductivity of Carbon Fiber-Reinforced Epoxy Composites by Forming Layer-by-Layer Contact of Inorganic Crystals.Materials (Basel). 2019;12(19):

[8]Zhao Y, Sugio K, Choi Y, Gen S, Xu Z,Yu J. Effect of Anisotropic Thermal Conductivity of Graphite Flakes and Interfacial Thermal Resistance on the Effective Thermal Conductivity of Graphite Flakes/Aluminum Composites.Materials Transactions. 2021;62(1):98-104.

[9]Yang L, Miyoshi Y, Sugio K, Choi Y, Matsugi K,Sasaki G. Effect of graphite orientation distribution on thermal conductivity of Cu matrix composite.Materials Chemistry and Physics. 2021;257(123702.

[10]Tokunaga T, Takahashi K, Ohno M, Sasaki K, Imanishi T,Matsuura K. Fabrication

of Carbon Fiber Oriented Al-Based Composites by Hot Extrusion and Evaluation of Their Thermal Conductivity.Journal of the Japan Institute of Metals. 2016;80(10):640-645.

[11]Kontani H, Tokunaga T, Ohno M, et al. Fabrication of unidirectionally orientated carbon fiber reinforced cu-based composites by hot extrusion and evaluation of their thermal properties.Journal of the Japan Institute of Metals and Materials, 2018; 82(5): 125-129.

Acknowledgement

I would like to express my deepest gratitude to my supervisor, Professor Gen Sasaki, who has provided me with valuable guidance at every stage of the writing and publication of the paper. When I was helpless and difficult to continue my research, he gave me a lot of help and overcame the difficulties. Without his enlightened guidance, impressive kindness, and patience, I would not have been able to complete my dissertation. In addition, Prof. Sasaki gave me many opportunities to present my research, he led me to many domestic and international conferences and gave a perfect presentation. This has been a valuable experience in my life and has given me the confidence to face the coming challenge.

I am also greatly indebted to Associate Professor Kenjiro Sugio, who provided software guidance and technical support for my simulation calculations. Assistant Professor Zhefeng Xu, who have helped me learn the operation of some experimental equipment, supervised and provided suggestions for my experiments. Next, I would like to express my heartfelt thanks to the reviewers from the journal of Material Transactions for their useful comments on this thesis. Then, my thanks are extended to the past and present students of Material Physics Laboratory, in Department of Mechanical Science and Engineering, Hiroshima University, for their enthusiastic help to me. Especially Yan Zhao, we fully explored the orientation of carbon fiber in three-dimensional space, which provided great help for the establishment of mathematical equations for carbon fiber orientation in two-dimensional cross-section and three-dimensional space.

Finally, my gratitude also extends to my family, for their endless love and selfless support. Without them, I would not have come so far in my education.

Papers and Proceedings

1. Wu Di, Kenjiro Sugio, Gen Sasaki*, Estimation of Effective Thermal Conductivity of Copper-plated Carbon fibers reinforced Iron-based Composites by 2D Image Analysis. Material transactions,64(2023), (Chapter 3)
2. Wu Di, Kenjiro Sugio, Gen Sasaki*. Effective Thermal Conductivity and Thermal Resistance of Electroless Copper plated Carbon fiber and Fe Composite. Material transactions, 64(2023),586-595, (Chapter 4)
3. Wu Di, Takuro Morimoto, Kenjiro Sugio, Gen Sasaki*. Preparation and Thermal Conductivity of Copper Plated Carbon Fiber Dispersed Steel Matrix Composites. Material transactions, 61(2022),295-299, (Chapter 5).
4. Wu Di, Kenjiro Sugio, Gen Sasaki*. Effect of Copper-plated Carbon fiber Orientation distribution on Thermal Conductivity of Fe matrix Composite. 17th Japan International SAMPE Symposium & Exhibition (JISSE-17), (2021), 1A-06. (Chapter 3).

Presentations

1. Di Wu, Kenjiro Sugio, Gen Sasaki. The Preparation and Properties of Electroless Copper-plated Carbon Fiber and Iron Composites. 金属第 59 回・鉄鋼第 62 回中国四国支部講演大会，愛媛大学，城北キャンパス,. August.19,2019.
2. Di Wu, Kenjiro Sugio, Gen Sasaki. Evaluation of Effective Thermal Conductivity of Copper-plated Carbon fibers reinforced Iron-based Composites by 2D Image Simulation. The Japan Institute of Metals and Materials Annual Autumn Meeting 2020(167th), September.17,2020.
3. Di Wu, Kenjiro Sugio, Gen Sasaki. Effective Thermal Conductivity and Thermal Resistance of Electroless Copper plated Carbon fiber and Fe Composite. The Japan Institute of Metals and Materials Annual Spring Meeting 2021(168th), March.19, 2021.
4. Di Wu, Kenjiro Sugio, Gen Sasaki. Effect of Copper-plated Carbon fiber Orientation distribution on Thermal Conductivity of Fe matrix Composite. 17th Japan International SAMPE Symposium & Exhibition (JISSE-17), Decemember.1,2021.